Physical, Mechanical and Tribological Behavior of Metal Matrix Hybrid Composite Fabricated via Friction Stir Consolidation Process

Samuel Kefyalew Abebe

A Dissertation Submitted to the Department of Mechanical Engineering

School of Mechanical, Chemical and Materials Engineering

Presented in Partial Fulfillment of the Requirement for the Degree of

Doctor of Philosophy

In

Manufacturing Engineering

Office of Graduate Studies

Adama Science and Technology University

June, 2024

Adama, Ethiopia

Physical, Mechanical and Tribological Behavior of Metal Matrix Hybrid Composite Fabricated via Friction Stir Consolidation Process

Samuel Kefyalew Abebe

Main Supervisor: Dr. Habtamu Beri Tufa (Associate Professor)

Co-Supervisor: Dr. Devendra Kumar Sinha (Associate Professor)

A Dissertation Submitted to the Department of Mechanical Engineering

School of Mechanical, Chemical and Materials Engineering

Presented in Partial Fulfillment of the Requirement for the Degree of

Doctor of Philosophy

In

Manufacturing Engineering

Office of Graduate Studies

Adama Science and Technology University

June, 2024

Adama, Ethiopia

Declaration

I hereby declare that this Dissertation entitled “Physical, Mechanical and Tribological Behavior of Metal Matrix Hybrid Composite Fabricated via Friction Stir Consolidation Process” is my original work. That is, it has not been submitted for the award of any academic degree, diploma or certificate in any other university. All sources of materials used for this thesis have been duly acknowledged through appropriate citations.

Name of student	Signature	Date

Recommendation

We, the supervisors of this dissertation, hereby certify that we have read and revised the dissertation entitled "Physical, Mechanical and Tribological Behavior of Metal Matrix Hybrid Composite Fabricated via Friction Stir Consolidation Process" prepared under our guidance by Samuel Kefyalew Abebe submitted in partial fulfillment of the requirements for the degree of Doctor of Philosophy in Manufacturing Engineering.

____________________	____________________	____________
Major Supervisor	Signature	Date
____________________	____________________	____________
Co-supervisor	Signature	Date

Approval of Board of Examiners

We hereby certify that the recommendations and suggestions made by the board of examiners are appropriately incorporated into the final version of the dissertation entitled "Physical, Mechanical and Tribological Behavior of Metal Matrix Hybrid Composite Fabricated via Friction Stir Consolidation Process" by Samuel Kefyalew Abebe.

Major Supervisor	Signature	Date
Co-supervisor	Signature	Date

We, the undersigned, members of the Board of Examiners of the dissertation open defense by Samuel Kefyalew Abebe have read and evaluated the dissertation entitled "Physical, Mechanical and Tribological Behavior of Metal Matrix Hybrid Composite Fabricated via Friction Stir Consolidation Process" and examined the candidate during open defense. This is, therefore, to certify that the dissertation is accepted for partial fulfillment of the requirement of the degree of Doctor of Philosophy in Manufacturing Engineering.

Chairperson	Signature	Date
Internal Examiner	Signature	Date
External Examiner 1	Signature	Date
External Examiner 2	Signature	Date
Department Head	Signature	Date
School Dean	Signature	Date
Office of Postgraduate Studies, Dean	Signature	Date

ACKNOWLEDGEMENT

In the name of the Almighty, the Most Merciful, I express my deepest gratitude to God for providing me with the strength, guidance, and perseverance throughout the challenging journey of my doctoral studies.

I extend my sincere appreciation to my esteemed advisors, Dr. Habtamu Beri Tufa and Dr. Devendra Kumar Sinha, for their unwavering support, insightful guidance, and continuous encouragement. Their commitment to academic excellence, coupled with their ethical approach to research, has been the foundation of my doctoral endeavors. Beyond science, their integrity and ethics have taught me a lot about the qualities a doctor ought to possess. Genuinely witnessing, the mutual understanding and respect they showed with one another led to the smooth flow of this dissertation.

My heartfelt thanks go out to my family members and my girlfriend Miss Bethlehem Teklehaymanot whose love, encouragement, and sacrifices have been a source of inspiration.

I extend my appreciation to the members of my doctoral committee Dr. Gebisa Bekele, Dr. Fekadu Gochole and Dr. Esmael Adem; whose valuable insights and constructive feedback have played a pivotal role in shaping the outcome of this research. Additionally, I would like to thank the Head of Mechanical Engineering Department, Mr. Sintayehu Legesse for his ethical principles and humility.

A special acknowledgment is reserved for Adama Science and Technology University (ASTU), where my academic journey began a decade ago. From my bachelor's degree through the master's program and now completing my Ph.D., the university has been a nurturing ground for my intellectual development.

In memory of my late father Kefyalew Abebe Abaferda (Kefalye), who passed away just before I presented my proposal, I want to express my gratitude for his unwavering belief in my abilities. His legacy lives on in my academic achievements, and I **dedicate** this dissertation to his memory.

Contents

CHAPTER TWO

CHAPTER THREE

LIST OF TABLES

LIST OF FIGURES

Acronyms and Abbreviations

ANN	Artificial Neural Network
ANOVA	Analysis of Variance
ASTM	American Standards for Testing and Materials
CoR	Coefficient of Restitution
CYS	Compressive Yield Strength
DEM	Discrete Element Method
FSC	Friction Stir Consolidation
FSP	Friction Stir Processing
FSR	Friction Stir Riveting
FSS	Friction Stir Scribe
FSW	Friction Stir Welding
GA	Genetic Algorithm
MMC	Metal Matrix Composites
MMHC	Metal Matrix Hybrid Composite
MMSCs	metal matrix surface composites
MWCNTs	multi-walled carbon nanotubes
PM	Powder Metallurgy
RSM-BBD	Response Surface Method – Box-Behnken Design
SEM	Scanning Electron Microscope
UTS	Ultimate Tensile Strength
FDM	Fused Deposition Modelling

Abstract

Metal matrix composite materials are becoming a growing trend in the automotive and aerospace industries because of their mechanical, physical, tribological and fundamentally desirable strength to weight ratio properties. However, their availability in use is limited because of their manufacturing method difficulty and process extravagancy. The main aim of this research was to fabricate Metal Matrix Hybrid Composite (MMHCs) through Friction Stir Consolidation (FSC) process which is composed of AZ61 reinforced with SiC and ZrO_2. The investigation integrated Discrete Element Method (DEM) simulation, optimization using Response Surface Methodology (RSM), artificial neural network (ANN) model validation, Genetic Algorithm (GA), and experimental validations. The DEM simulation provides insight into the FSC process, offering a virtual platform to analyze material's porosity behavior *and optimize process parameters. RSM and GA were employed to optimize key parameters, including die rotational speed, applied load, thickness, consolidation time, and reinforcement composition of the MMHC. RSM predicted an optimal configuration at 800 rpm rotation speed, 500 N applied load, 12 mm thickness, 6 minutes of consolidation time, and 5%wt (2.5 %wt of SiC and 2.5 %wt of ZrO_2) composition of the metal matrix. This combination was projected to yield a minimum porosity response of 0.62%. In contrast, GA suggested an optimal configuration with identical rotation speed, applied load, thickness, and consolidation time, but a higher 15%wt (7.5 %wt of SiC and 7.5 %wt of ZrO_2) composition of the metal matrix. This prediction gave a lower minimum porosity response of 0.469%. In contrast, optimization through GA showed a better predicting accuracy. Experimental validation of the GA predicted optimal process parameter combination for minimum porosity was successfully carried out. The results of the fabricated samples showed hardness, compressive yield strength and wear rate properties of 339±1.5HV (3324.6±14.7MPa), 170±2.6MPa and 0.0054mg/m respectively. Furthermore, following FSC synthesis, a new phase of ZnO emerged upon characterization with XRD and Thermogravimetric analysis revealed that the thermal stability ranged from 375 to 480 ^oC. In conclusion, based on the findings of this study and the properties of manufactured MMHCs, FSC may generally be taken into consideration for an alternative approach for fabricating MMHCs.*

Keywords: *Friction Stir Consolidation, Porosity, Response Surface-Box-Behnken Design, Artificial Neural Network, Genetic Algorithm.*

CHAPTER ONE

INTRODUCTION

1.1 Background and Context in Metal Matrix Composite

Metal Matrix Composites (MMCs) are gaining a lot of attention in a wide range of technical applications due to their unique properties. MMCs are composed of a mixture of various materials. These materials consist of one or more non-metallic material types, such as ceramics or polymers, reinforced by a metal matrix. When contrasted to the base metal alone, the resulting composite has superior thermal, mechanical and electrical properties. Metal matrix composites were initially developed in the 1970's as a result of efforts made by researchers to find ways over the drawbacks associated with conventional monolithic metals (Miracle, 2005). However, start to attract attention in early 1980's when international organizations such as National Aero Space Plane (NASP) started giving attentions in the United State. Similarly, an investigation by Khalid et al., (2023) witnessed that the commercialization of metal matrix composites generally began after the second world war. In 1999, there were 2500 metric tons of MMC sold globally, worth at approximately $100 million (Miracle, 2005). The attractiveness of MMCs began to attract attentions for the reasons, conventional metals frequently suffered from issues like high densities, constrained strength-to-weight ratios, and weak corrosion and wear resistance. MMCs have shown to be a viable way to solve these restrictions and offer improved performance in applications that are demanding.

The goal of finding a balance between strength and weight is one of the main inspirations behind the invention of MMCs (Khalid et al., 2023). Engineers can produce composites with increased specific strength and stiffness by mixing lightweight reinforcement elements, such Silicon Carbide (SiC) or Alumina (Al_2O_3), into a metallic matrix such as titanium, magnesium and aluminum. This is especially helpful in the automobile and aircraft industries, where lightweight materials improve performance and fuel efficiency. When it comes to MMCs, the qualities of the composite are mostly determined by the reinforcing phase. Ceramics have great strength, hardness, and thermal stability, which make them a primary choice for reinforcement. The specific application demands also influence the choice of reinforcement. For instance, refractory materials such as tungsten or Boron Nitride (BN) can possibly be utilized when resistance to high temperatures is required.

MMCs are produced using a variety of manufacturing techniques, including stir casting, liquid infiltration, and powder metallurgy processes. Every processing technique has positive and negative impact on the final characteristics of MMCs. For instance, in powder metallurgy, reinforcing particles are dispersed in metal powders and then pressed and consolidated using techniques such as hot pressing or sintering operation. Likewise, metal matrix materials are melted and desired proportions of reinforcements are stirred in the case stir casting route (Miracle, 2005; Hashim et al., 1999).

Applications for metal matrix composites are found in different industries, such as sports equipment, automotive, electronics, and aerospace. In addition to this, MMCs are used in engine parts, structural components, and thermal control systems in the aerospace sector. MMCs are useful in lightweight components that improve fuel efficiency and lower emissions for the automotive sector. In general, the need for materials that are lightweight with improved mechanical, tribological and thermal properties make them useful in a variety of industrial sectors and this has driven the development of MMCs.

MMCs are materials made of a metal matrix mixed with other reinforcements in order to enhance particular characteristics. The selection of reinforcing materials which is a important part of MMC has an important impact on the MMC's overall strength. Different types of reinforcing materials have been studied; each has particular advantages and contributes to the desirable properties of the composite.

1. ***Ceramic Reinforcements***: Ceramic reinforcements can be produced into whiskers, particles, continuous fibers, or short fibers.
   a) Silicon Carbide (SiC): Among the most typical ceramic reinforcements in MMCs is SiC. It enhances and offers exceptional wear resistance, compressive and tensile strength; and high hardness (Fenghong et al., 2019; Chandradass et al., 2020). Applications areas for SiC-reinforced MMCs include brake rotors, aerospace parts and other high-wear applications.

b) ***Alumina (Al_2O_3):*** Due to its outstanding hardness and thermal stability, alumina is selected. It is commonly used in MMCs for applications, like cutting tools and automotive components, where resistance to wear and high temperatures is essential.

c) ***Boron Nitride (BN):*** a ceramic reinforcement BN is widely recognized by its attractive heat conductivity. It is used in MMCs where efficient heat dissipation is essential which makes it appropriate for thermal control systems and electronic packaging.

d) ***Zirconium Dioxide (ZrO_2):*** according to various studies a metal matrix reinforced with zirconia has enhanced tremendously the wear resistance of the composite (Radhakrishnan et al., 2019).

e) ***Titanium Diboride (TiB_2):*** TiB_2 is a very hard ceramic with good wear resistance, oxidation stability, and heat conductivity. TiB2 is a good electrical conductor as well (Schmidt et al., 2007).

1.2 Bulk Metal Matrix Composite Fabrication Methods

Bulk Metal Matrix Composites (BMCs) are a class of state-of-the-art materials that combine the benefits of metals with enhanced performance features from the inclusion of reinforcing phases. There are various methods to process MMC materials; however stir casting and powder metallurgy are the two most common ways to fabricate MMC. (Behera et al., 2019). These techniques are essential for altering a composite’s mechanical and thermal characteristics for use in structural, automotive, and aerospace engineering, among other fields. However, researchers listed the general metal matrix fabrication processes as shown in Figure 1.1 (Behera et al., 2019).

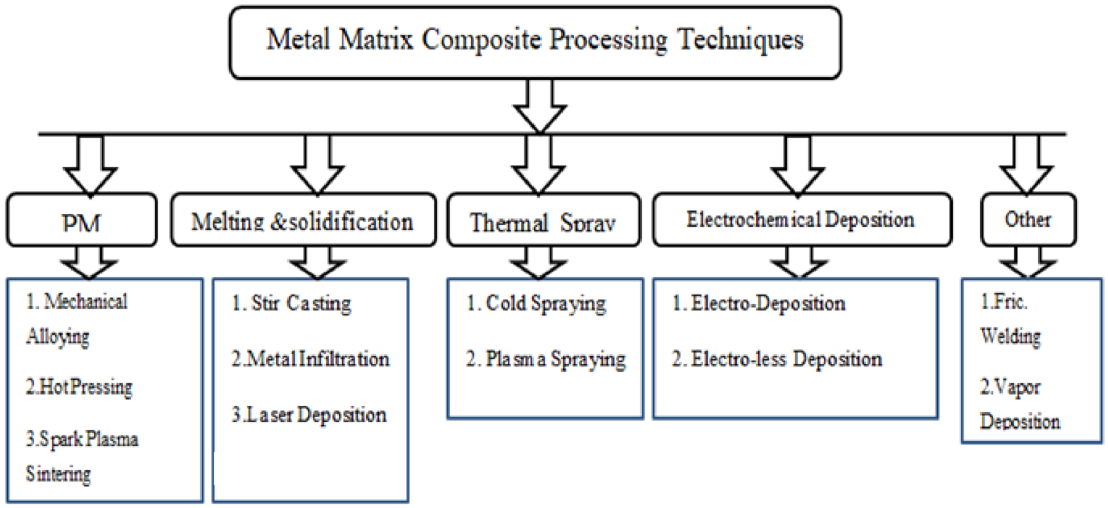

Figure 1.1 Metal Matrix Composite Processing Techniques

1.2.1 Stir Casting

Stir casting or Liquid-state processing is a commonly used technique for creating bulk MMCs. This method uses mechanical stirring to distribute reinforcement phases such as whisker or particles throughout a molten metal matrix material. The technique works well to develop composites with a range different reinforcing particle and is relatively simple to use. The homogenous dispersion of reinforcing particles inside the matrix made possible by mechanical stirring. Stir casting have certain disadvantages. For instance, The main drawbacks of the stir casting technique are; problem in an inadequate wetting, Agglomeration of reinforcements and non-uniform dispersion of reinforcements throughout the melted matrix (Annigeri & Veeresh Kumar, 2017). Furthermore, breakage of the reinforcing particle, local solidification and gas trapping (Shivalingaiah et al., 2022). Furthermore, during the experiment of Al-SiC metal matrix composite, researchers discovered that the high temperature during stir casting produced very brittle Aluminum carbide phase, which has an impact on the final mechanical property. (Lai & Chung, 1996). The creation agglomeration leads to undesired properties which leads the researchers to incline into surface friction stir processing (Parikh and Badgujar, 2022). The composite's mechanical characteristics could be impacted by this non-uniformity. Furthermore, the stir casting procedure frequently challenged with a lack of control over the positioning the distribution of reinforcement materials, which could potentially have an effect on the finished product's overall performance.

1.2.2 Powder Metallurgy Process

Another technique that is frequently used for the manufacture of bulk MMC is powder metallurgy (PM). Usually, the reinforcement material used in this technique is in the form of powders that are combined with metal powders to create a uniform mixture. The powders are then consolidated or pressed into a dense composite or green compact by compressing the mixture into the required shape and sintering it at high temperatures for further densification. Improved mechanical and thermal properties can be achieved by improved control over reinforcement distribution through powder metallurgy than stir casting. Powder metallurgy has advantages, but it also has drawbacks. Compared to stir casting, the manufacturing process is more time-consuming because it comprises more processes such as powder mixing, compaction, and sintering. Longer processing durations could be necessary to achieve a fully dense composite and the sintering process itself could increase production costs. Likewise, the quality of the finished composite is at concern due to the possibility of oxidation and contamination during the handling and processing of powder.

1.2.3 Drawbacks and Time-Consuming Nature of Stir Casting and Powder Metallurgy

There are comparable challenges as well as drawbacks with both powder metallurgy and stir casting processes. Producing parts with enhanced porosity continues to be a challenge, affecting the composites' performance in general. One significant difficulty with these fabrication techniques is their time-consuming nature, particularly in industries where quick production cycles are needed. Powder metallurgy's time-consuming nature is affected by its complex processing procedures, whereas stir casting's ease of use is compensated by the difficulties of creating a uniform distribution of reinforcements and presence of high porosities.

1.3 The Working Principle of Friction Stir Consolidation Process

Early in the 1990s, the Welding Institute in Cambridge, UK, developed friction stir processing. Up until the early 2010s, it was essentially ignored for years after that. Li et al., (2018), described that the Friction Forging was initially began into investigation in 1975 by Andrews and Gilpin. This drives the development of friction extrusion process which was invented and patented 1990's by W. Thomas (X. Li et al., 2018). Because of their excellent potential for recycling, friction processing and extrusion technologies have gained attention with the rise of additive manufacturing and the aerospace industry. Likewise, it is promising thermo-mechanical manufacturing process that modifies or improves the microstructure and mechanical properties of the material. In addition to this, friction stir consolidation process uses simple and inexpensive non-consumable rotating dies to create a frictional heat which will result in generation of heat.

The fundamental working principle of FSC is heat generation caused by friction between the precursor and the non-consumable dies. This will result the precursor in plastic deformation with the aid of compressive (applied load) force. The Figure 1.2 shows the arrangement of the rotating die, fixed chamber, precursors (AZ61, SiC and ZrO_2) and a Process Development System (PDS) or (Milling Machine). Heat will be generated inside the chamber as a result of the compressive force and rotational impact of the rotating die, and this heat will cause the precursor to plasticize. Li et al., (2018), used different equipment to run FSC such as chamber and backing plate which maintains the precursors and makes the particles accessible to the revolving die, during the recycling of Aluminum scraps. The friction rises by applying compressive force. Next, there would be a weldment or consolidation of the precursors due to the heat generated by the frictional pressure.

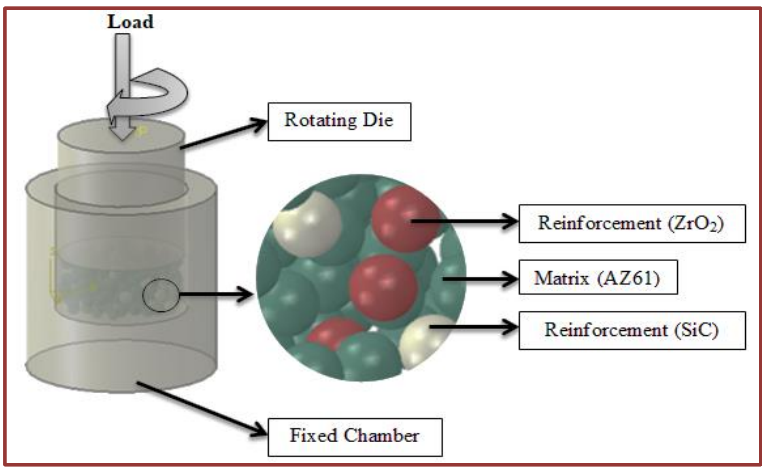

Figure1. 2 Procedure of FSC Process in Metal Matrix Composite Fabrication

The general working principle of FSC started by designing rotating die and fixed chamber to possibly be assembled on a PDS, then the designed fixed chamber was tightened or fixed on the table of a milling machine while the rotating die was assembled on the spindle of the machine, then the fixed chamber was loaded with the desired amount of matrix and reinforcement ratios based on the Box-Behnken design matrix, followed by aligning the rotating die in a fixed chamber simultaneously the desired amount of load was applied to create a frictional heat for a desired time, then spindle was stopped and the process was terminated. Finally, the produced MMC was taken out from the fixed chamber for characterization and tests. The fixed chamber was made split for ease of removal of the produced MMCs.

1.4 Application Areas

The application areas of friction stir consolidation process are related to the application areas of powder metallurgy and stir casting industries which are at aerospace industries, automotive, manufacturing industries and material production industries. Likewise, the most common application areas of Magnesium MMCs are; automotive spare parts like disk brake, aerospace parts, and engine valves (Chawla & Chawla, 2010). Similarly, the mechanical properties of this optimized metal matrix composite match with the properties of ELEKTRON EQ21 Magnesium alloy, which is used in different application areas such as aerospace, automotive and military applications. This material (ELEKTRON EQ21) has a compressive yield strength of 165 - 200 MPa, while the optimized MMHC has a compressive yield strength of 170±2.6MPa, which can suitably be used in the same application areas based on Material Catalogue Index (MatWeb, 2024).

1.5 Statement of the Problem

Aluminum based metal-matrix composites (MMCs) are increasingly being used in various engineering applications, such as in aerospace and automotive industries because of their high strength to weight ratio, low coefficient of thermal expansion, excellent corrosion and wear resistance. Apparently, Magnesium alloyed with Aluminum is one of the materials whose strength to weight ratio is much higher than Aluminum. Up to the present time, the stir casting process and powder metallurgy dominantly used for metal matrix composites production but as far as the economy and the tool life of the processes are concerned, these processes have lots of drawbacks such as material wastage, extended processing steps, shrinkage and porosity. Consequently, it is imperative to implement a manufacturing process which could tackle the drawbacks obtained in dominantly used MMCs processing techniques. Therefore, friction stir consolidation process has a capability to stand in a certain position to overcome and reduce the drawbacks recognized in the pre-existing MMC processing techniques. The present thesis aimed at attaining the needs of automobile and aerospace industries in the form of low weight and high strength material, fabricated via highly economical and efficient manufacturing process. Furthermore, exploration of the FSC process for MMCs fabrication were carried out through in-depth numerical simulations, optimization of the key parameters, and experimental validation of numerical findings, as previous researches have focused solely on producing MMC on the surface of the matrix metal. Ultimately, in this processing technology, wastages and processing steps were expected to be reduced with an enhancement of porosity and other desirable properties of developed material leading to its applications in various fields.

1.6 Objectives of the Research

1.6.1 General Objective

The general objective of this research is to investigate the Physical, mechanical and tribological behavior of metal matrix hybrid composite fabricated via friction stir consolidation process; through an integrated DEM simulation with optimization and validation**.**

1.6.2 Specific Objectives

The specific objectives of this research include:

- ➢ To analyze the particle size distribution of reinforcement and matrix powders, and numerically consolidate them using the Discrete Element Method (DEM) with a Box-Behnken Design (BBD) framework to optimize and develop a mathematical model.
- ➢ To validate the developed RSM-BBD model using an Artificial Neural Network (ANN) and optimizing the FSC process parameters using a Genetic Algorithm (GA), followed by experimental validation of the optimized parameters.
- ➢ To determine the porosity, compressive strength and hardness properties of optimized sample.
- ➢ To investigate the wear rate and thermal stability behavior of an optimized sample through a combined RSM-BBD and GA optimization approach followed by analysis of wear mechanism of the worn-out surface.

1.7 Significance of the Study

The overall significance of this research is to simplify the existing processing methods of metal matrix composites. The overall significance of this research is to simplify the existing fabrication methods of metal matrix composites. As previous researchers focused on the fabrication of surface composite on the matrix metal, the novelty of this investigation lies fabrication of the entire structure of MMHCs through FSC process. The following points are some of the significance of FSC process.

1. Enhanced Processing Efficiency: The use of Friction Stir Consolidation (FSC) offers a significant advantage over traditional processes like powder metallurgy and stir casting by eliminating the need for sintering and melting. This results in considerably reduced processing time, contributing to increased manufacturing efficiency. The absence of time-consuming steps such as sintering translates into quicker production cycles, providing a competitive edge in industries where time-to-market is critical.

2. Ideal for Magnesium-Based Metals: FSC appears as a superior choice, especially when dealing with magnesium-based metals. Unlike conventional methods that involve high-temperature melting and sintering, FSC avoids these processes. Magnesium tends to burst at high temperatures during melting and sintering, making FSC a safer alternative. The ability to consolidate magnesium-based metals without subjecting them to the risks associated with melting and sintering underscores FSC's significance in ensuring both material integrity and workplace safety.

3. High Material Recovery Rate: FSC stands out in terms of sustainability, offering a high material recovery rate compared to powder metallurgy and stir casting. As 38% of material is unrecoverable when material melting takes place (Samuel, 2003). Since there is no melting involved, hence there is minimal material loss during the consolidation process. This not only contributes to cost-effectiveness but aligns with environmentally friendly manufacturing practices. The high material recovery rate also positions FSC as an eco-friendly alternative, reducing the overall environmental impact of material processing.

4. Versatility in Application Areas: FSC's significance extends beyond its efficiency gains. Its unique characteristics make it applicable in diverse fields, from aerospace to automotive industries. The absence of melting not only preserves material properties but also broadens its use in applications where maintaining the original characteristics of the material is crucial. This versatility positions FSC as an easy method for industries requiring precision and reliability.

5. Potential for Advanced Material Combinations: FSC opens doors for the consolidation of materials that might face challenges in traditional processes. Its unique attributes allow for the joining of dissimilar materials without the need for melting. This becomes particularly significant in industries seeking advanced material combinations for enhanced performance. FSC's contribution lies in enabling the creation of novel materials and composites, paving the way for innovations in areas such as lightweight structures and advanced engineering materials.

6. The research explores the FSC process as a method to improve material consolidation and processing efficiency compared to traditional methods. Additionally, the research investigates the viability of using FSC for Magnesium-based Metal Matrix Hybrid Composites (MMHCs), demonstrating its effectiveness for these materials.

1.8 Scope of the Research

The scope of this dissertation was restricted or limited to the geometric design of dies, conducting computational experiments using the Discrete Element Method (DEM) simulation based on the Response Surface Method (RSM) derived from the Box-Behnken Design (BBD) experiment matrix. The progression of the FSC process was examined by considering the impacts of input parameters, including applied load, thickness, reinforcement composition, consolidation time, and die rotational speed, on porosity response. The validation of the RSM-BBD model was carried out using Artificial Neural Network (ANN). Additionally, this dissertation expanded its scope to include Genetic Algorithm (GA) optimization for enhanced accuracy. The GA-optimized samples were experimentally fabricated for mechanical properties testing (Hardness and Compressive strength) and physical properties (porosity). Furthermore, various characterizations were implemented, such as phase analysis using XRD, thermal stability through Thermogravimetric Analysis (TGA), Fractography of compressed samples, and wear morphology through Scanning Electron Microscope (SEM). Additionally, tribological behavior was investigated using the Pin-On-Disc apparatus.

1.9 Organization of the Dissertation

This dissertation has incorporated five main chapters despite appendices and reference sections. Appendices section incorporated machines used in the study and die drawings. The references cited from chapter one to chapter four provided in reference section. The composition of the five main chapters listed as:

Chapter One: Introduction: In the opening chapter, the dissertation begins by providing a comprehensive background on metal matrix materials, outlining their significance in the field.

Following this, the introduction delves into the principles of the Friction Stir Consolidation (FSC) process, exploring its working mechanisms. The chapter then presents the research objectives, outlining the specific aims of the study. The significance of the research is highlighted, emphasizing the potential contributions to the understanding and improvement of metal matrix composites. Furthermore, the chapter identifies and articulates the statement of problems, setting the stage for the subsequent chapters.

Chapter Two: Literature Review: This chapter undertakes a thorough exploration of key aspects related to the research. Subtopics include the identification of process parameters in friction stir consolidation, addressing gaps in existing bulk metal matrix composite fabrication techniques such as powder metallurgy and stir casting routes. Additionally, the chapter examines optimization techniques, focusing on Artificial Neural Networks (ANN), Genetic Algorithms (GA), and Response Surface Methodology (RSM). The literature review concludes with a research summary, synthesizing the key findings, and highlighting the existing gaps that the current study seeks to address.

Chapter Three: Methods and materials; a thorough explanation of the research's methodology is provided in this section. It explores the use of DEM simulation and clarifies the challenges that come with implementing it into practice. The optimization approaches, encompassing RSM, ANN, and GA, are expounded upon within this segment. Furthermore, the chapter outlines the testing and characterization procedures employed for the optimized samples, aiming to provide a thorough comprehension of the experimental methodologies.

Chapter Four: Results and Discussion: Building on the established methodologies, Chapter Four presents the results of preliminary studies. This encompasses the identification of process parameter levels, examination of particle size distribution, and DEM simulation for porosity response. The chapter delves into the optimization through RSM based on obtained porosity results, subsequent model validation through ANN, further optimization through GA, and the comprehensive characterization of the optimized samples. The detailed analysis includes Fractography, wear morphology, XRD analysis, Thermogravimetry, hardness properties, compressive strength properties, and the wear rate behavior. A significant portion of this chapter is dedicated to a thorough comparison of FSC with powder metallurgy and stir casting techniques.

Chapter Five: Conclusion and Recommendations: The final chapter synthesizes the findings, drawing conclusions based on the results obtained. The effects of each process parameter are summarized, and the implications of the research are discussed. Recommendations for future research avenues are provided, offering insights for researchers to build upon the current study. The chapter serves as a comprehensive conclusion, bringing the dissertation to a logical endpoint.

CHAPTER TWO

LITERATURE REVIEW

2.1 Processing Techniques of Metal Matrix Composites

There are several techniques to fabricate MMC materials, but stir casting and powder metallurgy processes are the most common ways to fabricate MMC. However, these processing techniques have a number of drawbacks. For instance, a study identified the three main problems with the stir casting process: inadequate wetting, uneven reinforcement distribution throughout the melted matrix, and reinforcement agglomeration (Annigeri & Veeresh, 2017). Additionally, the drawbacks of the stir casting method include local solidification, gas entrapment, and reinforcing particle breakage (Shivalingaiah et al., 2022). Furthermore, during the research study of Al-SiC metal matrix composite, researchers discovered that the high temperature during stir casting produced very brittle aluminum carbide, which has an impact on the final mechanical property (Lai & Chung, 1996).

The processing technique has a significant impact on the final characteristics of MMCs. Magnesium is a brittle metal with a hexagonal closed packed structure. Unlike aluminum, it is challenging to plasticize. Consequently, there is a limited processing window to produce effective magnesium based composite (Asadi et al., 2010). Hence, it is challenging to fabricate magnesium matrix composites via liquid metallurgical techniques, FSP is an appropriate method for producing such composites (Sunil et al., 2016). Fabrication techniques of a metal matrix composite generally classified into three broad categories as shown in Figure 2.1 (A. Kumar et al., 2020).

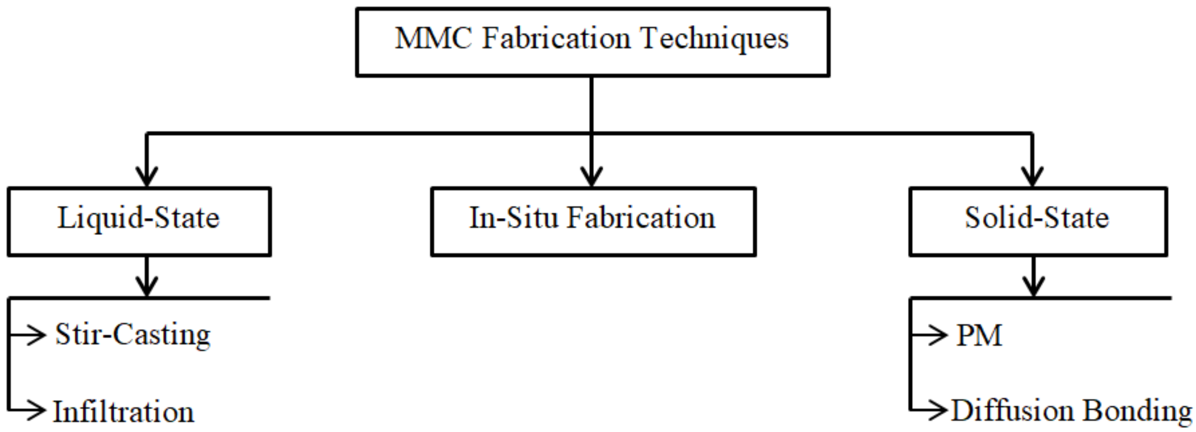

Figure 2.1 Classification of Fabrication Techniques of MMC

2.1.1 Overview of Stir Casting Process

Several researchers defined the stir casting process as liquid state process, where metal matrixes are melted at a melting temperature of base metal before the inclusion of reinforcing phases; researchers kept investigating the process parameters of stir casting route for enhanced property. Optimizing blade geometry, stirring speed and impeller position based on fluid vortex height and reinforced particle settling time is a crucial step in the stir casting process for the creation of metal matrix composites (Mariappan et al., 2020). The emphasis on process parameters shows that, how crucial it was for achieving a uniform distribution of reinforcing particles and preventing defects like porosity and agglomeration. The study of Rajmohan & Palanikumar, (2013), employed response surface methodology and Central Composite Design (CCD). In order to model, optimize, and analyze the effects of dominant machining parameters on thrust force, surface roughness, and burr height during the drilling of hybrid metal matrix composites made via stir casting. Their result depicted that, the measured and predicted values agree and well suggested that the proposed models were useful tool for predicting drilling responses in hybrid metal matrix composites fabricated through stir casting route. Weldability, joint macrostructure, mechanical characteristics, fracture mechanism, and tool wear are some of the difficulties encountered during friction stir welding of Aluminum matrix composites (Mir et al., 2022). The continuing investigation of stir casting process witnessed that the existence of unfilled gap in stir casting process.

Ozben et al., (2008) investigated an important aspect in the formation of a brittle structure is the dendritic air gap, which is created as a result of slow cooling. Particle segregation due to density, surface tension, and temperature gradient, excessive chemical reactions and wettability problems are not present in powder metallurgy as they occur with stir casting techniques (Sankhla et al., 2022). These problems could be minimized and overcome by employing proper and uniform mixture of reinforcement with matrix materials. This underscores that one of the main challenges of stir casting technique is uniform mixture of reinforcing particles and reinforcement segregation is a major disadvantage of the stir casting process since it is difficult to prevent. The powder metallurgy method does not have this problem. One of the key benefits of the powder metallurgy process over stir casting process is that, it is relatively easier to retain the reinforcement material without any phase change or chemical reaction. It also allows for reasonable control over the processing variables and the solid-state mixing of the reinforcement and matrix material (Sankhla et al., 2022).

2.1.2 Overview of Powder Metallurgy

In the powder metallurgy process, powdered metal or metal alloy is mixed with reinforcing particles or whiskers and pressed into the required shape using a die and punch at room temperature. Following compaction, a procedure known as sintering is carried out using heating. Using the ball milling process, a uniform mixture of powders is first produced in the powder metallurgy process. The mixed powder is then introduced into a chamber die and strike under load to transform it into a solid or green compact. The green compact part will then be heated to a certain elevated temperature and is called sintering operation. The fusing of powder particles with one another occurs during the sintering process without involving melting. The production of MMCs of copper matrix alloys and aluminum alloys (Kaczmar & Kainer, 1992; Han & Chan, 1996) are common application of powder metallurgy. The Figure 2.2 shows the general procedure of powder metallurgy processing technique (Kumar et al., 2020).

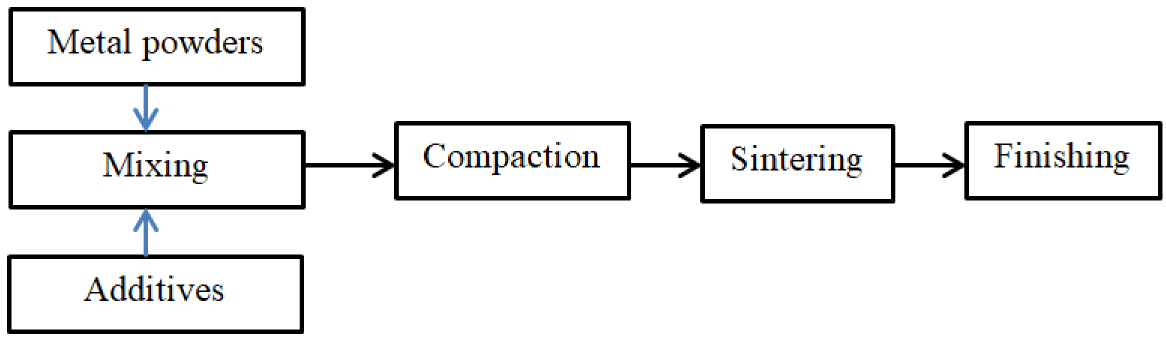

Figure 2.2 Powder Metallurgy Processing Technique

Zhang & Tan, (1997) stated that the approaches used in PM's powder mixing and blending steps provide its greatest benefit; however, when mixing fine powders, aggregation and clustering continue to be problematic. Furthermore, the biggest advantage of powder metallurgy was its capacity to produce materials based on both metals and non-metals.

Even if there are numerous advantages of powder metallurgy process, there are also different types of disadvantages. For instance, Zhang & Tan, (1997) stated one of the disadvantage existed in PM is the size limitation of a part that could be produced. i.e. large sized components could not be produced through this process. Additionally, when there is variation in powder sizes of matrix and reinforcement, the probability of getting good distribution is difficult to achieve. Similarly, as another advantage of PM is that parts could be manufactured to their final shape and geometry. However, if parts contain thread and slots it would be very difficult to machine the hard and porous part produced by PM (Behera et al., 2019).

2.2 Historical Development of FSP in MMCs

The development of Friction Stir Processing (FSP) is considered as a practicable solid-state technique to efficiently fabricate surface MMCs. Friction Stir Welding (FSW), a state-of-the-art solid-state welding technique developed at The Welding Institute in 1991, served as the inspiration for FSP. Fabrication of MMCs using FSP, researchers published their initial article in 2003 (Mishra et al., 2003). The matrix material is often prepared as plate, which can be either extruded or rolled. To accommodate the reinforcing particles, a groove is machined into the top of the plate. The volume percentage and needed processing depth are taken into consideration while determining the groove's size. The groove can be cut using a milling machine or a wire electric discharge machine. Then, the particles are manually packed into the groove or pre-

pressed powders can be used (Lee et al., 2006). During processing, particles can escape through the groove's top opening. Processing can be done first with a pin-less tool to prevent this. The tool consists of two parts, a shoulder and a pin, and is not consumed. The material becomes plasticized as a result of the frictional heat produced by the tool's shoulder rubbing and the pin's shearing action. The tool's stirring motion blends the packed particles with the plasticized material to form the metal matrix composite. Generally, in friction stir processing, the metal matrix composite is fabricated totally at its solid state (Arora et al., 2012; Bajakke et al., 2019; Ma, 2008; Sharma et al., 2015; Rathee et al., 2018).

It is critical to comprehend how different processing parameters affect the behavior and distribution of reinforcement particles in the stir zone. According to several research investigations, machine variables such tool rotation speed, traverse speed, material melting point, thickness of the material, and number of passes significantly affect dispersion, microhardness, and wear characteristics (Sathiskumar et al., 2014). Tensile strength and hardness improved up to a certain point while tool rotational speed and axial load rose in the process when researchers used underwater Friction Stir Welding (FSW) for increasing the quality of the weldment while implementing a range of welding temperatures. However, when the maximum point was reached, these qualities became less prominent. (Liu et al., 2010; Muthu et al., 2018).

2.2.1 Magnesium alloys under Friction Stir Processing in MMCs

Surface metal matrix composites based on magnesium were effectively produced via friction stir processing, and these materials have potential use in the power, automotive, aerospace, and biomedical industries (Sunil et al., 2016). Moreover, another study investigated defect-free AZ31 magnesium matrix composites with improved corrosion resistance and tribological behavior are produced by friction stir processing; Al-SiC particles exhibit the highest potential for self-corrosion, while Al-Si particles exhibit the lowest current for self-corrosion (Liu et al., 2021). This indicates that, the improvement in corrosion resistance and tribological behavior is noteworthy, as these are crucial properties for many engineering applications. Utilizing friction stir processing, fly ash-reinforced metal matrix composites based on Copper, Magnesium, and Aluminum were investigated by Dinaharan & Akinlabi, (2018). The produced composite exhibited encouraging outcomes in terms of lower manufacturing costs and improved microhardness.

2.2.2 Advantages and Challenges of FSP in MMCs

Casting defects can efficiently be reduced using FSP; hence, FSP could be used as post casting method to eliminate the casting defects (Sun & Apelian, 2011). This depicts that the superiority of FSP over stir casting process in eliminating defects. For instance, research studied on the possibility of using the FSP technique to create a silicon carbide (SiC) reinforced surface composite layer on Aluminum (Al) 5083 alloy was conducted during the past decade and found positive results (Mishra et al., 2003).

Avettand-Fènoël & Simar, (2016), raised some of the challenges associated with FSP; as metal matrix composites involve number of difficulties especially for FSW, including microstructure, tool wear even if it possesses the capacity for more or extended time applications, friction stir weld characteristics, and reinforcing behavior during joining. Additionally, Prater et al., (2013), also added the main challenge to friction stir welding (which works based on frictional heat generation) of metal-matrix composites is the welding tool pin severe wear caused on by extended contact with the tougher reinforcements.

2.2.3 Die and Tool Materials in FSP

The FSP tool's two main purposes are to heat the workpiece and to deform the material of the workpiece (Sharma et al., 2015). This dictates that the die material should withstand the stress occurred at stir zone during the FSP techniques at higher temperatures. The FSP tool and dies should have high hot toughness property. In addition FSP tool desired to have the ability to fabricate surface composites in any variation with little to no interfacial reactivity to the reinforcement and matrix (Sharma et al., 2015). Puviyarasan & Senthil Kumar, (2015), used a hardened H13 tool to fabricate AA6061/B_4C metal matrix composite through FSC process and their result depicted that H13 tool successfully withstood the process. A defect free microstructure resulted in 112HV and 192MPa of tensile strength were obtained during investigation of shoulder diameter to pin diameter effect on the fabrication of LM25AA-5%SiC particles through friction stir processing by using HSS (High Speed Steel) (Vijayavel et al., 2014). This showed that the inevitable property of HSS during FSP process.

Dolatkhah et al., (2012), studied the process parametric effects on the mechanical property and microstructural characteristics of Al5052/SiC metal matrix composite fabricated through FSP. Their result witnessed that an ultrafine grained microstructure with an average grain size of 0.9 micrometer replaced and obtained the original microstructure, which had an average grain length of 243 micrometer, thanks to FSP. During their experimental investigation they have used H13, the tool was heat treated and hardened to 52 HRC. This showed that a die or tool material which had 52HRC could handle the FSP process in metal matric composite fabrications. Moreover, Lone et al., (2022), used pin-less High-Speed Steel (HSS) tool during experimental investigation of tool offset effects on the Mg-NiTi produced through FSP process. Tang et al., (2013), investigated AISI D2 tool material's wear property under different pre-conditions i.e. having 51-65 HRC. This witnesses that AISI D2 tool material has HRC value that can handle the FSP process. For instance, (Sharma et al., 2015) and Dolatkhah et al., (2012) emphasize the necessity for high hot toughness and hardness, but do not address the potential limitations such as increased tool wear or cost implications of using materials like H13 and HSS. Additionally, the review does not compare the long-term performance and durability of various tool materials in diverse operational conditions.

2.2.4 Process Parameters of Friction Stir Processing

The mechanical properties of a composite materials processed through FSP can easily be controlled by varying the process parameters (Ma, 2008; Węglowski, 2018). The general name FSP includes methods such as friction stir welding, friction stir extrusion, Friction Stir Scribe (FSS), friction surfacing and Friction Stir Riveting (FSR). Zykova et al., (2020), investigated and explored the most commonly process parameters in FSP. These process parameters are tool rotation speed, force applied on the upper die, friction time (duration). The amount of heat generated during FSP technique could range from 0.6 to 0.9 times the melting temperature of the base materials (Padhy et al., 2018). Amancio-Filho et al., (2011) listed out the process parameters of FSR process as tool rotational speed, time, pressure, frictional torque, temperature and burn-off temperature. The FSW process parameters were found to influence the final property of the weld quality according to researchers; these process parameters are tool tilt angle, traverse speed, rotational speed of the tool and plunge depth (Zykova et al., 2020). In addition to this, Zykova et al., (2020), studied the influencing factors of Friction Stir Scribe (FSS) process. These PPs were plunge depth, tilt angle, traverse speed and rotational speed of the tool. There are three main categories into which the friction stir extrusion process parameters classified; (a) tooling related parameters: linear velocity; (b) parameters associated with the machine: plunge force or depth, spindle speed, axial force rate, extrusion speed etc. and (c) die related parameters: die material, texture of die and tool, size of the die etc. A cause-and-effect diagram is used and investigated to represent the influencing process parameters of the FSP (Sathiskumar et al., 2014).

Additionally, these factors affecting FSP process were strongly supported by (Sharma et al., 2015). As they stated the process variables of FSP to be machine related, tool related and material related. Maurya et al., (2020), listed the process parameters of FSC process as shown in the Figure 2.3.

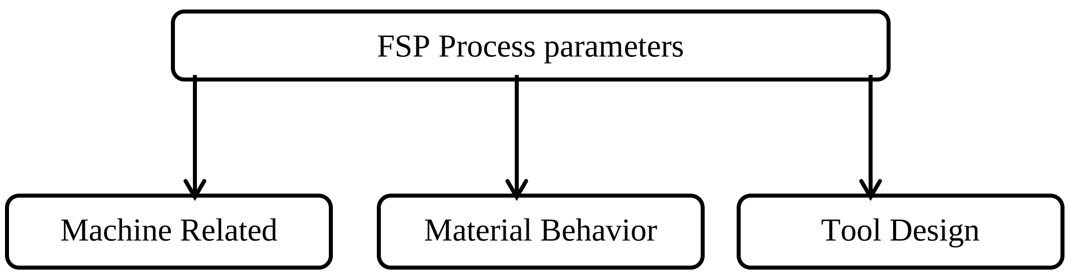

Figure 2.3 Process Parameters of Friction Stir Processing

Maurya et al., (2020), listed machine related process parameters as tool speed, tool traverse speed and tool tilt angle. In addition to this, the material behavior includes aspects such as mechanical and thermal property. Moreover, they listed tool design aspects such as shoulder diameter and profile and probe height profile and diameter could influence the FSP processes.

2.3 Levels Considered in Magnesium Alloys under Friction Stir Processing

The appealing characteristics of magnesium and its alloys continue to be favored by various researchers, mainly due to their high strength-to-weight ratio, reduced weight, and electromagnetic shielding properties. However, employing magnesium and its alloys as a metal matrix presents challenges, particularly in terms of formability, especially at room temperature. Enhancing magnesium's ductility is crucial, and grain refining and texture weakening are considered effective methods for achieving this goal. Friction Stir Processing (FSP) is a technique that can be employed to alter the microstructure of the alloy, significantly improving its ductility without compromising its tensile strength (Peng et al., 2019; Wang et al., 2017; Shang et al., 2019). Dinaharan et al., (2022), used the following parametric levels shown in Table 2.1 to produce AZ31 reinforced with Ti-6AL-4V particles MMCs through friction stir processing. The result showed that the mixture of the Ti-6Al-4V particles was obtained and maintained from of any undesirable chemical reactions or degradation with magnesium and its alloying elements.

Table 2.1 Friction Stir Processing Parametric Condition

S.No.	Process Parameters	Values
1	Tool Rotational speed (rpm)	950
2	Tool Traverse speed (mm/min)	30
3	Passes (Number)	5
4	Tool’s Shoulder diameter (mm)	24
5	Tool’s Shoulder concavity (mm)	0.2
6	Pin diameter (mm)	7-5
7	Pin length (mm)	5.7
8	Pin shape	Frustrum of core
9	Tool material	H13 Steel
10	Tool tilt angle (°)	1
11	Groove width (mm)	0, 0.4, 0.8 and 1.2
12	Groove depth (mm)	5
13	Ti-6Al-4V content (Vol. %)	0, 7, 14 and 24

Kalashnikov et al., (2017) have used Al-Cu-Mg with an average grain size of 137micrometer to process through FSP by employing tool rotation speed of 450 rpm with a single number of pass. Results depicted that FSP showed an improvement of hardness value of 15% and UTS of 9% improvement. Similarly, Shang et al., (2019) have used AZ31 magnesium alloy to process through FSP under the variables of tool rotational rate and traverse speed of 200rpm and 50mm/min respectively. Their finding depicted that there was an improvement of 4% and 9.5% in UTS and percentage elongation respectively. Another investigation by Peng et al., (2019) witnessed an improvement of 22.2%, two times and 1.5% in hardness, UTS and percentage elongation respectively by using tool rotational speed of 400rpm and traverse speed of

50mm/min.. Babu et al., (2018) investigated the impact of tool rotational speed and traverse speed on the hardness property of AZ31 under FSP process as shown in Table 2.2.

Table 2.2 Improvements in FSP of AZ31

Process Parameters	Levels					
Tool Rotational Speed (rpm)	600	600	600	800	800	800
Traverse speed (mm/min.)	20	30	40	20	30	40
Improvement in Hardness (%)	17.8	24.3	38	44.6	48.7	53.7

The table generally witnessed that the impacts of tool rotational speed in hardness property of the sample increases as the tool rotational speed increases. Shahraki et al., (2013), noted that at both high and low traversal speeds, there was a dispersion imbalance of ZrO_2 nanoparticles in the stir zone of the AA5083 alloy. Similarly, the impact of tool rotation was investigated by Salehi et al., (2012), that the variables influencing the Ultimate Tensile Strength (UTS) of the AA6061/SiC Nano-composites made by FSP using the Taguchi design approach. With a 43.70% contribution, rotating speed was found to be the most significant process parameter. Transverse speed came in third, pin profile at 11.22%, tool penetration depth at 4.21%, and transverse speed at 33.79%.

2.4 Materials Used in Friction Stir Consolidation of Metal Matrix Composites

In employing FSP technique, mostly non-ferrous metal such as Magnesium, Aluminum and Copper have been used generally by several researchers. Similarly, in the development of surface composites reinforcement such as carbon nanostructures and micron or Nano size of SiC, Al_2O_3, B_4C, TiC, etc. are frequently used as reinforcement (Arora et al., 2012). The impact of micron and Nano sizes of SiC particles on the fabrication of SiC/AA5052 surface composites through FSP was examined (Dolatkhah et al., 2012). Their result depicted that, when compared to 5 micrometer size of SiC particles, they discovered that 50 nm size of SiC particles reduced grain size by more than twice as much. The average grain size was decreased to 0.9 micrometer by the incorporation of nanoparticles.

2.5 Computational Study on Metal Powder Processing

The Discrete Element Method (DEM) is an advanced numerical technique rooted in the discrete representation of material. Cundall Peter initially introduced the theoretical formulation of DEM and its application with spherical particles in 1971 (Rojek et al., 2015). DEM autonomously identifies contacts between existing and emerging pairs of discrete elements or particles, describing finite displacements and rotations of these elements. The particle interaction model within DEM can encompass various effects such as elasticity, friction, viscosity, damping, cohesion, and adhesion. Widely accepted, the discrete element approach has become a favored and practical tool for modeling discrete systems, particularly in geomechanics and powder metallurgy processes.

The modeling of powder behavior in metal matrices holds significant importance in materials science and engineering, especially in metal matrix compression applications. Understanding the intricate interactions among different particles is crucial for predicting the mechanical properties and overall performance of these composite materials. The Discrete Element Method (DEM) stands out as a robust numerical methodology that has gained prominence in this specific field of study, offering a unique perspective compared to more traditional approaches like the Finite Element Method. By treating individual particles as separate entities with different sizes, shapes, and interaction forces, the Discrete Element Method focuses on modelling the discrete behavior of individual particles. When used in powder modelling within metal matrix compression, DEM proves to be an effective instrument for capturing the complex interactions and particle properties of powders during deformation processes (Gethin et al., 2003).

The Discrete Element Method (DEM) is a recently developed numerical technique that is based on the discrete model of material. The DEM’s theoretical formulation and initial introduction to use the DEM formulation with spherical particles was first presented by Cundall Peter in 1971 (Rojek et al., 2015). The DEM method must automatically recognize the contact between existing and emerging pairs of discrete elements; describe finite displacements and rotations of discrete elements. The DEM’s particle interaction model can incorporate a variety of effects, including elasticity, friction, viscosity and damping; and cohesion and adhesion. The discrete element approach is now a widely accepted technique and a well-liked and practical tool for modelling discrete systems, particularly in geomechanics and powder metallurgy processes. On the other hand, a popular numerical method for modelling the behavior of continuous materials is the Finite Element Method. By assuming a uniform material distribution inside each element, it discretizes a domain into smaller ones (Remacle et al., 2012).

Gethin et al., (2003), described DEM as "When compared to experimental results, the discrete deformable element modelling approach produces encouraging results in simulating powder compaction and yield characteristics". On another study focused on effects of inter granular friction and grain structure on material behavior in uniaxial compression; experimental and DEM modelling was investigated. The result of the investigation depicted that in comparison to experimental investigations, the DEM accurately predicted bulk stiffness for a spherical assembly (Wiacek et al., 2012).

There are numbers of DEM simulation investigation where friction coefficient values calculated based on coulomb's law. The particle-particle and particle-wall friction formulas are reduced to Coulomb's law of friction in the majority of DEM simulations, which is expressed as $Fs = \mu N$, where μ is the coefficient of friction and N is the normal load (Horabik & Molenda, 2016). The important terms such as coefficient of restitution, coefficient of rolling friction and coefficient of static friction have to be taken care of during DEM simulation. Horabik & Molenda, (2016), added that rolling friction was incorporated to the contact model, which greatly increased the DEM's ability to precisely predict granular material behavior under different conditions. On another study about rolling friction it was noted "Instead of considering contact points, the resistance to rolling concept considers contact regions. Rolling resistance emerges as a force couple that hinders particle rotation and can be transferred between particles through the contact area." (Horabik & Molenda, 2016; Jiang et al., 2005). Additionally, another important note was that it is not possible to fully define complicated shapes using a commonly used simplified measure of shape, such as a set of three dimensions: length, width, and thickness (Boac et al., 2010). Therefore, this shows that as it is not possible to fully define particles with only their three-dimensional measure, other property such as density, poison's ratio, young's modulus and shear modulus needs to be added for the DEM simulation understanding.

2.6 Optimization Model Validation Techniques

Optimization techniques have been playing critical roles in analyzing the impact of process parameters on the intended responses. Compared to standalone methods, hybrid optimization techniques have been used in recent years, according to observations (Srinivasan et al., 2020). Optimization techniques often led researchers to refined and effective conclusions. For instance, the process of machining composite materials is difficult; additionally, finding a suitable combination of process parameters for this issue is more difficult unless effective optimization techniques employed. For example, Puviyarasan & Senthil Kumar, (2015), optimized the process parameters of FSP during the fabrication of AA6061 reinforced with B_4C; they successfully optimized and analyzed the impacts of process parameters effectively through Taguchi method. Periyasamy et al., (2013), used desirability approach for Al/SiCp MMCs, the optimal friction stir welding parameters are 88.9 mm/min welding speed, 9.6 kN axial force, and 1370 r/min tool rotation to yield 201 MPa notch tensile strength and 265 MPa ultimate tensile strength. This shows that how the optimization techniques led investigators to an effective conclusion. Beyond this, optimization techniques often led the study to be more flexible by developing a mathematical or regression model which would help the upcoming researcher not to start from the scratch.

The effects of FSW process parameters such as stirrer shape, rotational speed, and traverse speed on the mechanical properties of composite combinations of AA5083 and AA1050 were studied by SarsIlmaz & Çaydaş, (2009). Following this, high tensile strength and the hardness of the welded joints were obtained. To obtain the process parameter impacts, the entire factorial test setup was performed. The main impact design and investigation of Analysis of Variance (ANOVA) were used to identify the significant parameters and determine where each parameter has an optimal value. Each yield attribute was predicted using a linear regression analysis. With 0.82 R square values for the exploratory and expected qualities, and 0.93 for the hardness and UTS, respectively, the results were in favorable accord. This additionally implies how the optimization techniques effectively led researchers to minimized labor, time and material costs.

Simulation models can be optimized and validated faster with statistical approaches like Response Surface Methodology and regression analysis, yielding more comprehensive results (Kleijnen, 1995). ANN, ANN-GA, and RSM-GA are a few examples of hybrid statistical techniques that optimize Fused Deposition Modelling (FDM) process parameters and improve dimensional precision in FDM devices (Deswal et al., 2019). Their findings demonstrated that a variety of hybrid statistical techniques, including ANN, RSM-GA, and ANN-GA, are excellent methods for optimizing the parameters of the FDM process. In another study, Vickers microhardness of AA6061 friction stir welded plates was reliably predicted by the ANN approach, with mean absolute percentage errors not exceeding over 5.4% and 7.48%, (Dehabadi et al., 2016). While the literature highlights the effectiveness of hybrid statistical techniques such as ANN, RSM-GA, and ANN-GA in optimizing FDM process parameters, it lacks a detailed comparison of the computational costs and accuracy trade-offs among these methods. For instance, the above researchers (Dehabadi et al., 2016) and (Deswal et al., 2019) demonstrate the predictive capabilities of these models but do not critically evaluate their scalability or practical implementation in diverse industrial contexts. Additionally, the potential limitations and assumptions inherent in these models are not sufficiently addressed, which is crucial for understanding their applicability and robustness in real-world scenarios.

The microhardness of the stir zone and the parameters of friction stir processing are correlated using ANN modelling, and the results of experiments demonstrate good agreement between input and output response; specifically, microhardness was increased by friction stir processing of mild steel plates with Al_2O_3 Nano-powder; higher microhardness values were obtained by increasing passes and tool rotational speed (Ghasemi-Kahrizsangi et al., 2015). Moreover, The Levenberg Marquardt method with three neurons was the most effective solution found by the ANN model for friction stir welding, which produced predictions with a high degree of consistency (Sonmez et al., 2017). By simulating parameters using a well-trained Artificial Neural Network (ANN) model with the help of grey relational grade obtained from the GRA, the best tool and process parameters for friction stir welding were found (Wakchaure et al., 2018). This leads to a summary of how model validation techniques were effective. Response Surface Methodology (RSM) and multivariate quantifiable techniques including central composite design, three-level factorial, and Box-Behnken test designs can be used to improve the quality and productivity of friction stir processing (Chanakyan et al., 2020). Response Surface Methodology successfully implemented to optimize the parameters of the friction stir welding process, leading to improved joint properties in different Aluminum alloys (Elatharasan & Kumar, 2012).

2.6.1 Response Surface Methodology

Engineers frequently are interested in what the input process parameter values ought to be in order to get the best possible responses or optimum response. Under the process input parameters, the optimal value of a given function may be either a minimum or a maximum (Periyasamy et al., 2013). Response Surface Methodology (RSM) is a set of statistical and mathematical techniques that are helpful in the analysis of issues where the objective is to optimize the response and a number of independent variables affect a dependent variable or response.

Different researchers employed RSM technique to reach on refined and effective conclusions. The tensile strength of AA2219 Aluminum alloy joints was optimized in friction stir welding by using the RSM optimization technique, which developed a mathematical model and optimized process parameters (Babu et al., 2009). These investigators used four different process parameters such as tool profile (Straight Cylindrical pin profiled tool, threaded cylindrical pin profiled tool, Square pin profiled tool, Triangular pin profiled tool and Tapered cylindrical pin profiled tool), tool rotational speed (1400, 1500, 1600, 1700 and 1800 RPM), welding speed (0.25, 0.5, 0.75, 1.00 and 1.25 mm/sec) and axial force (8, 10, 12, 14 and 16 KN). Based on their experimental findings, it was discovered that the joints produced with a square pin profiled tool with a welding speed of 0.75 mm/s, an axial force of 12 KN, and a rotational speed of 1600 RPM had superior tensile characteristics than the other joints. Response surface methodology was utilized by Premnath et al., (2012), to optimize the milling process parameters and a minimum cutting force of 132.8 N and a surface roughness of 0.28 m were achieved, when milling hybrid metal matrix composites.

By optimizing process parameters through RSM-CCD optimization technique in friction stir processing allowed for the fabrication of the best predicted mechanical properties of 1050 aluminum alloy (Martin et al., 2018). This study incorporated four different process parameters to study their impact on the yield strength, ultimate tensile strength, % elongation and hardness properties. Rotation speed (500, 100, 1500, 2000 and 2500RPM), feed rate (58, 87, 116, 145 and 174 mm/min), number of passes (1, 2, 3, 4 and 5) and tool shape (conical, triangle, square, pentagon and hexagonal) had been considered. The findings of their study depicted that the optimized result found to be at 1500 RPM, 116 mm/min, 3 numbers of passes and square tool shape. Srinivasa Rao & Ramanaiah, (2018), experimentally approved that, Al-Mg-Mn-Sc-Zr alloy's maximum hardness; tensile strength, percentage elongation, impact strength, and bending strength could be achieved by optimizing the FSW process parameters using response surface methodology. Similarly, Zamani et al., (2021), experimentally validated the influence of traverse speed and rotational rate on the mechanical properties of friction stir welding of Al-SiC composite sheets with the help of the RSM optimization technique.

2.6.1.1 Response Surface Method Box-Behnken Design

Using the stir casting method, Rajeswari & Amirthagadeswaran, (2018)**,** created three distinct combinations of metal matrix composites with dimensions of 130 mm by 100 mm by 50 mm. These combinations were 90Al7075/5SiC/5Al2O3, 85Al7075/10SiC/5Al2O3, and 80Al7075/15SiC/5Al2O3. They have used RSM-BBD in integration with genetic algorithm optimization techniques. Through the use of analysis of variance, they evaluated the adequacy of the resulting mathematical models at 95% confidence interval; additionally, they underscore the parameters are more significant when the F value is higher and the p value is lower than 0.05. This implies the application of ANOVA to assess model adequacy at a 95% confidence interval adds a level of rigor to the study. This statistical validation ensures that the findings are reliable and that the models developed are statistically significant. Additionally, the use of advanced statistical and optimization techniques such as RSM-BBD and genetic algorithms shows a sophisticated approach to model and optimize the properties of MMCs.

2.6.1.2 Response Surface Method Central Composite Design

The RSM-CCD optimization technique ensures lowest thrust force, surface roughness, and burr height during the drilling of hybrid metal matrix composites (Al 356-aluminum alloy/SiC/mica) by efficiently predicting responses such as Roughness, thrust force and Burr height; when process variables such as Spindle speed (1000, 2000 and 3000RPM), Feed rate (50, 100 and 150 mm/min) and wt% of SiC (5, 10 and 15) considered. Their result depicted that global optimum result found to be at Speed (1855, 1517.64 and 1539.22RPM), Feed rate (50, 50 and 50mm/min) and wt% SiC (15, 12 and 10) during drilling of parts produced through stir casting route (Rajmohan & Palanikumar, 2013). In another study, the RSM-CCD optimization technique contributed in the prediction of the tensile strength and grain size of AA7075-T6 Aluminum alloy friction stir welded joints and well predicted the response as verified experimentally by (Rajakumar & Balasubramanian, 2012). The literature does not compare RSM-CCD with other optimization methods, such as Genetic Algorithms (GA) or Artificial Neural Networks (ANN). A comparative analysis could highlight the relative advantages and limitations of RSM-CCD, providing insights into when and why this technique should be preferred.

2.6.2 Artificial Neural Network

Artificial neural networks, often known as ANNs, are powerful simulation tools that are inspired by the real-world use of neural networks in living things (Karkalos et al., 2016). They consist of several components, representing biological neurons, and different weighted connections, representing synapses. Artificial neural networks are trained by exposure to input/output data samples, and in order for them to adapt to supplied data and develop predictive capabilities; numerical algorithms control the weights of their connections. The network design, activation functions, and training algorithms of neural network models are some of the factors that affect their efficiency. Three distinct algorithms such as the gradient descent method, the Broyden-Fletcher-Goldfarb-Shanno (BFGS) algorithm, and the Levenberg Marquardt algorithm are compared in order to determine how effective the training process was. The earliest and most used technique for minimizing the error function in multi-layer back propagation neural networks is the gradient descent approach (Karkalos et al., 2016). The Levenberg-Marquardt approach is popular as an ANN training procedure produces an approximate computation of the Hessian matrix which leads to quick convergence. While the literature highlights the advantages of the Levenberg-Marquardt algorithm, it lacks a thorough comparative analysis with other training algorithms under various conditions. Such comparisons would provide a clearer understanding of the contexts in which Levenberg-Marquardt is most beneficial.

2.6.3 Genetic Algorithm

Natural selection and natural genetics serve as the foundation for the intelligent process known as a Genetic Algorithm (GA) which finds the most effective solutions to search problems (Liu et al., 2020; Rong et al., 2015). The biologically inspired operations, such as selection, crossover or combination, and mutation, form the foundation of this algorithm. The accuracy of composite pressure vessels with metallic liners is increased by the adaptive response surface method combined with genetic algorithm (Vafaeesefat, 2011). In metal matrix composites the Taguchi method integrated with genetic algorithm optimization produces better outcomes when it comes to drilling parameter optimization as assessed by (Rao et al., 2021). Thiagarajan et al., (2012), assessed this optimization technique performance during large-scale production, they noted that genetic algorithms can improve material removal rate and dimensional accuracy for Al/SiC composites by optimizing grinding parameters; they additionally noted the estimation degree of

GA was incredible. GA's provide a powerful optimization framework capable of handling complex, multi-dimensional search spaces. Their ability to mimic natural selection processes allows for effective exploration and exploitation of solution spaces.

2.7 Properties of MMCs processed through FSC

Investigations on metal matrix composite have been conducted by different researchers and mechanical properties are one of set of properties that researchers used to determine the quality of the produced MMCs. For instance, As mentioned by Roebuck et al., (1989), mechanical properties of metal matrix composites such as tensile, compressive, bend, impact, fracture toughness, fatigue, and high temperature tests, could be used to assess their quality. The quality of advanced metal matrix composite materials can be assessed by examining their mechanical and physical characteristics (Christian & Campbell, 1973; Reddy et al., 2020). El-Sabbagh et al., (2012), added that enhanced mechanical property can increase product quality to the desired level. While the literature comprehensively lists mechanical properties as key indicators of metal matrix composite (MMC) quality, it lacks a critical evaluation of how these properties correlate with different manufacturing processes and material compositions. For example, Roebuck et al., (1989) and El-Sabbagh et al., (2012) emphasize mechanical properties but do not address the variability in these properties across different composite formulations or processing methods. Additionally, the literature fails to critically assess the limitations of these mechanical tests in predicting long-term performance and real-world applicability of MMCs. Therefore, future research should focus on linking specific manufacturing variables to mechanical properties and evaluating their practical implications.

2.7.1 Mechanical Behavior of Metal Matrix Composites under Friction Stir Processing

FSP is an advanced method for producing nanocomposites. It was possible to create nano-composites with secondary phases, fine grains, and evenly dispersed reinforcements. Metal Matrix Surface Composites (MMSCs) based on magnesium alloy AZ91-D were developed using the multi-pass FSP method. Using the grooving approach, multi-pass FSP was used to add the reinforcements, which were nano-WC–Co–Cr and Multi-Walled Carbon Nano-Tubes (MWCNTs) by Bhadouria et al., (2017). The findings of their result witnessed that, Micro-hardness was greatest in the 0.7- 1:1-CNT-WC case. On the other hand, pure WC-Co-Cr reinforced Nano-MMSC was found to have a higher micro-hardness than pure CNT-reinforced Nano-MMSCs (Metal Matrix Surface Composites).

Sun et al., (2012), studied the mechanical property of Magnesium reinforced with nano-SiCp through FSP; and found that, when SiC-Mg bulk composites are produced via friction stir processing, they exhibit a notable improvement in strength when compared to as-cast magnesium alloy. Furthermore, the composite's ultimate tensile strength was 312 MPa, compared to the magnesium alloy's 160 MPa as-casted. Another study approved the positive impact of FSP by stating that, in magnesium AZ91 alloy surface composites, FSP enhanced mechanical characteristics and corrosion resistance (Abbasi et al., 2015). In order to study the microstructural and mechanical properties of the AA6082/TiC composite, (Thangarasu et al., 2015) manufactured MMCs using the FSP process. By adding 24 vol. % of TiC particles, the maximum microhardness and UTS were discovered to be 149 HV and 222 MPa, respectively.

2.7.2 Tribological Behavior of Metal Matrix Composites under Friction Stir Processing

The study of lubrication, wear, and friction on interacting surfaces is known as tribology. Sagar & Handa, (2020) investigated that the hardness and tribological characteristics of magnesium-based AZ61A/TiC composites are improved by increasing tool rotational speed during friction stir processing, which qualifies them for use in military and bicycle pedals, among other applications. Specifically, improved hardness was obtained for the composite that was manufactured at 800 rpm, or 95 HV, which is far higher than, when compared to the 60 HV hardness of the AZ61A base metal. Furthermore, the specimen prepared at 800 rpm and 1200 rpm had a high hardness and uniform particle distribution, resulting in the worn surface appearance of being smooth with few shallow grooves. A research review paper by Parray et al., (2020), summarized that the friction stir processing, or FSP, is a potentially useful technique for the automotive and aerospace sectors because it can improve the micro-hardness, mechanical characteristics, and tribological functioning of magnesium-based surface composites. While the literature underscores the benefits of friction stir processing (FSP) in enhancing the hardness and tribological properties of magnesium-based composites, it lacks a critical evaluation of the variability in performance based on different processing parameters. For example, Sagar & Handa, (2020) highlight the improvements in hardness and surface characteristics at specific rotational speeds but do not explore the potential drawbacks or limitations of FSP, such as increased tool wear or energy consumption. Additionally, Parray et al., (2020) broadly endorse FSP for automotive and aerospace applications without addressing the long-term durability and cost-effectiveness of the process. Future research should focus on a comprehensive assessment of these factors to provide a balanced view of FSP's practical implications.

The effects of various compositions on the microstructure properties, corrosion resistance, tribological behavior, and reinforcement particles on phase compositions of the AZ31 Magnesium Matrix Composites (MMCs) were examined by Liu et al., (2021). Their result summarizes that a defect-free AZ31 magnesium matrix composites with improved corrosion resistance and tribological behavior are produced by friction stir processing. Sagar & Handa, (2020), reviewed different research findings; they summarized that magnesium-based metal matrix composites with outstanding characteristics are successfully produced using Friction Stir Processing (FSP) and are available for application in the automotive, aerospace, and biomedical industries. Additionally, their review paper investigated various studies which employed magnesium alloys under FSP process with different tool rational speeds. The following table 2.3 summarizes the findings of several studies of FSP process with the results of tribological characteristics.

Table 2.3 The Influence of FSP on Magnesium Alloy Based MMCs on their Tribological Characteristics

Composite	**Machine parameters**	**Wear test specifications**	**Findings**
AZ91/Al_2O_3/SiC	730-1800 rpm, 14-80 mm/min with 1-4 passes	Tri pin on disc, load 50 N, sliding speed 1 mm/s for 500 m	Wear rate decreases as number of pass increases AZ91/ AZ91/Al2O3 & AZ91/SiC gives almost same wear rate
AZ91/TiC	900 rpm, 40 mm/min with PD = 0.3 mm	Pin on disc, load 5-10 N, sliding speed 1 m/s for 2000 m	Wear rate of composite decreases half to the base metal

AZ31/TiC	800 rpm, 40 mm/min	Pin on disc, load 5–20 N, sliding speed 1 m/s for 1.5 km	At 20 N higher wear resistance was noticed
AZ31/ Al_2O_3	800, 1000, 1200 and 1400 rpm, 45 mm/min and 2° tilt angle	Pin on disc, load 10, 50 and 90 N, sliding velocity 0.12m/s for 600 m	Wear rate at 1000 and 1200 rpm is higher as compared to 800 rpm
AZ31/Fly ash	1200 rpm and 40mm/min	Pin on disc, load 20 N, sliding velocity 1.0 m/s for 3000 m	FSP exhibits 33% lower wear rate as compared to stir casted composite
AZ91/ Al_2O_3	900–1200 rpm, 40–80 mm/min with 3° tilt angle	Pin on disc, load 50 N, sliding velocity 1.0 mm/min for 500 m	Wear rate decreases more than three times to the base metal

Another study examined the impact of hard inclusions on the microstructural changes that occurred during the friction stir processing of an aluminum-magnesium alloy. The impact of microstructural changes on the mechanical characteristics was examined. Grain structure was improved by FSP from 50μm to approximately 10μm which led to improved wear resisting property (Khodabakhshi et al., 2015).

The mechanical and wear properties of A413/SiC and A413/SiC/MoS2 composites made by FSP were examined by Janbozorgi et al., (2017). The MoS2/SiC lubricant content decreased the A413/SiC/MoS2 composite's microhardness. This resulted from the MoS_2 lubricant's decreased hardness. The greatest hardness of the non-lubricated A413/SiC composite was 105 HV; MoS_2 lubricated the SiC particles, reducing wear loss. In another study by Abreu et al., (2017), used the FSP approach to create an AA2024/SiC composite in order to study its tribological properties. The AA2024/SiC composite's microhardness was increased to 145 HV by the SiC inclusion.

2.8 Literature Summary

In the context of friction stir processing using metal powders, this literature review examines and hovers focusing the integration of Discrete Element Simulation (DES) with validation and optimization methodologies. The reviewing structure of this section focused on the die materials used in FSP, Discrete Element Simulation conducted related to metallic powders especially under FSP, different optimization techniques which helped researcher conclude, and analyze process parameters effectively, model validation techniques and genetic algorithm approaches conducted in FSP process during metal matrix composite fabrication. Based on the reviewed literatures the following points could be raised.

- Various die materials, such as High-Speed Steel, H13 tool, and D2, with hardness value close to 50 HRC, were employed by several researchers for friction stir processing. Based on their results all those die or tool materials successfully handled the FSP.
- The need of using optimization techniques such as RSM-BBD-GA-ANN was underlined as a valuable means of examining the current status of the friction stir consolidation process in the production of metal matrix composites.
- Determining the effects of process parameters on the porosity of the generated sample may also be accomplished effectively by using discrete element method simulation for the FSC process. According to the review literature, Altair EDEM simulation software offers a decent degree of accuracy and would be useful.
- It was examined the FSP process parameters from a number of perspectives. Based on previous research and preliminary studies, the following levels and parameters were set in order to study the FSC process for the fabrication of MMCs: load at [400, 450, and 500N], time at [4, 5 and 6 minutes], thickness at [12, 16 and 20mm], composition of reinforcement at [5, 10 and 15%], and tool rotation speed at [200, 500, and 800 RPM].
- To the present time, the MMC's strength property is now inadequate and could be enhanced by adding more phases, for instance, previous study suggests that ZrO2 is important for increasing compressive strength. While, adding SiC can improve the tribological or specifically wear characteristics of the MMCs. Research into the AZ61/SiC/ZrO_2 material combination is required.

Wear morphology, XRD, SEM, TGA, and other characteristics are thought to define the quality of MMCs. Such characterizations were employed in earlier studies to determine the MMC quality developed by FSP.

2.9 Research Gaps and Limitations

In this literature review section different aspects were reviewed regarding metal matrix fabrication techniques, optimization techniques, numerical simulation of discrete elements and the current status and history of friction-based metal matrix processing. Based on the reviewed literatures, there are number of research gaps such as material recovery rate, time issue, process effectiveness, metal matrix composite materials property and characteristics found to be major challenges in metal matrix composite fabrication.

Analyzing and assessing the literatures an integration of DEM simulation, optimization technique and data validation have never been used, optimization techniques such as RSM-BBD, GA and a model validation technique ANN which could help in a systematic approach to validate models without going to experimental validation for all design matrix have never been used.

I. There is a gap in studying properties such as tribological, hardness and compressive strength of MMCs materials processed through FSC process, as previous researches focused solely on fabricating surface composite on the matrix metal (Sharma et al., 2015; Li et al., 2018).

II. There is a gap in mixing reinforcement of SiC and ZrO_2 with AZ61.

III. There is a gap in integration of optimization techniques which could lead researcher to an effective conclusion. Additionally, there are several studies conducted through RSM-CCD; however, there are few researchers conducted RSM-BBD.

CHAPTER THREE

MATERIALS AND METHODS

3.1 Introduction

The mechanical, metallurgical and tribological behavior of Metal Matrix Hybrid Composites (MMHCs) plays a crucial role in their application across various industries. The present dissertation focuses on investigating these properties for MMHCs fabricated through the FSC process. This section provides a detailed description of the materials and methods employed in the research, including the parametric optimization of FSC process, numerical simulations, and experimental characterization techniques. Moreover, to achieve an optimal set of process parameters for the fabrication of MMHCs, a comprehensive approach combining numerical simulations and experimental techniques were adopted.

The first step involved was parametric optimization through the use of Discrete Element Method (DEM) software. DEM simulations were employed based on RSM Box-Behnken design (46 experiments) to analyze the effects of different process variables such as; Speed (rpm), Load (N), Thickness (mm), Time (min.) and Composition (%wt) on the FSC process followed by identifying the parameter ranges that would result in desirable material properties for minimum porosity. Once the initial parametric optimization was performed using response surface methodology (RSM) Box-Behnken design, an Artificial Neural Network (ANN) was carried out to validate the model using MATLAB 2014a. The ANN model was trained using the data generated from the numerical simulations data. By comparing the predicted values from the ANN model with the actual experimental data of optimum sample, the accuracy and reliability of the optimized parameters were evaluated. After model was once validated, additional optimization process was conducted using a genetic algorithm by MATLAB 2014a, which efficiently explored the parameter space to further find the global optimal combination of parameters (Sreenivasan et al., 2019).

The optimized MMC samples were characterized using several analytical techniques to assess their microstructural, tribological, and thermal properties. X-ray Diffraction (XRD) analysis was employed to determine the crystallographic phases present in the MMHCs. Scanning Electron

Microscopy (SEM) was utilized to examine the microstructure and morphology (worn out and fractured surfaces) of the consolidated composites at various magnifications. Thermogravimetric characterization was performed to investigate the thermal stability and decomposition behavior of the MMCs under controlled heating conditions. In addition to the characterization techniques mentioned above, mechanical tests were also conducted to evaluate the performance of the optimized MMHCs. Hardness tests were performed to assess the resistance of the material to scratches and to determine its overall strength. Compressive strength tests were carried out to measure the load-bearing capacity and structural integrity of the MMHCs under compression load.

The combination of numerical simulations, parametric optimization, statistical analysis, ANN modeling, and experimental characterization techniques provides a comprehensive framework for understanding and optimizing the mechanical, metallurgical, and tribological behavior of MMHCs fabricated through the FSC process. The subsequent sections of this dissertation will explore the results and discussions derived from the implementation of these materials and methods section.

3.2 Materials

The investigation of this study incorporates materials such as SiC, ZrO_2 as reinforcement and AZ61magnesium alloy as a matrix. Likewise, the FSC process involves using a rotating tool material D2 to consolidate the SiC and ZrO_2 particles within the magnesium alloy matrix (AZ61). To evaluate the mechanical properties of the composites, hardness testing and Universal Testing Machine (UTM) were utilized. Hardness testing machine is employed to measure the resistance of the composite material to scratches and provides an indication of its strength. UTM, on the other hand, allows for a comprehensive assessment of mechanical properties such as compressive strength. Furthermore, the tribological behaviors of the composites were analyzed using a pin-on-disc wear test machine. This machine applies controlled sliding contact between the composites and a counter surface. The wear characteristics and wear rate of the composites were determined, providing insights into their performance under dry sliding contact. Table 3.3 represents the detail materials, machines and equipment used.

3.2.1 Die Materials

D2 tool steel is a popular choice for die-making due to its exceptional properties. D2 tool steel is known for its outstanding wear resistance; withstand the high-stress and abrasive conditions encountered in die-cutting and forming processes. Its high carbon and chromium content contribute to its hardness, making it suitable for extended use without significant wear. Additionally, D2 steel exhibits good dimensional stability under high heat zones. Its ability to maintain sharp edges and resist deformation under heavy loads makes it a preferred material for producing dies that demand durability. In general, the following factors led to the selection of D2 tool steel:

1. High Wear Resistance: D2 tool steel is known for its exceptional wear resistance, which is crucial in the friction stir consolidation process (Patel & Bhavsar, 2019). During the consolidation process, the die comes into contact with the metal powders being consolidated, which can lead to significant frictional forces and wear. By using D2 tool steel, which has high hardness and wear resistance, the die can withstand the abrasive wear encountered during the process, resulting in prolonged die life and improved process efficiency.

2. Good Thermal Conductivity: Friction stir consolidation involves generating significant heat due to the friction between the rotating tool and the workpiece. Effective heat dissipation is essential to prevent localized overheating and thermal deformation of the die. D2 tool steel offers good thermal conductivity, allowing for efficient heat transfer and minimizing the risk of thermal damage to the die (Ajay et al., 2018).

3. High Compressive Strength: D2 tool steel possesses high compressive strength, making it suitable for withstanding the compressive forces exerted during the consolidation process. The intense pressure applied to the material being consolidated requires a die material that can withstand these forces without deformation or failure. D2 tool steel's high compressive strength ensures the die's structural integrity, enabling it to maintain its shape and functionality throughout the process.

4. Excellent Dimensional Stability: Dimensional stability is crucial in the friction stir consolidation process to ensure accurate and consistent consolidation of the workpiece material (Patel & Bhavsar, 2019). D2 tool steel exhibits excellent dimensional stability,

minimizing any dimensional changes or deformation that may occur during the process. This characteristic ensures the die maintains its original shape, resulting in precise consolidation and improved product quality.

Considering the above reasons, selecting D2 tool steel as a die material for the friction stir consolidation process found to be worthy.

Table 3.1 Chemical Composition of AISI D2 Tool Material

Composition	C	Cr	Mo	V	Si	Mn	Fe
% Weight	1.55	11.3	0.8	0.8	0.3	0.4	Balance

Its high wear resistance, high compressive strength and excellent dimensional stability make it a suitable choice to ensure efficient and reliable consolidation of metal matrix composites in the study. The composition of D2 die material is presented in Table 3.1 (Bourithis et al., 2006; Tang et al., 2013).

3.2.2 Materials Used for Investigation

The following materials listed in Table 3.2 were used to assess the feasibility and effectiveness of FSC process for MMCs fabrication, understand the process's effects on the final product, and optimize it for minimum porosity. Different variety of reinforcement and matrix powder compositions were mixed to optimize and identify the optimum material composition for a superior product property. As this FSC process was noble investigation (initial investigation) for the fabrication of full metal matrix composite, the AZ61 matrix material, which possessed attractive malleability or excellent formability and less density characteristics, was selected for the evaluation of the status of the FSC process. Additionally, the lesser melting point made AZ61 a better candidate prior to Aluminum alloys and grain refinement of magnesium alloys could be achieved by severe plastic deformation (Luo et al., 2020). The remarkable mechanical properties of SiC, such as its high strength and stiffness, are well known. It can greatly improve the composite material's overall strength and stiffness when incorporated into a metal matrix (Subramani et al., 2022). In the same way, SiC is a lightweight material, making it a desirable option for applications where weight reduction is crucial. It makes it possible to create strong, lightweight components, which is very useful for the aerospace and automotive industries. It is also superior fatigue resistance, reduced thermal expansion, high thermal conductivity, and improved stability at high temperatures (Anggara et al., 2019). In addition to this Silicon carbide has excellent thermal stability and can withstand high temperatures without significant degradation.

Table 3.2 Materials Used for Investigation

S.No.	Materials	Type	Purpose
1	SiC	Reinforcement	Investigation
2	ZrO_2	Reinforcement	Investigation
3	AZ61	Matrix	Investigation

This property is valuable in applications that involve exposure to elevated temperatures or rapid temperature changes. The other attractive property of SiC is highly wear-resistant, making it suitable for applications where the composite will be exposed to abrasive conditions, such as in brake pads, clutch plates, or cutting tools.

Zirconium dioxide (ZrO_2) is one of the most researched ceramic elements, which is the crystalline oxide of zirconium, sometimes known as zirconia. Zirconia (ZrO_2) was used as the reinforcing particle due to its high temperature compatibility and ease of access (Juliyana et al., 2022). The findings in previous investigation demonstrated that the AZ31/ZrO_2 composite material achieves homogeneity, densification, and grain refinement after FSP in comparison to the base metal (Qiao et al., 2021). In the same way researchers investigated that as ZrO_2 additions rose in weight percentage, hardness and yield strength improved as well when added to Al-Zn-Mg alloy (Aziz & Bedien, 2020). Similarly zirconia material has a number of benefits that make it preferable in some aspects such as high strength and fracture toughness (Haja et al., 2022). These benefits include improved corrosion resistance, flexural strength, and fracture toughness that can inhibit crack growth and prevent catastrophic failure (Ben-Nissan et al., 2019). In this experimental investigation Zirconium dioxide (ZrO_2) was selected to impart the aforementioned characteristics to the magnesium alloy matrix composite.

3.2.3 Equipment and Machines Implemented

Friction Stir Consolidation (FSC) technique requires specialized machines and equipment, as well as precise characterizing techniques. The primary machine used was the conventional milling machine, which comprises of a spindle where the upper rotating die was assembled to generate friction and heat as it is plunged into the chamber where the powders being consolidated. A high-torque spindle and precise control system were essential components to maintain the required process parameters. The machines and equipment used in FSC process are tabulated in the Table 3.3. Mechanical properties testing such as hardness and compressive strength, tribological property are crucial for ensuring the quality of the consolidated composite material. These techniques help detect any defects and stance of the final product. Moreover, advanced material characterization methods like X-ray Diffraction (XRD) and scanning electron microscopy were used to examine the material's phases, as well as its fracture and worn-out surfaces.

Table 3.3 Machines used with their Corresponding Model and Purpose

S.No.	Machines	Model
1	Milling machine (PDS)	FU 281
2	Universal testing machine	WP 310 Materials Testing, 50kN
3	Furnace (heat treatment)	Fours Nagat Furnace44550 Montoir De Bretagne, France
4	Hardness testing machine	HVS-50 Hardness Tester
5	Wear testing (Pin-on-Disc)	DUCOM TR-20 Instrument (instruments Pvt. Ltd. Company in Peenya Industrial Area, Bangalore, India).
6	SEM (particle size and Fractography)	JCM/6000PLUS BENCH TOP SEM, Joel Japan
7	Diffractometer- XRD (Phase identification)	XRD7000 X-RAY DIFFRACTOMETER Maxima, shimadzu Corporation Japan)
8	Powder mixing machine	HIGH ENERGY BALL MIXER/MILL -RIST
9	Milling machine (Dies fabrication)	HARRISON M460

As detailing machines with their respective models is essential for the transparency, credibility, and replicability of research, each machines model are listed in the Table 3.3. To ensure that the tests or procedures described in a study can be duplicated or verified by other researchers for use in future research.

3.3 Methodologies

This section provides the methodologies of computational work, optimization techniques, data validation techniques, global optimization techniques, die design processes, fabrication processes for dies, specimen preparation techniques and finally specimen testing and characterization techniques.

3.3.1 Methodology for Computational Work

The initial step is ensuring that the idea or technique of FSC should be implemented directly in the simulation. In FSC, a rotating tool is used to mix metal powder and reinforcements with predetermined process parameters, forming a strong binding between them. Consequently, the same idea had to be created or simulated. The next step in the computational process was to determine the sizes of the powders that would be used in the experiment. Then, based on a thorough literature review, several parameters or properties of the powders and dies utilized in the simulation were determined. Therefore, the powders size in hand (as received powder) had to be analyzed so as to apply in the simulation. The Altair EDEM 2022.1 software was used to simulate the FSC process.

3.3.1.1 Particle Size Distribution

The as received particles and ball milled particles were observed through scanning electron microscope (SEM) Model: JCM/6000PLUS BENCH TOP SEM, Joel Japan. The main requirement of analyzing particle size distribution is that, the particle type and size affects both the composite and alter the efficiency of the manufacturing process especially when ceramic particulates are used as a reinforcements (Moradkhani & Baharvandi, 2018). Particle sizes have also influence on the coefficient of friction, strength and toughness of the composite materials (Katiyar et al., 2021). Therefore, as they have a considerable impact on the composite, it is crucial to analyze the particle size distribution in order to determine the processing method’s position. The sizes of the particles were determined using Image J software following the obtaining of the SEM image.

3.3.2 Methodology for Optimization and Data Analysis

In this dissertation RSM-Box-Behnken optimization and followed by artificial neural network model validation was implemented prior to genetic algorithm optimization approach. The decision not to study a full experimental design with all possible combinations of parameters and levels is often triggered by considerations such as resource constraints, efficiency and optimization goals and statistical analysis feasibility. Box-Behnken designs and genetic algorithms provide researchers with a more efficient and effective approach to experimental design and analysis, enabling them to provide relevant results.

3.3.2.1 Response Surface Methodology

The RSM Box-Behnken response surface methodology was selected for experimentation, optimization and data analysis. Response Surface Methodology (RSM) combines mathematics and statistics to model and analyze engineering challenges where the outcomes of interest were simultaneously influenced by a number of variables (Danish et al., 2017; Aslantas et al., 2020; Liu et al., 2020; Kumar Parida & Maity, 2019).

3.3.2.2 Box-Behnken Response Surface Design

Box-Behnken designs are used to create higher order response surfaces, requiring fewer runs than a traditional factorial method (Rao & Kumar, 2012). Considering the properties, interaction behaviors of matrix, reinforcement and die materials, the following numerical simulation set ups were run as conveyed in Table 3.4. The Box-Behnken experimental design of response surface methodology of five factors and three levels was generated by Minitab 2019 as depicted in Table 3.4. Full quadratic polynomial model which effectively illustrates the impact of a single factor and the interactions of factors on the responses was selected (Khajeh, 2009; Lahlali et al., 2008).

Table 3.4 Factors with their corresponding higher, lower and medium levels of Box-Behnken

Parameters	Units	Codes	Levels		
			Low	Medium	High
			-1	0	1
Composition	%wt	X_1	5	10	15
load	N	X_2	400	450	500
Speed	Rpm	X_3	200	500	800

Thickness	mm	X_4	12	16	20
Time	Min.	X_5	4	5	6

The levels of higher and lower values of every factor were set in Minitab 19 statistical software depending on literature and preliminary results. However, the medium levels were picked out by the software automatically. As indicated in Table 3.5; -1, 0 and 1 indicates the lower, Medium and higher-level values respectively. Finally, the effect of variation in those process parameters against porosity was analyzed through Altair EDEM 2022.1 software.

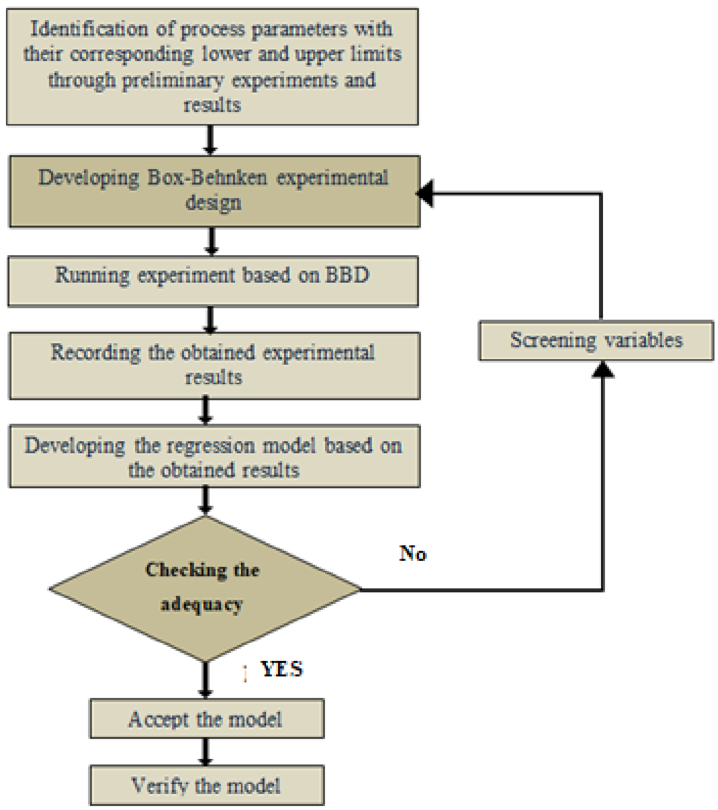

Figure 3. 1 RSM Box-Behnken design flow

Generally, procedures followed for BBD optimization which is presented in Fig. 3.1 was implemented to reach on the final conclusion (Palanikumar & Davim, 2013).

Table 3.5 RSM with Box-Behnken experimental design

	FACTORS				
Exp. No.	SPEED	LOAD	THICKNESS	TIME	COMPOSITION
1	0	1	0	1	0
2	0	-1	-1	0	0
3	1	0	0	0	-1
4	0	0	1	-1	0
5	0	0	0	-1	1
6	0	1	0	0	1
7	0	1	1	0	0
8	-1	0	0	-1	0
9	-1	-1	0	0	0
10	0	-1	0	0	1
11	0	0	0	1	1
12	0	-1	0	1	0
13	0	-1	0	0	-1
14	0	0	1	0	1
15	-1	0	0	0	-1
16	-1	0	1	0	0
17	0	0	1	1	0
18	0	-1	0	-1	0
19	0	0	-1	0	1
20	0	0	0	0	0
21	-1	0	0	0	1
22	0	0	0	0	0
23	0	0	0	1	-1
24	0	0	1	0	-1
25	0	0	0	-1	-1
26	1	0	0	0	1
27	0	-1	1	0	0
28	0	0	0	0	0
29	0	0	0	0	0
30	0	0	-1	-1	0
31	1	1	0	0	0
32	-1	0	0	1	0
33	-1	1	0	0	0
34	0	0	0	0	0

35	1	0	0	1	0
36	1	0	0	-1	0
37	-1	0	-1	0	0
38	0	0	-1	0	-1
39	1	-1	0	0	0
40	0	0	0	0	0
41	0	0	-1	1	0
42	0	1	0	-1	0
43	0	1	0	0	-1
44	1	0	-1	0	0
45	1	0	1	0	0
46	0	1	-1	0	0

Generally, 46 numbers of experimental combinations were determined by the RSM Box-Behnken approach for the five factors. After data analysis of RSM (Box-Behnken), ANN (Artificial Neural Network) was carried out to determine the correctness or the fitness of the model. Finally, Genetic Algorithm (GA) selected for the global optimum of the porosity.

3.3.2.3 Genetic Algorithm

The Genetic Algorithm (GA) is a method for solving both constrained and unconstrained objective functions. It is based on natural selection, the process that promotes the evolution. Furthermore, GA is an intelligent method for identifying the most suitable answers to search problems that is based on the principles of natural selection and genetics (Liu et al., 2020; Rong et al., 2015). The genetic algorithm repeatedly modifies a population of unique solutions. The genetic algorithm chooses parents at random from the current population at each stage in order to create the offspring for the upcoming generation. The population "evolves" toward the optimal solution over the course of upcoming generations. The algorithm starts with a population of candidate solutions and evolves them through selection, crossover and mutation, in a procedure similar to natural selection (Cardoso-jaime et al. 2022; Sheelwant et al., 2021; Cao et al., 2021; Panwar et al., 2020; Fan et al., 2017; Álvarez et al., 2009). At each stage, the genetic algorithm uses three main types of rules to create the next generation from the present population (Bahloul et al., 2014):

- *Selection rules* choose the individuals, called "parents," who will contribute to the population of next generation.
- *Crossover rules* combine two parents to produce the offspring of that generation.
- *Mutation rules* Random alterations are made to each parent to produce offspring.

MATLAB R2014a was used to run GA after RSM-Box-Behnken parametric optimization to achieve an even better result. To determine the best outcome, the regression equation was converted into a minimization problem in MATLAB R2014a. The upper and lower limitations were chosen based on the levels of each process parameter.

Table 3.6 Parameter function along with their values in GA for porosity optimization

Parameter Function	**Parameter Value**
population size	100
Population type	Double vector
Creation Function	Constraint dependent
Fitness Scaling Function	Rank
Selection Function	Roulette
Reproduction: Elite Count	Default (0.05* Population size) = 2.5
Reproduction: Crossover Fraction	Default: 0.8
Mutation Function	Uniform: Rate at 0.15
Crossover Function	Constraint Dependent
Number of Generations	300
Function Tolerance	1e-6
Constraint Tolerance	1e-6

A double vector population type was selected for the demography (Panwar et al., 2020). Creation function of constraint dependent was set. Crossover fraction was adjusted at 0.8 and uniform mutation was used with a mutation function at a rate of 0.15 as illustrated in Table 3.6. Moreover, roulette parent selection was preferred (Panwar et al., 2020).

A genetic algorithm was developed in MATLAB to verify the global and local minima of the Box-Behnken model. The accuracy of the optimization process was ensured by comparing the optimized results of GA with the Box-Behnken model. The basic flow chart followed in this study is tabulated Figure 3.2 (Panwar et al., 2020).

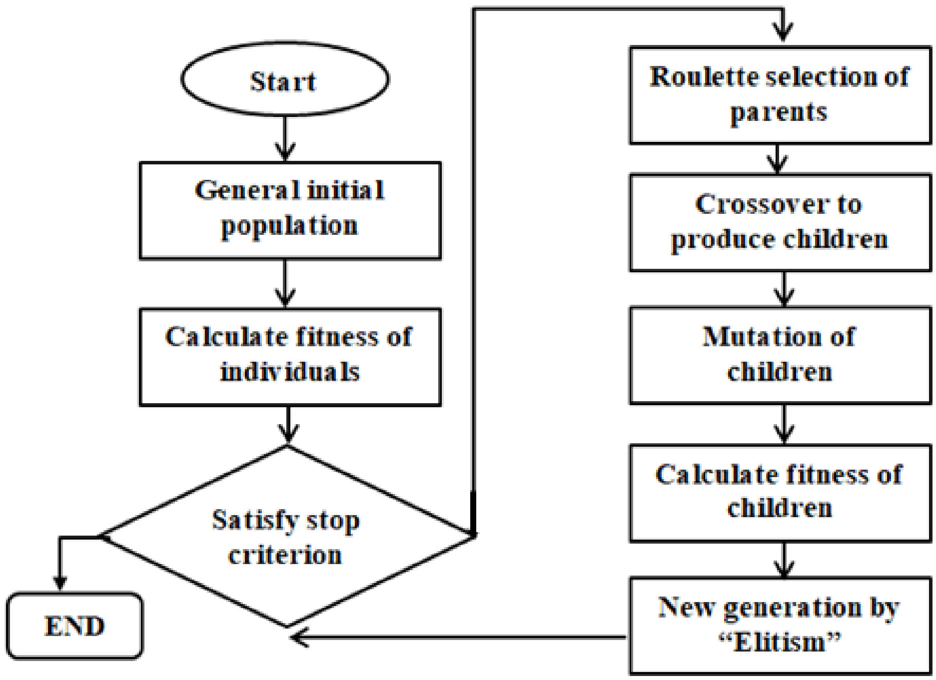

Figure 3.2 Flow chart of basic Genetic Algorithm procedure

When compared to the majority of traditional optimization techniques, the genetic algorithm plays a crucial role in predicting an exceptional optimal solution (Panwar et al., 2020).

3.3.2.4 Artificial Neural Network Data Validation

Artificial Neural Networks (ANNs) are complex machine learning models that can be used to predict or classify data. The validation of an ANN involves evaluating its performance and assessing its accuracy and generalization ability. In artificial neural network model validation technique MATLAB 2014a software was employed. Levenberg-Marquardt training was selected to determine the minimum of a function (either linear or nonlinear) over a range of parameters ("CUDA for Machine Learning and Optimization," 2011). Levenberg-Marquardt training algorithm was used to randomly select 32 samples (70%) for training, 7 samples (15%) for validation and 7 samples (15%) for testing out of 46 samples. Likewise, 10 hidden layers was filled with several neurons needed for enhancing the output value's prediction quality (Sanjeevi et al., 2020), as shown in Fig. 3.3.

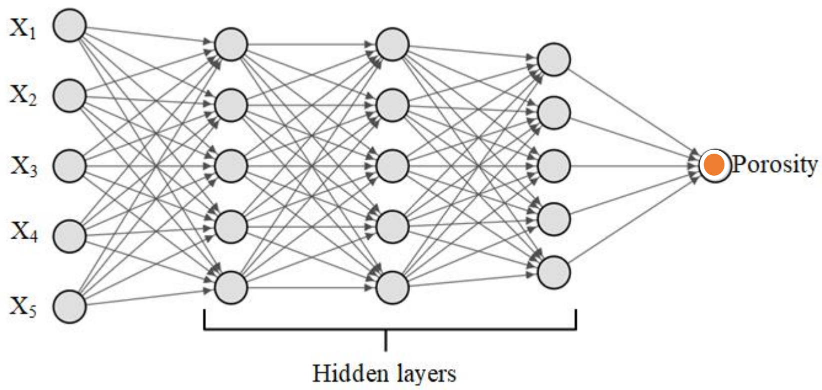

Figure 3.3 General hidden layer architecture of ANN showing coded input variables and the porosity output

3.3.3 Wear Behavior Investigation of a Pre-Optimized Sample

The pre-optimized sample against porosity was further examined its tribological or wear behavior property through optimization. The pre-optimized FSC process parameters were used to fabricate the hybrid composite samples made of magnesium alloy matrix tabulated in Table 3.7.

Table 3.7 FSC parametric combinations used during sample manufacturing for wear behavior investigation

Factors				
Speed [rpm]	Load [N]	Thickness	Time [min.]	Composition
800	500	12	6	15

The experiments were designed with the Box-Behnken optimization technique. Efficient modelling of the response surface and estimation of the interaction effects between process parameters and quadratic effects could be made achievable by this design. It also allows optimization within the design space and offers a more thorough examination of the responses. Three independent variables such as load, sliding speed and sliding distance were selected as the input parameters. Each variable was varied at three levels (-1, 0 and 1) based on their low, central and high values, respectively, as presented in Table 3.8. Then, the experimental data obtained from the wear testing were analyzed using the statistical software Minitab 19 to develop a regression model to predict the wear rate as a function of the input process parameters.

The model was optimized to identify the optimum parametric combination for the minimum wear rate of the MMHCs.

Table 3.8 Factors with their corresponding levels

Factors	Coded	Unit	Level -1	Level 0	level 1
Load	X_1	N	20	30	40
Sliding Speed	X_2	Rpm	220	240	260
Sliding Distance	X_3	m	350	500	650

Likewise, a total of 15 experiments were performed to cover Box-Behnken design space and investigate the effect of the input variables on the wear properties of the AZ61 magnesium alloy matrix composite as shown in Table 3.9.

Table 3.9 Box-Behnken experimental design matrix

Run	**Coded Factors**			**Actual Factors**		
	X_1	X_2	X_3	Load	Sliding Speed	Sliding distance
1	-1	-1	0	20	220	500
2	0	-1	1	30	220	650
3	1	-1	0	40	220	500
4	0	0	0	30	240	500
5	-1	0	-1	20	240	350
6	0	0	0	30	240	500
7	1	0	1	40	240	650
8	1	1	0	40	260	500
9	0	-1	-1	30	220	350
10	0	1	1	30	260	650
11	1	0	-1	40	240	350
12	0	0	0	30	240	500
13	0	1	-1	30	260	350
14	-1	1	0	20	260	500
15	-1	0	1	20	240	650

Dry sliding wear tests were performed in compliance with ASTM G99-05 to examine the tribological (Specifically Wear Rate) behavior of the composites. A pin-on-disk wear tester of model: DUCOM TR-20 instrument (Instruments Pvt. Ltd. Company in Peenya Industrial Area, Bangalore, India) was utilized. The length-to-diameter ratio must not be greater than two units, according to ASTM G99-05. As a result, samples measuring 6 mm in diameter and 12 mm in length were manufactured and mounted on wear testing apparatus as a pin to counteract the rotating disc device. At 20 ˚C room temperature, the dry sliding wear rate test was carried out. Various studies state that the method used to calculate wear rates is to use the associated densities to convert the mass loss values into volume loss (Yilmaz & Buytoz, 2001). In this study, Eq. 1 was used to compute the metal matrix composites' wear rates (Sivanesh et al., 2019).

$$\text{Wear rate} = \frac{(Mass\ of\ pin\ before\ wear\ test - Mass\ of\ pin\ after\ wear\ test)}{Sliding\ distance} \qquad \text{eq. (1)}$$

3.3.4 Wear Behavior Optimization through GA of a Pre-Optimized Sample

When compared to the majority of traditional optimization techniques, the genetic algorithm plays a crucial role in predicting an exceptional optimal solution (Panwar et al., 2020). A genetic algorithm optimization was carried out in MATLAB 2014a to find the global minima of the response. Following this, the accuracy of the optimization process was ensured by comparing the optimized process parameters with the Box-Behnken model's optimized result. The following genetic algorithm parameters tabulated in Table 3.10 had been used in MATLAB 2014a.

Table 3.10 Parameter function along with their values in GA for wear optimization

Parameter Function	Parameter Value
Size of the population	50
Type of the Population	Double vector
Creation Function	Constraint dependent
Fitness Scaling Function	Rank
Selection Function	Roulette
Reproduction: Elite Count	Default (0.05* Population size) = 2.5
Reproduction: Crossover Fraction	Default: 0.8
Mutation Function	Uniform: Rate at 0.15
Crossover Function	Constraint Dependent
Number of Generations	100

Function Tolerance	1e-6
Constraint Tolerance	1e-6

3.3.5 Numerical Simulation Method of Discrete Element Method

The method followed during powder mixing was depending on, by considering percentage weight of reinforcement and matrix powders on the software. The powders were mixed to the ratio of matrix to reinforcement as shown in Table 3.11.

Table 3.11 Composition of Reinforcements to matrix ratio

Materials	Different Composition (% wt.)		
	A	B	C
AZ61	85	90	95
SiC	7.5	5	2.5
ZrO_2	7.5	5	2.5
Total reinforcement ratios	15%	10%	5%

For instance, according to the Altair EDEM software the volume of the factory should be filled with the desired amount of powders to be embraced in the simulation. The powders were generated inside factory in such a way that the optimum placing to pack the powders inside the chamber was carried out by the software. Therefore, the software was set to place the powders by considering 20 times of trials to pack the volume of the chamber until where a single place was not remained to situate a single powder. In order to attain the fully filled volume of factory inside the chamber, the fill section and static type of factory option was selected in the factory and as an environment gravity of 9.81m/s^2 was considered in negative Z direction. The following properties were set to every material as shown in Table 3.12.

Table 3.12 DEM base simulation parameters

Materials	Properties			
	v	ρ in g/cm^3	E	Thermal Conductivity
AZ61	0.35	1.8	44.8 GPa	70 W/m·K
SiC	0.19	3.2	700 GPa	350 W/m·K
ZrO_2	0.22	5.68	200 Gpa	1.7 W/m·K
D2	0.285	7.7	209 GPa	20.5 W/m·K

Model	Hertz-Mindilin

In the interaction portion the coefficient of restitution is the ratio of speed of detachment to speed of advance towards in a collision (Manual of EDEM). The coefficient of static friction is a scalar value applied to identify what amount of force is needed preceding an inert object, of a specific material, at rest on another predefined substance, be able to set into motion. In addition to this, the coefficient of rolling friction determines the interaction between powders as; when a powder rolls on a surface, both the powder and the surface can deform to counteract this rolling motion. This is generally constituted as a torque being exerted to each of the powders. The coefficient of rolling friction is a scalar value applied to identify what amount of torque is required to be exerted to an object of a predefined stationary material on a flat surface to set it into motion. The Coefficient of Restitution (CoR) is one if there is no energy dissipation and completely elastic collision whereas CoR taken zero if the powders after collision remain stick together and called completely plastic collision (Ramírez-Aragón et al., 2018). Therefore, in this DEM simulation the coefficient of restitution was considered as a completely plastic collision in the interaction cases of AZ61-AZ61, AZ61-SiC, AZ61-ZrO_2 and AZ61-D2 (Tool). However, the CoR for the interactions of reinforcement to reinforcement and reinforcement to tool materials were considered as a completely elastic collision. Generally, the CoR depends on varies parameters such as; mechanical property of powders, property of the surface, collision medium, kinetic parameters and mechanisms (Yu & Tafti, 2016).

3.3.5.1 Scales of Actual Experimentation and Simulation

It is suggested that the numerical model can precisely replicate the mechanical behavior of a physical model under three similarity assumptions, namely geometric, mechanical, and dynamic. The first obvious requirement is that the scaled model developed in the simulation must comply precisely with the physical phenomenon. The classical principle of geometric similarity must be strictly followed (Feng et al., 2009). Scaling a Discrete Element Method (DEM) simulation to match actual experimental conditions for quantities such as force, volume, particle size, time, density, and length requires careful consideration of the scaling factors for each parameter. A step-by-step guide to follow on how to scale these quantities is presented:

I. **Identify the Reference System**: Before scaling, it was needed to define the reference system, which is either the DEM simulation or the actual experiment. It was assumed that the reference system was the actual experiment (where the preliminary study was carried out to verify the process).

II. **List the Parameters**: Make a list of the parameters which needs to be scaled, including force, volume, particle size, density, and length.

III. **Determine the Scaling Factors**:

A) **Force Scaling**: To scale forces, the principle of stress equivalence had been used. The forces should be scaled so that the stress levels (force per unit area) in the DEM simulation match those in the actual experiment. The Force Scaling Factor (FSF) is given by:

FSF = (Stress in actual experiment) / (Stress in DEM simulation)

B) **Volume Scaling**: Volume scaling is necessary to maintain the correct particle packing density. The volume scaling factor (VSF) is given by:

VSF = (Volume in actual experiment) / (Volume in DEM simulation)

C) **Density Scaling**: To scale density, the following equation had been used:

Density Scaling Factor = (Density in actual experiment) / (Density in DEM simulation)

D) **Length Scaling**: Length scaling is essential to ensure that the geometrical features of the system are accurately represented in the simulation. The Length Scaling Factor (LSF) is given by:

LSF = (Length in actual experiment) / (Length in DEM simulation)

IV. **Apply Scaling Factors**: Once it was determined the scaling factors for each parameter, apply these factors to DEM simulation was applied. This involves adjusting particle sizes, forces, volumes, densities, and lengths based on the calculated scaling factors.

V. **Validate and Adjust**: The next step after applying the scaling factors was, validating scaled DEM simulation by comparing its results to the actual experimental data. If necessary, adjustments are recommended to the scaling factors to better match the experimental observations.

In this research, it was assumed that the physical model consists of particles that are randomly packed in a domain and have different size distributions. The particles may be driven by phases such as fluid, electrical, or magnetic fields, or by predefined displacement and/or velocity on the domain boundaries. They may also be subject to the influence of external forces (applied and/or gravitational) (Feng & Owen, 2014). The corresponding discrete element model, which was assumed to have been scaled, was a geometrically exact representation of the physical phenomenon; that was, both models have the same number of particles, configuration and the only difference between them in terms of their particle sizes and domains was a constant scale factor h. Additionally, it was predicted that the scaled model would experience the same loading and boundary conditions as the actual model. The overbar (⁻) used in the formulation to represent a quantity associated to the scaled model in a general 3D context. Furthermore, in this research, spherical particles were assumed; however, the conclusions that can be made generally apply to particles of various shapes as well.
Let D and $\bar{D}$ stand for the typical lengths of the domains in both models, and let R and $\bar{R}$ repre sent the radii of an arbitrary particle in the physical and scaled models, respectively as presented in Eq.2.

$$\bar{R} = h\mathrm{R}; \quad \bar{D} = h\mathrm{D}; \quad \bar{S}\mathrm{n} = \mathrm{Sn} \qquad \text{eq. (2)}$$

For both models, the scale number Sn remains the same. As a result, the scaled model adheres to the geometric similarity concept as stated in previous research (Feng & Owen, 2014).

3.3.5.2 Governing Equation for Mechanical Motion of the Particle System for Scaling

The second law of Newton governs the mechanical motion of the particle system entirely. A general formulation of the governing equation for an arbitrary particle expressed as Eq. 3:

$$m\ddot{u}(\mathrm{t}) + F_d\,(\mathrm{t}) + F_{int}(\mathrm{t}) = F_{ext}(\mathrm{t}) \qquad \text{eq. (3)}$$

Where, m is mass of particle, $\ddot{u}$ is the acceleration, where u can be viewed as the displacement/position, F_d is the damping force responsible for energy dissipation in the system, F_{ext} is external applied force and F_{int} is interaction force between particles. The particle in the scaled system can have the same equation as presented in Eq. 4.

$$\bar{m}\ddot{\bar{u}}(\mathrm{t}) + \bar{F}_d\,(\mathrm{t}) + \bar{F}_{int}\,(\mathrm{t}) = \bar{F}_{ext}\,(\mathrm{t}) \qquad \text{eq. (4)}$$

The precise scaling laws provide the conditions necessary to ensure that the physical system and the scaled model are equivalent, i.e., that the two sets of Eq. 3 and 4 are mathematically equivalent or only deviate by a constant factor. Researchers implemented relatively simple approach which sustains the scaled model and physical phenomenon proportional (Feng et al., 2009) as presented in Eq. 5:

$$\frac{\bar{m}\ddot{\bar{u}}(\mathrm{t})}{m\ddot{u}(\mathrm{t})} = \frac{\bar{F}_d\,(\mathrm{t})}{F_d\,(\mathrm{t})} = \frac{\bar{F}_{int}\,(\mathrm{t})}{F_{int}(\mathrm{t})} = \frac{\bar{F}_{ext}\,(\mathrm{t})}{F_{ext}(\mathrm{t})} = \lambda \text{ (Constant)} \qquad \text{eq. (5)}$$

Let λq represent (Eq. 6) any physical quantity in the system, solving a scale factor λq for q results in

$$\bar{q} = \lambda_q q \qquad \text{eq. (6)}$$

The best technique to determine a quantity's scale factor is to explain its dimension in terms of the basic quantities, which can then be converted to scale factors (λ). For instance, applying $\mathrm{M} = \rho\mathrm{V}$ to mass results in Eq.7:

$$\mathrm{M} = [\rho][\mathrm{L}]^{3};\ \lambda_M = \lambda_\rho\, \lambda_L^3 = h^3 \qquad \text{eq. (7)}$$

Likewise, for force; using $\mathrm{F} = \mathrm{ma}$; gives Eq. 8:

$$[\mathrm{F}] = [\mathrm{M}]\,[\mathrm{L}][\mathrm{T}]^{-2} = [\rho][\mathrm{L}]^{3}[\mathrm{L}][\mathrm{T}]^{-2} = [\rho][\mathrm{L}]^{4}[\mathrm{T}]^{-2}\ ;\ \lambda_F = \lambda_\rho\, \lambda_L^4\, \lambda_T^{-2} = h^3 \qquad \text{eq. (8)}$$

Generally, when all the scale factors for all the physical quantities are identified, the whole set of scaling rules could be defined as indicated in the Table 3.13.

Table 3.13 Selected Physical Quantities, Symbols, Dimensions and Scale Factors

Quantity name	Symbol	Dimension	Scale factor (λ)	Category
Length	L	[L]	h	Basic
Density	ρ	[ρ]	1	Basic
Time	T	[T]	h	Basic
Position (sapatial)	X	[L]	h	Geometrical
Area	A	$[\mathrm{L}]^{2}$	h^2	Geometrical
volume	V	$[\mathrm{L}]^{3}$	h^3	Geometrical
Force	F	$[\rho][\mathrm{L}]^{4}\,[\mathrm{T}]^{-2}$	h^2	Mechanical
Stiffness	k	$[\rho][\mathrm{L}]^{3}\,[\mathrm{T}]^{-2}$	h	Mechanical
Mass	M	$[\rho][\mathrm{L}]^{3}$	h^3	Material

Acceleration	a	[L][T] $^{-2}$	h^{-1}	Kinematic
Young's modulus	E	[ρ][L] ^{2} [T] $^{-2}$	1	Material

Scaling relationship calculations:

In order to calculate force that can be used in the DEM simulation, copied or derived from the actual experimentation. The scale factor used for actual experiment to the DEM simulation considered to be quadruple (four times) less than the actual experiment.

***Force Scaling*:** For instance, the stress in actual experimentation should be equivalent with DEM simulation's stress. The method employed for actual force and DEM simulation's force scaling calculated as:

$$P = \frac{F}{A}; \frac{500N}{0.000134m^2} = 1{,}592{,}356.68 \text{ Pa},$$

Whereas the equivalent force that has to be applied for simulation was calculated as:

$P = \frac{F}{A}$ where, F = PA, to equalize the pressure for actual experimentation with the simulation, the same amount of pressure had to be determined. Hence, the pressure in actual experimentation determined to be 1,592,356.68 Pa, the pressure had to be calculated with the corresponding area of the die used in the simulation. The cross-section area of the rotating die (by which the load is applied) is $A = \pi r^2$; where r is the radius of rotating die which was applied in simulation was 0.0025m. Therefore, F = PA becomes 31.25N. Generally, the equivalent of 500N force applied for actual experiment was considered to be 31.25N in DEM simulation.

Comparing the scale factor (Eq. 9) depending on the Table 3.13, the scale factor for force conversion h^2 presented in Eq.10, this means that:

$$\text{Scale Factor} = \frac{Force\ in\ Actual\ Experiment}{Force\ in\ DEM\ simulation} \qquad \text{eq. (9)}$$

$$h^2 = \frac{Force\ in\ Actual\ Experiment}{Force\ in\ DEM\ simulation} \qquad \text{eq. (10)}$$

$$4^2 = \frac{500N}{X};\ X = (500N)(16); X = 31.25\text{N, where } X \text{ is force in DEM simulation.}$$

Geometric Scaling: the geometric scaling for actual to simulation was considered to be quadruple. The Fig. 3.4 depicts the geometrical dimensions used for actual experimentation and

DEM simulation. Based on the table conversion scale, h^3, the volume for the DEM simulation's chamber was estimated, with the actual chamber volume considered to be four times bigger than the chamber volume used in the simulation. The volumes taken into consideration for the actual experiment and simulation were 0.00000628 m^3 and 0.00000009813 m^3, respectively.

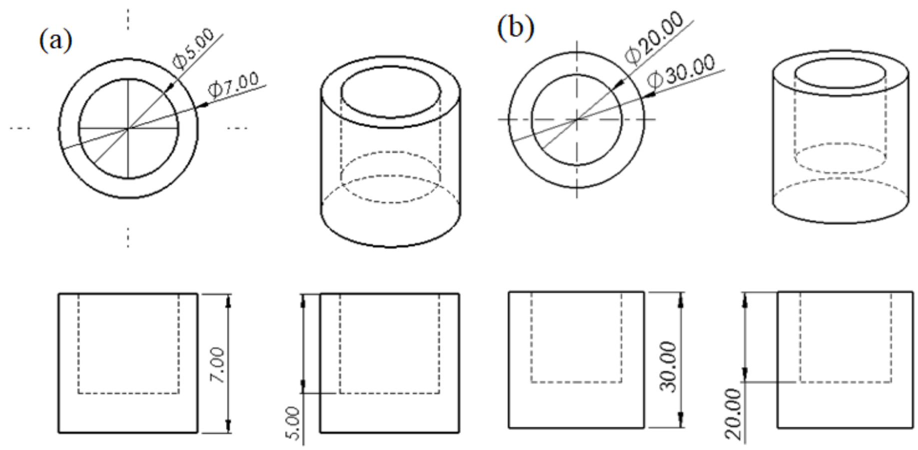

Figure 3.4 Geometrically Scaled Internal Chamber Sizes (a) DEM Simulation and (b) Actual Experiment (all dimensions are in mm) (see also APPENDIX 5)

3.3.5.3 Basic Assumptions in Numerical Simulation of FSC Process

For the discrete element model of a Friction Stir Consolidation process, the following presumptions such were made: a) powder grains of matrix and reinforcements were represented by spherical particles b) The size and distribution of the particles were considered to match with those of the original powder c) At the consolidation stage, the interaction of the particles were considered to make friction at the contact point and plastic deformation d) The specimen's temperature distribution will be presumed to be uniform e) Modelling of powder-mold interaction was done under the assumption of frictional contact. The discrete element model created using the aforementioned premises has been utilized in the discrete element method using Altair EDEM Hertz-Mindilin model.

3.3.5.4 Hertz–Mindlin–Deresiewicz Model for Contact and Particle Representation in DEM

The initial step in the FSC process is a powder compaction step which results in the formation of a green body of a particulate material. The sufficient solidness of the compacted powder counter backs the rotating die to create frictional heat. The discrete element method (DEM) approach was used to simulate particle packing of spherical particles. In DEM, discrete particle dynamics are modelled, and the interactions between the individual particles control the behavior of the entire system (Tangri et al., 2017). Studies revealed that the normal contact interaction is represented by Kelvin-Voigt element where spring and a dashpot are connected in parallel, in addition to this thermal element should be summed up in series to the spring effect. Rojek et al., (2015), derived the contact interaction model for powder compaction starting from Eq.11-22, as:

$$F_n = F_n^e + F_n^d \qquad \text{eq. (11)}$$

Where; F_n = Normal contact force, F_n^e = Elastic force and F_n^d = Viscous component.

The viscous element F_n^e can further be analyzed by assuming linear force-displacement relationship as:

$$F_n^e = K_n U_{rn}^e \qquad \text{eq. (12)}$$

Where K_n represents the normal contact stiffness and U_{rn}^erepresents the penetration of two particles, which further analyzed using the following equation:

$$U_{rn}^e = d_{ij} - r_i(\mathrm{T}) - r_j(\mathrm{T}) \qquad \text{eq. (13)}$$

Where d_{ij} is the distance of the particle centres, and r_i (T), r_j (T) representing their radii dependent on the temperature, and related by the equation:

$$r_a(\mathrm{T}) = r_a^0(1 + \alpha\Delta\mathrm{T}),\ a = i, j \qquad \text{eq. (14)}$$

Where α is the linear coefficient of the thermal expansion, ΔT is the temperature increment, and r_a^0 ($a = i, j$) is a^{th} particle radius at the initial temperature.

On the other hand F_n^e or elastic part of normal contact force can be given in terms the overlap U of Hertz interaction model as justified for particle collision (Johnson, 2013).

$$F_n^e = K_n {U_{rn}^e}^{3/2} \qquad \text{eq. (15)}$$

Depending on the Hertz theory, the normal stiffness for the i^{th} sphere can be expressed as (Johnson, 2013b):

$$K_n = \frac{3}{4}\,\dot{\mathrm{E}}\sqrt{\dot{\mathrm{r}}} \qquad \text{eq. (16)}$$

Where Ė is effective elastic modulus and it is given in the following relation:

$$\frac{1}{\dot{E}} = \frac{1-v_i^2}{2E_i} + \frac{1-v_j^2}{2E_j} \qquad \text{eq. (17)}$$

And the effective radius ṙ can be expressed in terms of the following equation as:

$$\dot{r} = \frac{2r_i\,(T)r_i\,(T)}{r_i\,(T)+r_i\,(T)} \qquad \text{eq. (18)}$$

The normal force's viscous component is thought to be a linear function of the normal relative velocity(u_{rn}).

$$F_n^d = c_n u_{rn} \qquad \text{eq. (19)}$$

$$\text{Where } u_{rn} = (u_i - u_j) \bullet n_{i.} \qquad \text{eq. (20)}$$

For the system of two rigid bodies with masses m_i and m_j coupled by a spring of stiffness K_n, the value of the viscosity coefficient (c_n) can be interpreted as a fraction of ξ the critical damping C_{cr}.

$$c_n = \xi\, C_{cr} \qquad \text{eq. (21)}$$

Where, C_{cr} is an equation for calculating the critical damping (Rojek et al., 2016).

$$C_{cr} = 2\sqrt{\frac{m_i m_j k_n}{m_i+m_j}} \qquad \text{eq. (22)}$$

3.3.5.5 Governing Equation

The friction stir consolidation process involves the use of frictional heat to consolidate the powders. This equation considers heat generation due to friction and heat conduction within the material. The heat transfer to the surrounding assumed to be negligible. The partial differential equation showed in Eq. 23 describes the heat distribution (the variation in temperature) in a particular body over time.

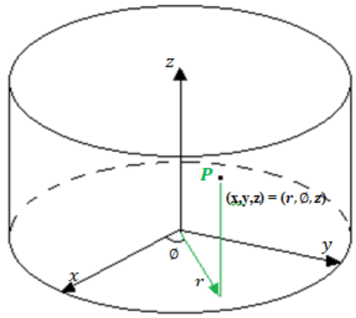

Figure 3.5 Conduction at Any Point P on Cylindrical Coordinates ($\boldsymbol{r}, \emptyset, \boldsymbol{z}$)

The governing equation for the heat transfer process is given as:

$$\rho c \frac{\partial T}{\partial t} = \frac{1}{r}\frac{\partial}{\partial r}\left(kr\frac{\partial T}{\partial r}\right) + \frac{1}{r^2}\frac{\partial}{\partial \emptyset}\left(k\frac{\partial T}{\partial \emptyset}\right) + \frac{\partial}{\partial z}\left(k\frac{\partial T}{\partial z}\right) + Q \qquad \text{eq. (23)}$$

For cylindrical coordinate given in Fig. 3.5 (Heat et al., 2007) represents the conductive heat transfer at any arbitrary point. Where ρ is the density, c is the specific heat, T is temperature, t is the time and k is the thermal conductivity. While r, $\emptyset$ and z are coordinates, and Q is the volumetric heat source term.

3.3.5.6 Boundary Conditions

To define a boundary condition for the rotating die, it is required to specify how the die interacts with the chamber. Important aspect to consider is the heat generated due to the friction between the rotating die and the metal powder. Since the die is rotating, frictional forces at the interface will generate heat. Therefore, a suitable boundary condition to capture this heat generation could involve specifying the heat flux at the surface of the die.

At the surface of the rotating die, it is important to set up a heat flux boundary condition that accounts for the heat generated due to friction with the metal powder. This heat flux (q) would depend on the frictional force and the angular velocity of the die:

$$q = (F_{\text{friction}})\,(\omega) \qquad \text{eq. (24)}$$

Where; q is heat flux, F_{friction} is Frictional Force and ω is Angular Velocity

The friction force F_{friction} can be calculated using the coefficient of friction (μ) and the normal force F_{friction} pressing the die against the compacted powder:

$$F_{\text{friction}} = \mu \cdot F_{\text{normal}} \qquad \text{eq. (25)}$$

Coefficient of friction could be calculated based on the applied load, rotating die radius and torque generated by the rotating die (Bhardwaj et al., 2020).

$$\mu = \frac{T}{2R_r P} \qquad \text{eq. (26)}$$

Where; T is torque applied by the rotating die, R_r is rotating die radius and P is axial applied load by the rotating die (Bhardwaj et al., 2020).

Here, the frictional force can be calculated from the applied load and the coefficient of friction between the die and the metal powder. The angular velocity is given by the RPM (rotations per minute) of the die.

From the relation:

$$q = -k\,\frac{dT}{dx} \qquad \text{eq. (27)}$$

Combining eq. 24 and 27, the surface heat flux at the contact point can be achieved as presented in eq. 28.

$$-k\,\frac{dT}{dx} = (F_{\text{friction}})\,(\omega) \qquad \text{eq. (28)}$$

From the relation in eq. 18, T_f could be calculated and the effect of the angular velocity of the rotating die integrated into the heat generation. By specifying this heat flux boundary condition, it is possible to effectively model the heat flux generated at the surface of the rotating die due to friction.

Calculation of heat energy transferred (Q) through the material per second described in Eq. 29 as (Kosky et al., 2021):

$$\frac{Q}{t} = \frac{kA\Delta T}{X} \qquad \text{eq. (29)}$$

Therefore, the heat energy transferred through the material is presented in Eq. 20.

$$Q = \left(\frac{kA\Delta T}{X}\right) t \qquad \text{eq. (30)}$$

Where; Q is heat energy in joule per second or Watt, t is time in second, k thermal conductivity constant, ΔT change in temperature and X is the thickness of the material. Therefore, Q was calculated theoretically for each simulation runs based on the parameters listed in design Table 5. Finally, the theoretically calculated heat energy Q was inserted into the DEM simulation which is responsible in powders deformation. These calculations provide a theoretical estimation of the heat energy transfer generated due to friction.

3.3.5.7 Time Integration Scheme

The second strategy that is frequently employed is founded on the idea that energy cannot move from a particle beyond its nearby neighbouring in a single time-step (Remacle et al., 2012). Additionally, regardless of where the contact point is, the Rayleigh wave always arrives at any contact at the same average time. For ease of use, the simulations employ a portion of the critical time step, which is depending on the average particle size. Therefore, the following Eq. 31 provides the key terms to decide Rayleigh time-step (Li et al., 2005; Lupo et al., 2021).

$$\nabla t_c = \frac{\pi r}{\beta}\sqrt{\frac{\rho}{G}} \quad \text{eq. (31)}$$

Where G is the particle shear modulus 17GPa, ρ is the particle density 1800 kg/m^3, and r is the average particle radius of AZ61 65µm = 0.000065m, β can obtain obtained from the following eq. 32. The value of β was approximated to be 0.93365 by using eq. 33.

$$(2-\beta^2)^4 = 16\,(1-\beta^2)\left[(1-\beta^2)\left(\frac{1-2v}{2(1-v)}\right)\right] \quad \text{eq. (32)}$$

$$\beta = 0.8766 + 0.163v \quad \text{eq. (33)}$$

Where; v is Poisson's ratio of the matrix material (AZ61) 0.35 and the result for the critical time-steps of the simulations evaluated was 7.113e^{-8}s.

3.3.6 Methods of Die Fabrication

As explained in the following sections, the fabrication of dies and samples includes the 3D design process, die manufacturing process, die heat treatment process, and sample fabrication process.

3.3.6.1 Die Geometrical Design and 3D Modelling

Prior to fabrication dies were geometrically designed and modeled by using SOLIDWORKS 2019 software.

I. ***3D Model of rotating die***: The 3D model of rotating die was modeled using SOLIDWORKS 2019 software. The size of the spindle on the milling machine where the die will be assembled was taken into consideration when determining the die's dimensions especially upper rotating die shown in Fig. 3.6 (see also APPENDIX 11).

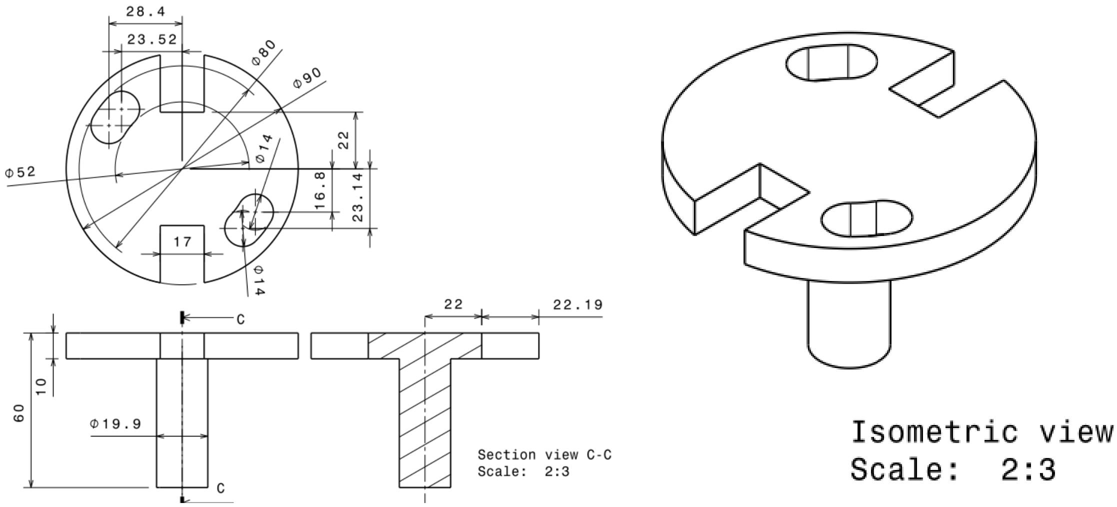

Figure 3.6 3D Model of Rotating Die with Its Corresponding Dimensions in mm

II. ***3D Model of fixed chamber die***: The exterior shape of the fixed chamber shown in Fig. 3.7 was preferred to be cubical for ease of griping, and it was also symmetrically split to make sample removal simple. The four holes are designed so that the two symmetrical dies can be fastened together (see also APPENDIX 11).

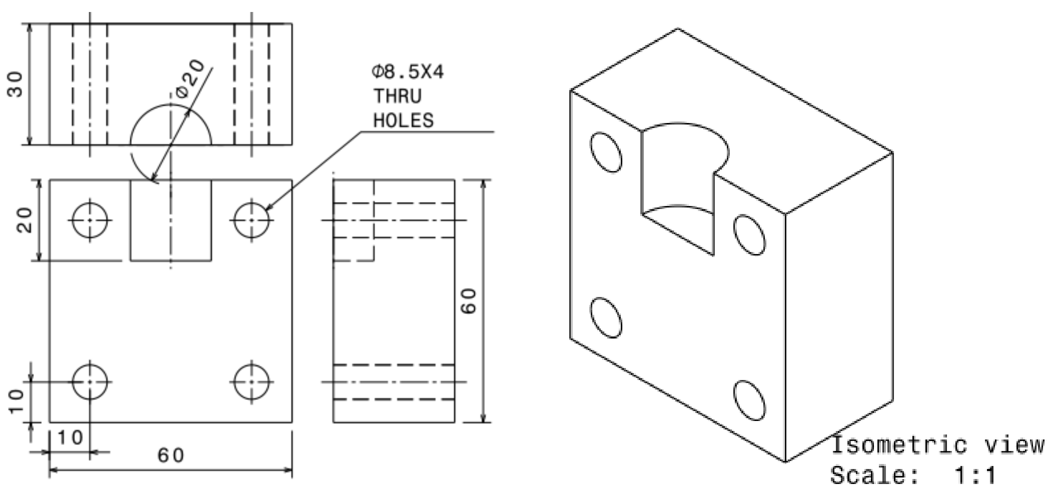

Figure 3.7 3D Model of Fixed Chamber Die with Its Corresponding Dimensions

3.3.6.2 Die Manufacturing Process

The die manufacturing processes are categorized into two sections I) production processes of rotating die and II) production processes of fixed chamber.

I. ***Production Process of Rotating Die:*** The rotating die was manufactured using lathe machine for diameter reduction and the slots indicated on the rotating die was manufactured by milling machine using end mill cutter as shown in Fig. 3.8. The larger portion of the rotating die especially the surface would be exposed to the actual experimentation was reduced or cut to a desired final dimension by using lathe machine (see also APPENDIX 2). The slots at the top right and left part of the rotating die was first drilled in order to allow entrance for the end mill cutter. As it was clearly presented in the 3D model, the drilled portion and the slot opening on the top portion of the rotating die permits the die to be assembled on the spindle of a milling machine (process development system) where the actual experimentation takes place.

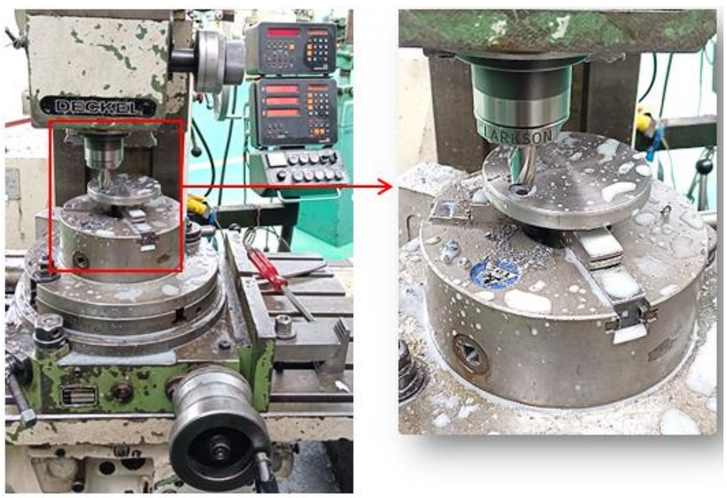

Figure 3.8 Upper Rotating Die Manufacturing Milling Machine

II. ***Production Process of Fixed Chamber Die:*** Prior to final dimension machining on the milling machine, the D2 die material for the fixed chamber was first cut into the appropriate shape to its close dimension using an automatic saw. The two symmetry D2 die material was then reduced to its nearly final dimension, which was 60 mm x 60 mm x 30 mm on a milling machine as shown in Fig. 3.9a. Next, drilling operation was carried out at the top center of the two symmetry D2 tool metals to a depth of 20 mm, and finally boring operation was carried out to bring the final diameter to 19.9 mm on a lathe machine as shown in Fig. 3.9b. Four symmetry holes with an 8.5mm diameter were drilled in order to securely fasten the two symmetry dies together.

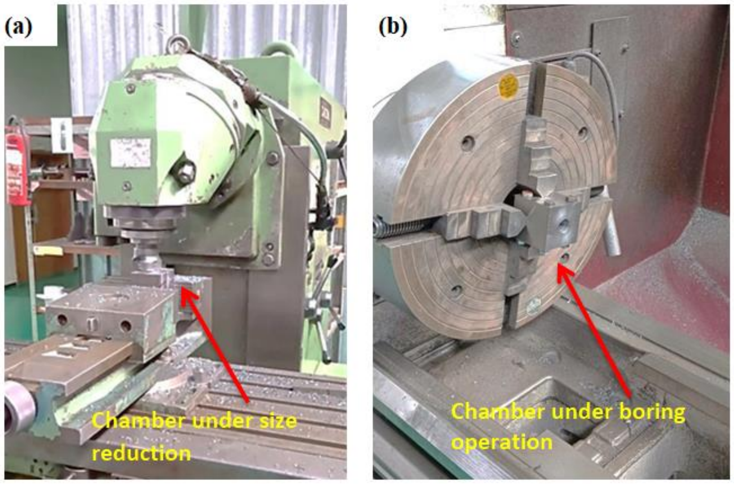

Figure 3.9 Chamber Preparation (a) Milling (Model: MAQUINARIA CMC-FU3) (b) Lathe for Boring (Model: Harrison M460)

3.3.6.3 Die Heat Treatment Process

Following the completion of manufacturing process, dies need to be heat treated for a better performance during their operation. Due to its strong hot toughness and wear resistance qualities, D2 die material is chosen (Azevedo et al., 2022).

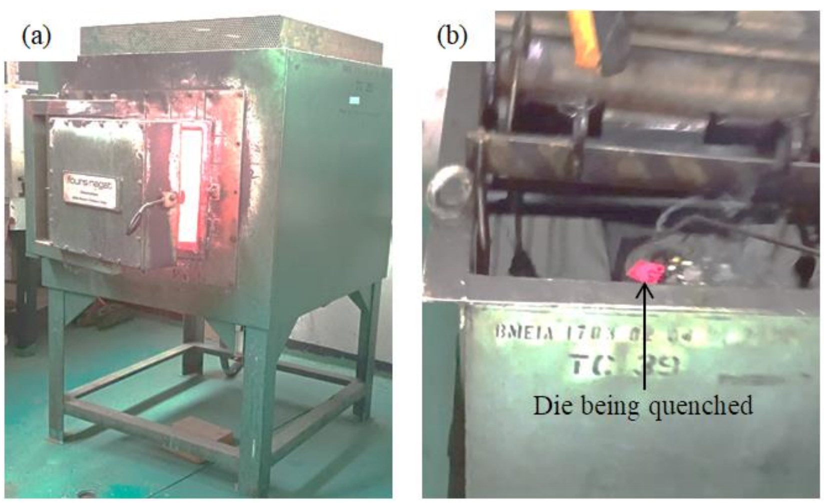

Figure 3.10 Machines Used for Heat Treatment (a) Furnace and (b) Oil Tanker (see also APPENDIX 10)

Quenching heat treatment procedure has been carried out to improve or increase the hardness of the D2 die material from 19 HRC to 44 HRC. In which the D2 material was heated at 900^{o}C (Fours Nagat Furnace-44550 Montoir De Bretagne, France) shown in Fig. 3.10a which has maximum heating capacity of 1200°C and soaked for 30 minutes of time duration followed by oil quenching medium shown in Fig. 3.10b. The improvement in hardness property of die material was measured using a hardness testing machine (Brooks Hardness Tester-Ras Model) with a 150 Kg load and a diamond indenter at a 120° inclination in accordance with ASTM E 18-07 standard.

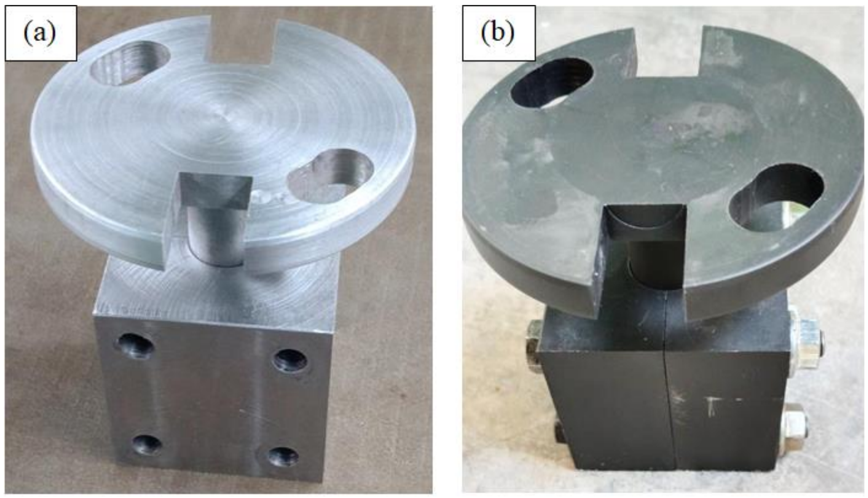

Figure 3.11 Heat Treatment Process (a) Before and (b) After

The heat treatment process was carried out for all dies except for bolts as shown in Fig. 3.11a and b.

3.3.7 Specimen or Sample Fabrication Method

Sample fabrication process incorporates processes such as powder weighing, powder mixing and powder consolidation through friction stir consolidation process.

I. ***Powder preparation method:*** First, powders were weighed using the Box-Behnken design matrix. In this study, weight percentages of 5%wt (2.5% SiC and 2.5% ZrO2), 10%wt (5% SiC and 5% ZrO2), and 15%wt (7.5% SiC and 7.5% ZrO2) were taken into consideration while examining reinforcement compositions. For simplicity, the reinforcement compositions were therefore often taken as 5%, 10%, and 15% weight, with the remaining %wt being regarded as AZ61 matrix material. For example, the powders were weighed as illustrated in the Fig. 3.12 for the 15% weight proportion of reinforcements (APPENDIX 3).

Figure 3.12 Weighing and Adjusting Proportion of the Matrix and Reinforcing Materials

II. ***Powder mixing method:*** prior to friction stir consolidation, using a high-energy ball mixer, the AZ61 magnesium alloy powder and the reinforcements (SiC and ZrO_2) were mixed to the required proportions for 20 minutes to provide a homogeneous distribution of reinforcements, depicted in Fig. 3.13a. Similarly, 10 mm diameter zirconia balls were employed, as illustrated in Fig. 3.13b, and ½ balls to powder ratios were used during the mixing operation. To create the magnesium alloy matrix hybrid composite, the mixture was then put into a chamber of friction stir consolidation on process development system and consolidated under the proper process parameters, such as applied load, consolidating time, speed, thickness, and composition. The magnesium alloy hybrid composite samples were fabricated based on the BBD matrix.

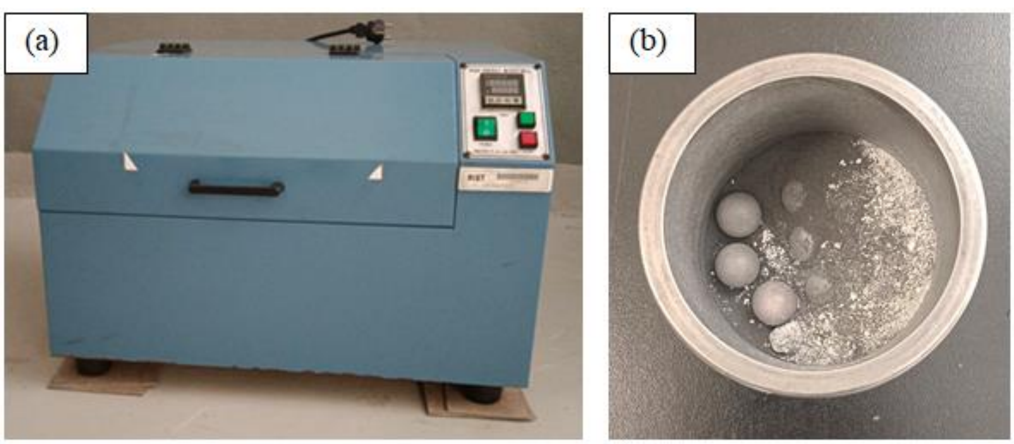

Figure 3.13 Mixing Methods (a) High Energy Ball Mixer and (b) Powders and Zirconia Balls before Mixture

After the mixture process was completed, the powders were directly fed into the fixed chamber in the appropriate amount to run the friction stir consolidation process. The FSC equipment was composed of the following parts as shown in Fig. 3.14: rotating die, fixed chamber and process development system.

The general procedure of FSC process covers the following steps:

i. Align the fixed chamber with the rotational axis of the rotating die which was assembled on the spindle of the conventional milling machine.

ii. Fill the chamber with the required amount of powders (use gravity to pour the particles or load them until the desired thickness is reached).

iii. Apply a 20N load to the reinforcement and matrix material to pre-compact it until the powders' spongy effect is gone.

iv. Begin the die rotation, once the die rotation has begun and the spindle is rotating at desired speed, the compaction force is raised uniformly to the desired level and maintained for the specific time based on the Box-Behnken design matrix.

v. Withdraw the die from the MMC chamber, terminate the process and finally remove the sample.

vi. Finally, by varying process parameters, the mechanical and physical properties were studied (APPENDIX Figure IV and V).

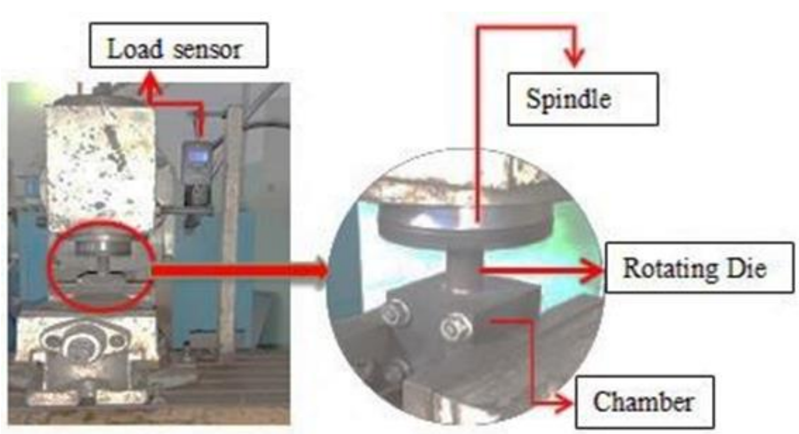

Figure 3.14 Friction Stir Consolidation Process on a Conventional Milling Machine

3.3.8 Testing and Characterization Method

3.3.8.1 Porosity Analysis Method

Porosity analysis experiments are commonly used to determine the porosity of materials, which is a measure of the void spaces or pores within a substance. The specific method chosen for porosity analysis depends on the type of material being studied, its characteristics, and the desired level of accuracy. In this study the porosity calculations for simulation and for actual experimentation was analyzed according to the following methods below. For instance, the porosity calculation in case of actual experimentation was depends on the theoretical and actual density of the optimized sample. However, porosity calculation for simulation was based on the Eq. 34.

I. ***Porosity Analysis in case of Simulation:*** The porosity was considered as the yield for the progression of the process evaluation. In which the porosity can truly determine the stance of the FSC process and how the densification occurred. The post-processing for porosity prediction was based on the manner in which the powders were compressed using certain process parameters. Porosity was estimated based on the volume of the powders at preprocessing and the volume of the die covered by the powders after processing. Similarly, based on the Eq. 34 predicted the porosity (Chen & Miedema, 2007).

$$n\ (\%) = 1 - \frac{\text{volume of solid particles in the cube}}{\text{volume of the cube}} = 1 - \frac{Vp}{Vc} \times 100 \qquad \text{eq. (34)}$$

$$\text{Porosity}\ (\%) = 1 - \frac{\text{volume of solid particles in the Die before compaction (at preprocess)}}{\text{volume of the die after compaction (at postprocess)}} \times 100$$

II. ***Porosity Analysis in case of actual experiment:***

The Archimedes principle, represented by Eq. 35, was employed to assess the experimental density. Furthermore, the theoretical density was calculated using the formula in Eq. 36.

$$\rho c = \frac{\rho_l - W_{\rho c}}{\Delta W_{\rho c}} \qquad \text{eq. (35)}$$

$$\rho c = \rho_r\ \textit{(Ratio of reinforcement \%)} + \rho_m\ \textit{(Ratio of matrix \%)} + ... \qquad \text{eq. (36)}$$

Where, ρc is magnesium matrix hybrid composite (AZ61) density, ρ_l is liquid (water at room temperature) density, $W_{\rho c}$ is weight of magnesium matrix hybrid composite in air, $\Delta W_{\rho c}$ is change of magnesium matrix hybrid composite in air and in liquid (Nayak et al., 2022). Likewise, the theoretical densities were calculated using Eq.36. Where ρ_c is the hybrid composite density, ρ_r is the density of reinforcement multiplied by its ratio in percentage volume and prior to calculation of theoretical density, the percentage weight converted into percentage volume of reinforcements. Generally, relative porosity could be calculated based on the Eq. 37 (Tosun & Kurt, 2019).

$$p_r\ (\%) = \left(\frac{\rho_t - \rho_a}{\rho_t}\right) \text{x } 100 \qquad \text{eq. (37)}$$

Where; p_r is the relative porosity, ρ_t is the theoretical density and ρ_a is the actual density of an optimized sample. The weights of the MMHCs in the liquid were measured as shown in Fig. 3.15.

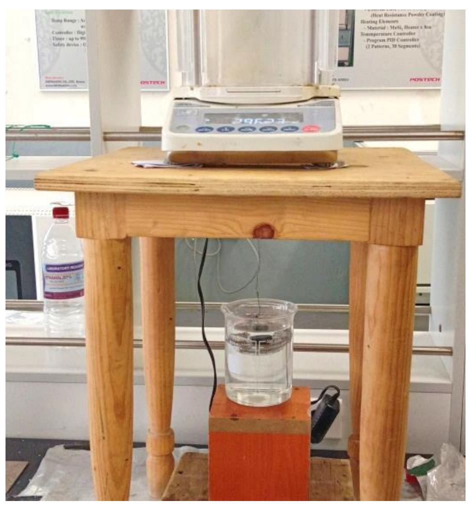

Figure 3.15 Weight Measurements in a Liquid

3.3.8.2 Hardness and Compressive Strength Testing Method

To provide a clear illustration of the impact of the FSC process on hardness properties, the samples were examined at the various surface zones depicted in Figures 3.16a and b. Applying the HVS-50 hardness tester and the ASTM E384-22 standard, test force of 10 kgf, 10x magnification, and dwell time of 7 seconds were taken into consideration, shown in Fig. 3.16a.

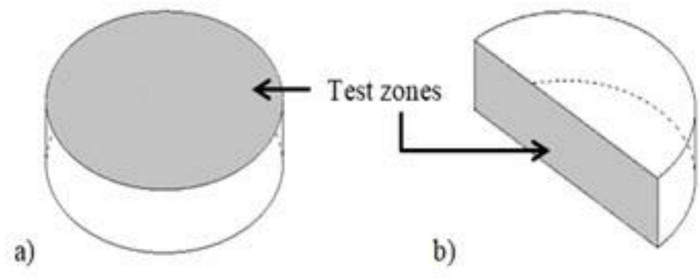

Figure 3.16 Sample Test Zones a) Top Surface b) Cross-Sectioned Surface

The desire to perform hardness testing at various cross-sectional surfaces was raised due to the nature of the FSC process, which causes the powders at the top surface to consolidate initially and the frictional heat to progressively spread to the perimeter of the chamber consolidating the powders. Similarly, the hardness results at various surface zones of the sample found to be infinitesimally differed. Therefore, the average HV (Vickers Hardness) value was taken into consideration. Likewise, as illustrated in Fig. 3.17b, the Compression Yield Strength (CYS) was measured using a universal testing machine (Model: WP 310 Materials testing) with a maximum capacity of 50kN, at room temperature and at a rate of 50 mm/minute. Additionally, it is presented in APPENDIX 7 and 8.

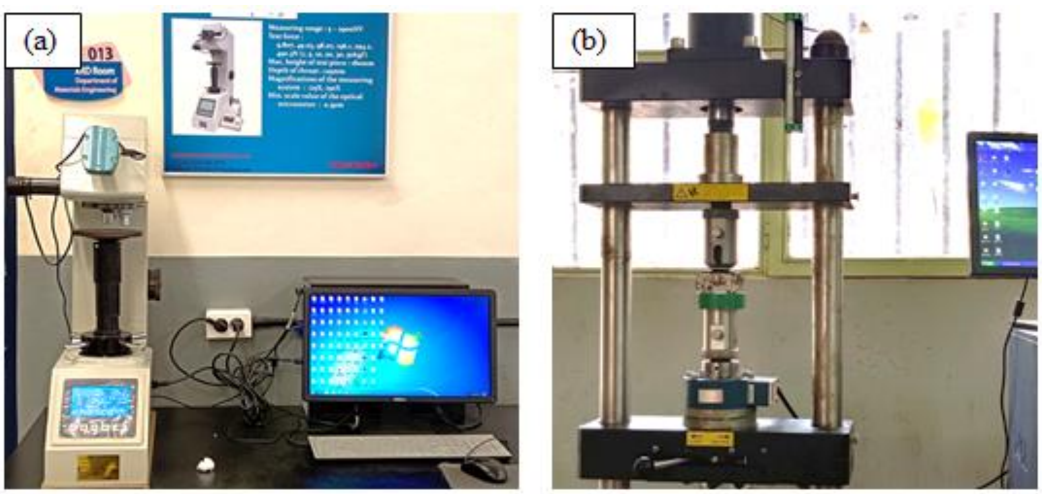

Figure 3.17 Hardness and Compressive Strength Testing (a) HVS-50 Hardness Tester and (b) Universal Testing Machine

3.3.8.3 Wear Testing Methods

Pin-on-disc apparatus was implemented to analyze the wear property of the sample. The basic principle of a Pin-on-Disc apparatus involves two main components: a stationary pin or a material to be tested hanged on the stationary part and a rotatable disc. The fixed pin is brought into contact with the rotating disc under controlled conditions to study aspects of wear rates.

Pin-on-Disc Wear Testing: The pin-on-disc apparatus of wear testing machine was employed to assess the wear rate of the magnesium alloy matrix hybrid composite. The apparatus uses a steel disc as the counter face material, and the samples were subjected to predetermined parametric combinations (based on RSM-BBD) at room temperature for a desired sliding distance. Finally, evaluations of the wear rates of the samples were performed and obtained. Figure 3.18 illustrates a sample ready for mounting and testing (See APPENDIX 1). Dry sliding wear rate tests were performed in compliance with ASTM G99-05 to examine the tribological behavior of the composites. A pin-on-disk wear tester of model: DUCOM TR-20 instrument (Instruments Pvt. Ltd. Company in Peenya Industrial Area, Bangalore, India) was utilized. The length-to-diameter ratio must not be greater than two units, according to ASTM G99-05. Therefore, samples measuring 6 mm in diameter and 12 mm in length were manufactured and held on the wear testing machine's sample holder device. At 20 °C of room temperature, the dry sliding wear rate test was carried out. Various studies state that the method used to calculate wear rates is to use the associated densities to convert the mass loss values into volume loss (Yilmaz & Buytoz, 2001). However, Eq. 38 was utilized in another study to calculate the wear rates of metal matrix composites (Sivanesh et al., 2019). Additional details for wear rate conversions and calculations have been elaborated in (APPENDIX 6).

$$\text{Wear rate} = \frac{(\text{Mass of pin before wear test} - \text{Mass of pin after wear test})}{\text{Sliding distance}} \qquad \text{eq. (38)}$$

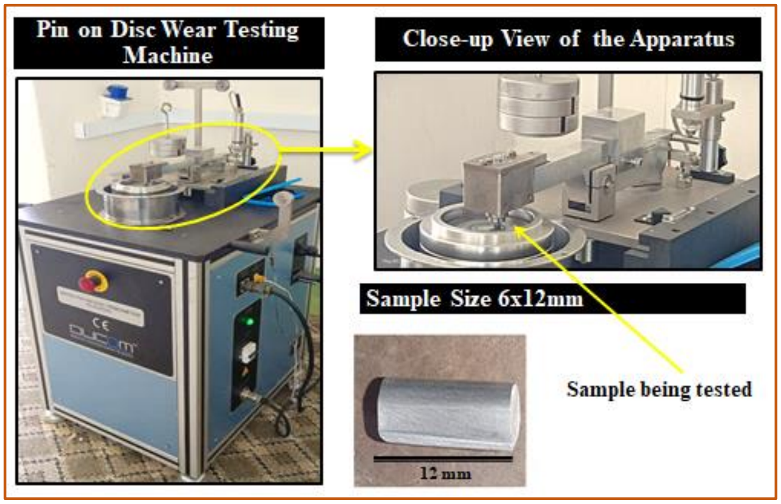

Figure 3.18 Pin-On-Disc Wear Testing Machine

3.3.8.4 X-ray Diffraction

X-ray diffraction is a method mainly used to assess the phases of the materials when the intensity of the reflected X-rays is analyzed or detected, as the detector and sample rotated (Prasad et al., 2020). Angles ranging from 10^o to 80^o were taken into consideration when using the X-ray diffraction apparatus (Model: XRD-7000 X-RAY DIFFRACTOMETER Maxima, Shimadzu Corporation, Japan) in this investigation.

3.3.8.5 Thermogravimetric Analysis

A thermal analysis technique called Thermo-Gravimetric Analysis (TGA) measures a material's weight gain and loss over time at different temperatures. TGA was evaluated in order to confirm that the friction stir consolidated sample may be used in environments where it can meet stability under different temperatures. Similarly, the temperature at which the sample begins to deteriorate or break down over time could also be disclosed by the TGA analysis and it is also a technique that is employed to investigate the thermal decomposition of materials. Furthermore, TGA is a commonly used technique to analyze certain properties of materials that exhibit mass gain or loss as a result of oxidation, decomposition, or loss of volatiles (like moisture), according to Nasrollahzadeh et al., (2019). In this study, a DTG-60H detector was used to analyze the TGA of an optimized sample weighing 10.215 mg. The sample was heated at a rate of 15 ^oC per minute in nitrogen gas at a flow rate of 50 ml per minute, covering a temperature range of 15 to 700 ^oC.

3.3.8.6 Scanning Electron Microscope

Scanning Electron Microscope (SEM) is commonly used to analyze the fracture surface of MMCs. SEM provides high-resolution images that help to identify the fracture origin and crack propagation path. For example, Fractography analysis of Al/SiC MMCs revealed that the SiC particles acted as a stress concentrators and initiated the cracks, which propagated through the matrix (Kane et al., 2016). Another study conducted Fractography analysis on Al/B4C MMCs and found that the fracture occurred due to the presence of voids in the matrix (Alizadeh et al., 2013). In this study, Fractography of SEM images using (Model: JCM/6000PLUS BENCH TOP SEM, Joel Japan) was employed to examine the worn-out and fractured surfaces.

3.3.9 General Methodology Flowchart

This detailed flow chart illustrated in Fig. 3.19, represents the methodology flow for the materials and methods section of this dissertation. It outlines the various steps involved, including parametric optimization, numerical simulation, RSM Box-Behnken optimization, genetic algorithm, and model validation with ANN, sample characterization with XRD, SEM, and Thermogravimetric analysis, as well as mechanical testing. The flow chart provides a comprehensive overview of the methodology employed in this study, leading to the conclusion of the research.

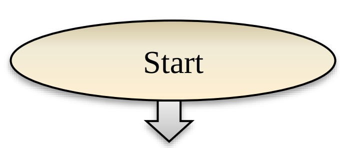

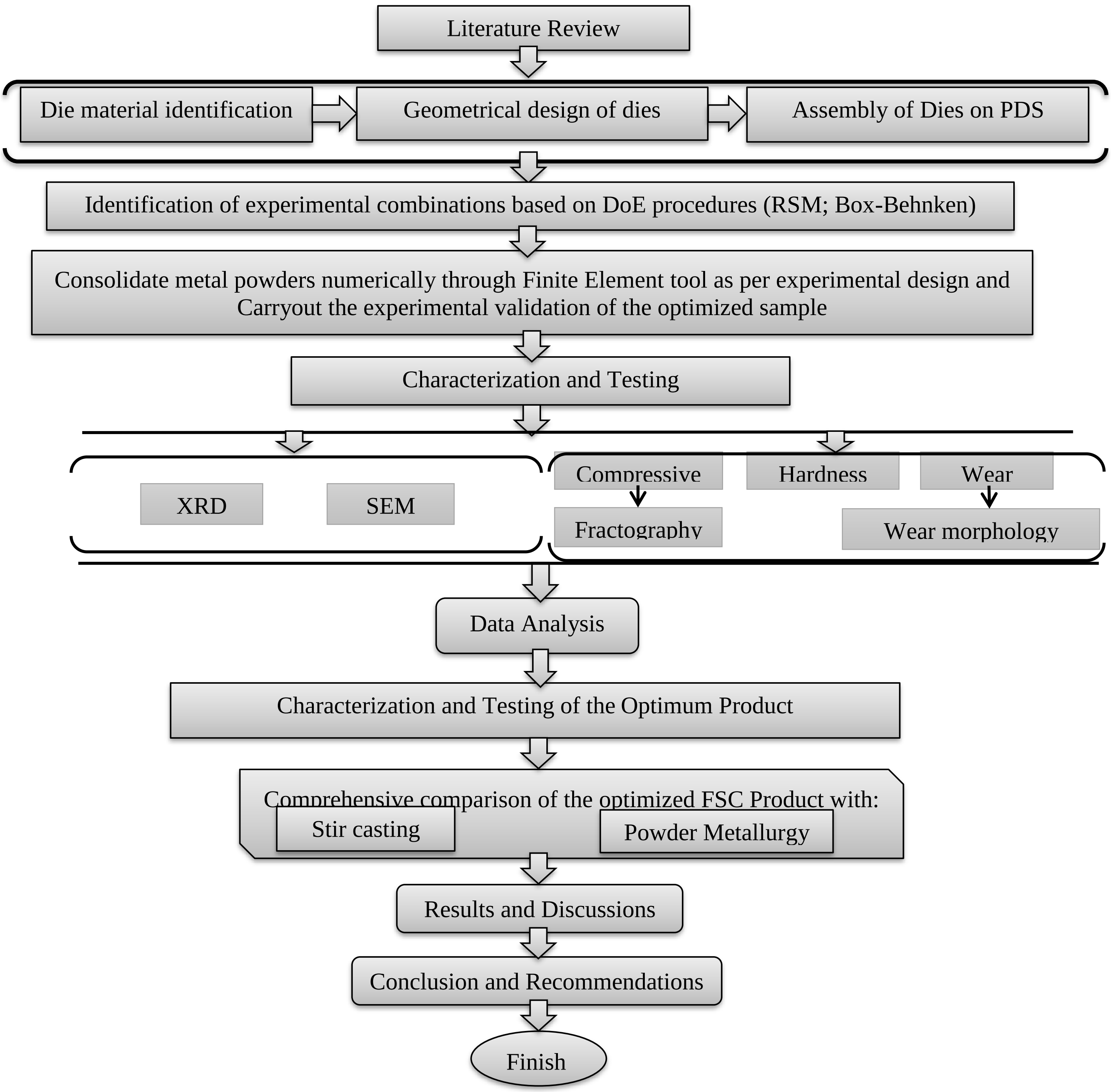

Figure 3.19 The General Flowchart of Methodologies

CHAPTER FOUR

RESULTS AND DISCUSSIONS

4.1 Introduction

This section examines a systematic and thorough exploration of the optimization of process parameters of FSC process using a combination of innovative approaches. The optimization journey began with a comprehensive DEM (Discrete Element Method) simulation of the FSC process. By employing the Box-Behnken design, five pivotal process parameters namely composition, load, speed, thickness, and time systematically varied. The overall objective was to identify the ideal combination of these parameters that would yield the lowest or minimum possible porosity in the resulting composite material. Prior to DEM simulation preliminary experiments were conducted to identify the upper and lower limits of process parameters.

Subsequently, the insights obtained from the Box-Behnken Design-led simulation led to two parallel validation processes: one involving the use of Artificial Neural Networks (ANN) through MATLAB 2014a software and the other employing a Genetic Algorithm (GA) to search for the global optimum for minimum porosity. The purpose of these validation steps was to carefully evaluate the correctness and efficiency of the derived optimization model. Once the global optimum for porosity was determined through the GA, optimum sample was experimentally fabricated via FSC process. The performance of this sample was then evaluated through a number of tests and characterizations, including hardness and compressive strength, Thermogravimetry and wear property providing experimental validation for its porosity property.

Moreover, an additional aspect of improvement was conducted by further optimizing the wear resistance of the optimized sample, representing another dimension of enhancement. This section's discussion will provide insight into how the FSC manufacturing process can be optimized and how the resulting material properties align with the desired characteristics for different applications.

4.2 Preliminary Experiments for Process Parameters' Level Determination

In order to determine the lower and upper limit or ranges of the process parameters such as time, thickness, load and speed; preliminary experiment was carried out at different values until comparable results were obtained as compared to previous studies. While, for the level of process parameter of reinforcement composition, intensive literature review from the previous studies were taken and experimented. Seven different samples were fabricated under different parametric condition of compositions as tabulated in Table 4.1.

Table 4.1 Sample Codes and Their Composition

	Sample codes and their Compositions (%Vol.)						
Materials	1	2	3	4	5	6	7
Matrix (AZ61)	85	90	95	90	90	85	85
Reinforcement (ZrO_2)	7.5	5	2.5	2.5	7.5	10	5
Reinforcement (SiC)	7.5	5	2.5	7.5	2.5	5	10

Figure 4.1 illustrates the successful fabrication of magnesium alloy (AZ61) matrix reinforced with SiC and ZrO_2 hybrid composites using a friction stir consolidation processing technique. In order to prevent the particles at the top surface from becoming at plastic state before the heat dispersed towards the periphery edges, the load was applied, controlled and adjusted. By doing this, the powders at the periphery would receive enhanced heat distribution from friction and consolidation. Within a period of seven minutes, the rotating spindle's applied load was allowed to progressively increase until it reached maximum load of 500N.

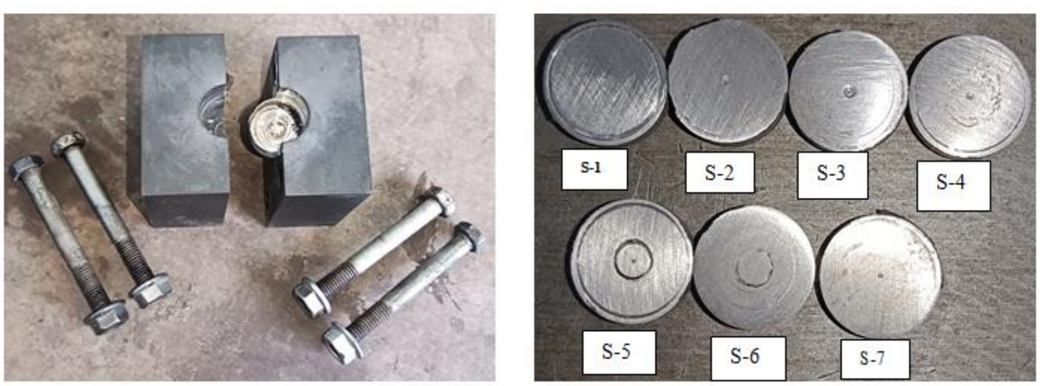

Figure 4.1 Composite Samples Produced by Friction Stir Consolidation Process

4.2.1 Density and Porosity Study

Using the Archimedes principle, as shown in Eq. 39, the experimental density was investigated. Similarly, the theoretical density was calculated using the formula of Eq. 40 (Nayak et al., 2022; Vijayakumar et al., 2022).

$$\rho c = \frac{\rho\, l - W\rho c}{\Delta W \rho c} \qquad \text{eq. (39)}$$

$$\rho_c = \rho r \textit{ (ratio of reinforcement \%)} + \rho m \textit{ (ratio of matrix \%)} + ... \qquad \text{eq. (40)}$$

Where ρ_c is density of magnesium alloy matrix hybrid composite, W ρ_c is weight of magnesium matrix composite in air, ρ_l is density of liquid, $\Delta W\rho_c$ is change of magnesium matrix composite in air and in liquid (Nayak et al., 2022). Where ρ_c is the density of hybrid composite, ρr is the density of reinforcement multiplied by its ratio in percentage volume and prior to calculation of theoretical density, the percentage weight converted into percentage volume of reinforcements. The theoretical, actual density and porosity of the samples have been shown in Table 4.2. The density analyzed theoretically is a higher than the actual density and this result strongly aligns with the previous study (Rangrej et al., 2020).

Table 4.2 Density and Porosity of Samples: Theoretical and Experimental Perspectives

Sample No.	Density g/cm3		
	Theoretical	Actual	Porosity (%)
1	2.196	2.13	3.00
2	2.064	2.003	2.95
3	1.932	1.871	3.16
4	2.002	1.941	3.05
5	2.126	2.065	2.87
6	2.258	2.2	2.57
7	2.134	2.073	2.86

From the friction stir consolidated sample, S-6 had the lowest porosity percentage of 2.57% and the highest porosity at 3.16% of S-3. Consequently, based on previous studies, the metal matrix composite made of Al, Mg, Si, and Bauxite Waste by stir casting method had a minimum porosity of 0.456% and a maximum porosity of 2.225 percent, which appears to be in the ranges of most porosity values (Verma et al., 2019). Additionally, synthesis of Al-Mg metal matrix composite/SiC and Al_2O_3 through powder metallurgy process at different reinforcement volume ratios of (15%-30%) showed that at SiC composition of 15% maximum porosity of 17% and 5.4% were obtained at experimental conditions of 300 MPa, 400 °C for 90 minutes and 600 MPa, 500 °C for 90 minutes respectively proving the current study is preferable for minimum porosity (Tosun & Kurt, 2019). Likewise, a MMC composed of Mg-matrix reinforced with SiC particle showed that Porosity of 10, 20 and 30 wt. % SiC particles samples were 5.94%, 10.28% and 14.42% respectively (Purohit et al., 2018); witnessing acceptability of the obtained porosity level in FSC. This showed that, prior to optimization the FSC process permits less amount of porosity for magnesium matrix composite.

4.2.2 Hardness Property

For the purpose of clear visualization of the effect of FSC process on hardness property, the samples were tested at different surface zones shown in Fig. 4.2a and b. Following ASTM E384-22 standard and by HVS-50 hardness tester considering test force of 10kgf, 10x magnification and dwelling time of 7 seconds. Table 4.3 shows the results of hardness test of the developed samples.

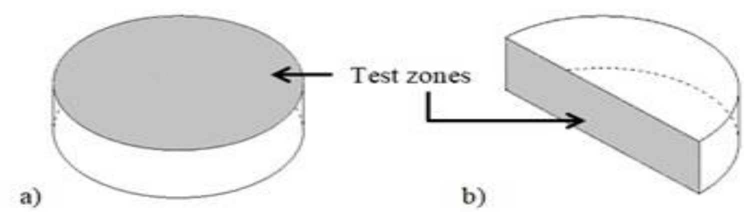

Figure 4. 2 Sample Test Zones A) Top Surface B) Cross-Sectioned Surface

Table 4. 3 Results of Hardness Test

Sample No.	Hardness Result in HV			Hardness in MPa
	Top surface average	Cross-sectioned average	Average	
1	324	318.5	321.76	3155.5
2	315	313.2	314.1	3080.4
3	312	309	310.5	3045.1
4	314	311	312.5	3064.7

5	316	314	315	3089.2
6	323	322	322.5	3162.8
7	324	319.52	321.25	3150.5

Because of the nature of the FSC process, which causes the powders at the top surface to consolidate first and the frictional heat to progressively expand to the perimeter or to the far edge, the need to conduct hardness tests at different cross-sectional surfaces was raised. Consecutively it was found that there was small variation in the hardness values of the sample at different surface zones. Therefore, the mean Vickers Hardness (HV) value was taken into consideration. The hardness result on friction stir consolidated composite samples demonstrated that the hardness value increases simultaneously with the increase of both SiC and ZrO2 reinforcing phases, with the exception of S-7 as shown in Fig. 4.3.

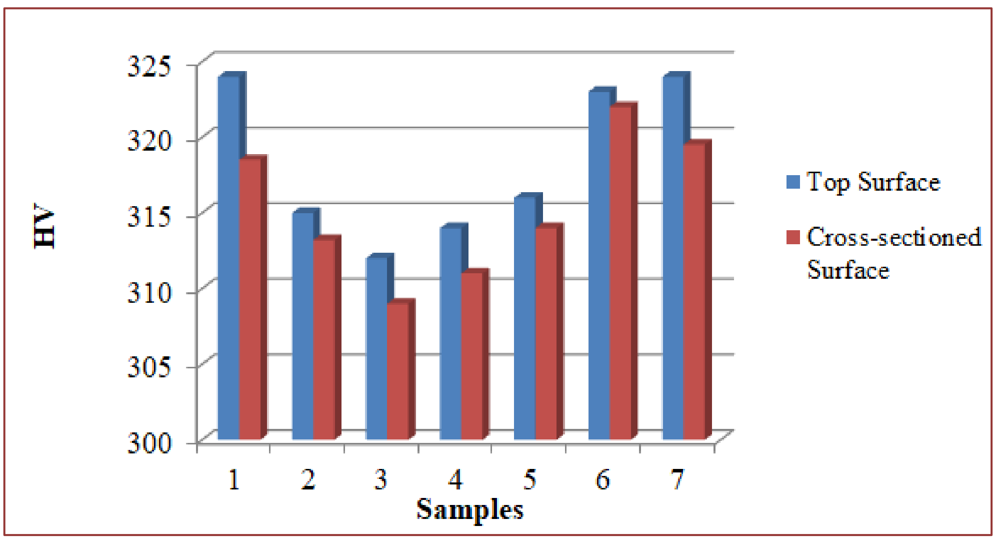

Figure 4.3 Vickers Hardness Results at the Top and Cross-Sectioned Surfaces

The results showed that the hardness values found to be slightly greater at the top surface. This reveals that, in comparison to powders around the perimeter and with those at the point of contact or close to the rotating die, the powders close to the rotating die interaction consolidate more effectively. Similarly, there was comparatively less consolidation at the sample's lower edges.

The sample number S-6 has a greater HV value; this is because SiC and ZrO_2 make up a larger percentage of the sample. Depending on the results, the hardness value increases as SiC and

ZrO_2 do. The hardness of 67 HRB, 86 HRB, and 90 HRB was found in the magnesium matrix reinforced with SiC particles at weight ratios of 10, 20, and 30% respectively; which is equivalent of 120 HV, 175 HV and 190 HV respectively (Purohit et al., 2018). This shows the increment of SiC to the magnesium matrix has a positive impact on the hardness of the MMC. The authors effectively demonstrated how the hardness of MMC rises with an increase in SiC content. However, the hybrid composite sample number S-3 rates lower in HV value; this is because the sample's specific composition, which includes 2.5ZrO_2%Vol, 2.5SiC%Vol, and 95AZ61%Vol, has a contributing influence.

4.2.3 Compressive Strength Study

Universal Testing Machine (UTM) with a maximum capacity of 50 kN was used to evaluate Compressive Yield Strength (CYS) at room temperature with a rate of 50 mm/minute. The result indicated that the reinforcement's composition is significant and plays a critical role. For example, composition ZrO_2 had a significant or noticeable effect on sample S-1, S-3, and S-6 as shown on Table 4.4. The compressive strength of S-6, which possesses higher compressive strength, was primarily influenced by the percentage contribution of SiC and ZrO_2 ($ZrO_2$10%Vol. and SiC5%Vol.) relative to S-3 (ZrO_2 5%Vol. and SiC 5%Vol.). The compressive yield strength increases from 147.51 to 160.4 MPa with an increase in the SiC reinforcement content. The observed increase in CYS from 147.51 MPa to 160.4 MPa with higher SiC reinforcement content aligns with the findings of (Sankhla et al., 2022), who also noted the positive impact of SiC on compressive strength in powder metallurgy-processed composites. The mechanical properties of the composite are influenced differently by the reinforcement materials, SiC and ZrO_2. ZrO_2 is a hard ceramic that improves the material's resistance to compressive stresses; this shows how reinforcement played a critical role. The exceptional strength and hardness of SiC adds even more to the total strength of the composite.

Table 4.4 Compressive Yield Strength to Weight Ratio of the Samples

Sample No.	1	2	3	4	5	6	7
CYS (MPa)	162.5	152.8	147.51	149.9	153.4	164.2	160.4
Actual Density (g/cm^3)	2.13	2.003	1.871	1.941	2.065	2.2	2.073
Strength to Weight Ratio	76.29	76.28	78.83	77.22	74.28	74.63	77.37
Rank	4	5	1	3	7	6	2

The strength to weight ratio is a critical metric for assessing material performance. Sample S-3 (AZ61 95%Vol., SiC 2.5%Vol., and ZrO_2 2.5%Vol.) achieved the highest strength to weight ratio (78.83), indicating an optimal balance of strength and density. In contrast, sample S-5 (AZ61 90%Vol., SiC 2.5%Vol., and ZrO_2 7.5%Vol.) had the lowest ratio (74.28), highlighting that beyond a certain threshold, increased ZrO_2 content may negatively impact the composite's overall efficiency. According to the obtained results, ZrO_2 has an enormous impact on compressive strength. This is demonstrated by the fact that when ZrO_2 composition increases, the Compressive Yield Strength (CYS) increases proportionally, with the exception of cases where CYS is between 5-7.5 %Vol. of ZrO_2; it is clearly shown from the Figure 4.4 that the effects of ZrO_2 and SiC. With the exception of a composition of 7.5 %Vol. of SiC, the effect of SiC is similarly directly proportional to compressive yield strength.

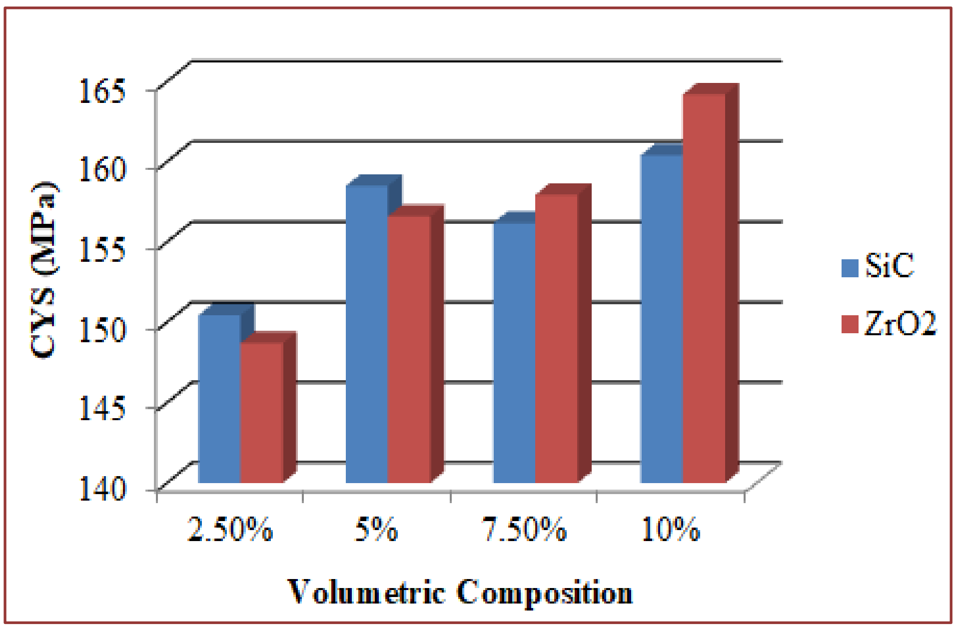

Figure 4.4 Effects of Reinforcements on Compressive Yield Strength

4.2.4 SEM Image Fracture Analysis

For fracture analysis the best sample (S-3) with the highest strength to weight ratio was proposed. To examine the fracture pattern, SEM was employed. Figure 4.5 demonstrates that during the compressive test, there were several different types of fracture or failure. SEM assessment confirmed the existence of crack propagation, dimple fracture, and crack development without plastic deformation. The micro-scale defects, such as inclusion and localized strain discontinuity were the cause of the cracks that developed without exhibiting plastic deformation. Researchers found that materials' excessive exposure to stress caused brittle fracture (no plastic deformation) and that inclusions and strain discontinuity caused unexpected catastrophic fracture (Ardebili & Pecht, 2009).

Figure 4. 5 SEM Fractography Observation of S-3 A) Longitudinal Surface B) Cross-Sectioned Surface

4.2.5 Summary of Preliminary Experiment

The preliminary experiments were aimed to determine the effects of various parameters such as speed, load, thickness, composition and time on the properties of friction stir consolidated samples. These properties include density, hardness, porosity, and compressive strength. The experiment involved a fine-tune range of values for each influential factor:

1. Speed: Varied between 100 and 1250 RPM
2. Load: Ranging from 100N to 900N
3. Thickness: Samples with thickness varying from 12mm to 20mm
4. Time: Processing times from 5 to 9 minutes
5. Composition: From 5 %wt (2.5SiC and 2.5 ZrO_2%wt) to 15 %wt (7.5SiC and 7.5 ZrO_2%wt).

In order to observe the hardness properties of the consolidated samples within these ranges and determine the upper and lower limits that align with existing literature values, it is important to compare the results obtained within these limits to ensure they meet or align closely with the established values in previous research. The upper and lower limits for these parameters, prior to any optimization, were established by the comparison of the experimental hardness results with the hardness properties reported in previous research. For every parameter, the following points could be raised in relation to the results obtained:

Speed (RPM)*:* The varying speed of 150 to 1200 RPM indicates a wide range, affecting the frictional heat generation and the material flow during the consolidation process. The upper and lower limits were chosen to cover both ends of the spectrum to observe the impact on hardness while ensuring that the speed variations were within the equipment's operational capabilities. For this parameter the range from 100-1250 RPM was tuned for an improved property, especially hardness and porosity property. When the speed was adjusted above 800 RPM, the top surface of a compacted sample gets consolidated before the heat distributed to the periphery of the die or sample. The powders at the contact area of rotating die consolidate and plasticized while the powders at the periphery or edge of the chamber remain un-plasticized. The higher the speed resulted in the quicker plasticization of powders. Increased speed demonstrated a marginal positive correlation with compressive strength within the range of 200-800 RPM. Beyond 800 RPM, the consolidation of powders reaches at a state of no change. Therefore, for preliminary experiment the speed was adjusted at constant 500 RPM to identify the other's parameter levels.

Load (N)*:* The load applied during consolidation, ranging from 100N to 900N, reflects the force exerted on the mixed powder. Within the load bearing capacity of the milling machine, these limitations were set to examine the hardness response under varying stress levels, covering the range from lower to higher loads. The fine-tuned 500N load found to be best to consolidate samples within favorable range of hardness property.

Thickness (mm)*:* Prior to sample consolidation, the height or thickness of the die chamber filled with loose powder was measured between 12 and 20 mm. It was found that this range greatly influenced heat dissipation and material flow. The range was selected to investigate the effects of thickness variations on hardness properties. Therefore, the median value 16mm was chosen to identify the impact of compositions for the preliminary experiment. Die Fill Level, in which the powders are permitted to fall into the empty chamber, was taken into consideration while measuring or quantifying the height or the thickness of a pre-consolidated powder.

Time (Minutes)*:* Processing times from 3 to 7 minutes indicated the duration of the consolidation process. The range covered different durations to observe the impact of time on the material properties, specifically hardness. The upper and lower limits ensured a comprehensive understanding of how time affected hardness within an actual processing time span.

Composition: At S-6, the compressive yield strength of 164.2 MPa was attained with a composition of 85% AZ61, 10% ZrO_2, and 5% SiC. When the die was rotated for seven minutes with a composite composition of 95% volume of AZ61, 2.5% volume of ZrO_2, 2.5% volume of SiC, and 500 N Load, sufficient heat was produced to cause powder consolidation and produce the optimum strength to weight ratio for sample S-3. Likewise, at a composition of 85%Vol. of AZ61, 10%Vol. of ZrO_2, and 5%Vol. of SiC, the highest Vickers hardness value was obtained on S-6 about 322.5 HV (3162.8 MPa).

This experiment is crucial in determining the initial feasibility of the parameters studied and providing a baseline for subsequent optimization, ensuring that the produced samples align well with existing literature values for hardness and other listed properties. Generally, preliminary experiments were successfully conducted and the following upper and lower limits of process parameters tabulated in table 4.5 were chosen for subsequent optimization.

Table 4. 5 Parametric Levels Determined Through Preliminary Experiments

Parameters	Units	Codes	Levels		
			Low	Medium	High
			-1	0	1
Composition	%wt	X_1	5	10	15
load	N	X_2	400	450	500
Speed	RPM	X_3	200	500	800
Thickness	mm	X_4	12	16	20
Time	Min.	X_5	4	5	6

4.3 Particle Size Distribution Analysis

Particle size distribution analysis is a necessary step prior to DEM simulation and MMC sample fabrication using the FSC method. It is also essential to conduct a particle size distribution analysis prior to sample fabrication in order to guarantee that the final composites fulfill the required performance standards and material attributes in relation to previous studies. Moreover, it is helpful to be aware of how the sample was produced and under what conditions. The position of FSC process investigated based on the circumstances of Figure 4.6, which presents, as received particle size distribution of a) SiC b) ZrO_2, c) AZ61 and d) mixed powder after ball milling operation, the average sizes of particulates are close to ≈17 µm, ≈15 µm, ≈130 µm and ≈91µm respectively.

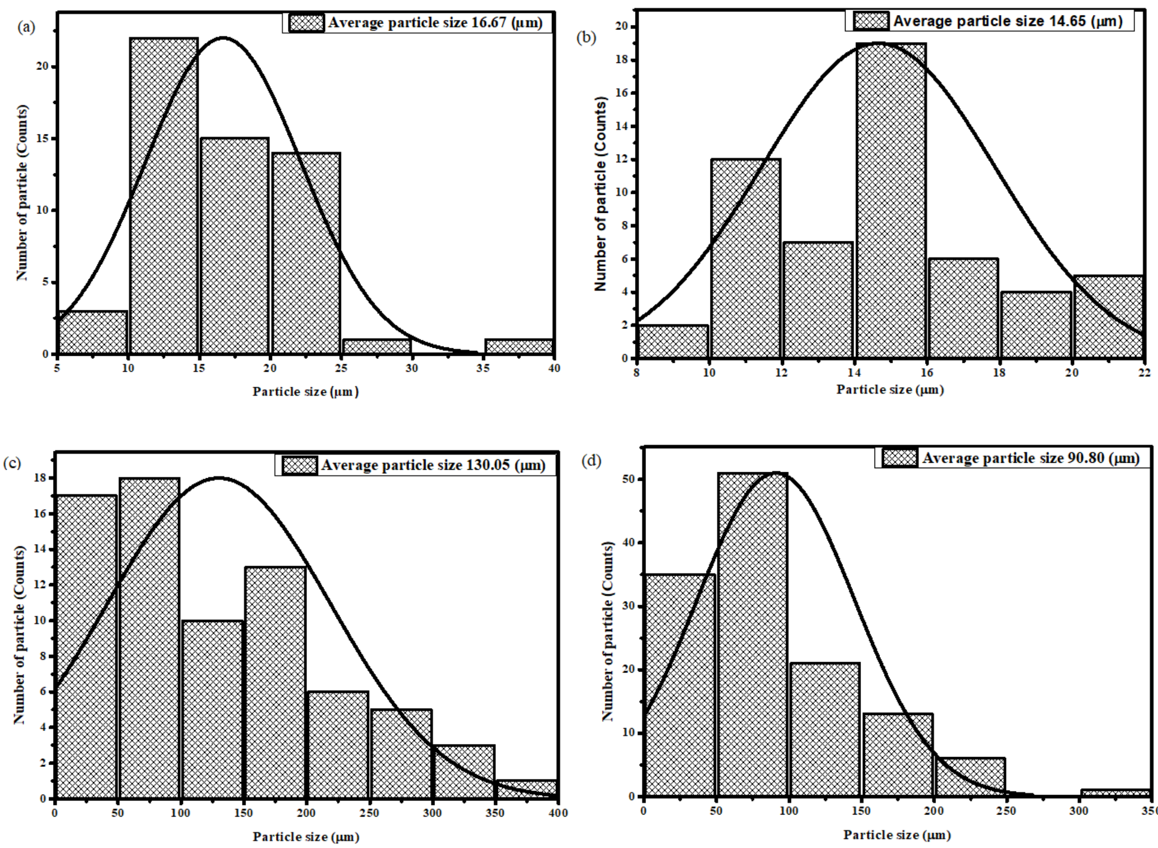

Figure 4. 6 Particles Size Distribution of (A) SiC, (B) ZrO_2, (C) AZ61 Of As-Received Particles and (D) Mixed Powder After Milling.

The particle size in Metal Matrix Composites (MMCs) has a significant impact on their mechanical, thermal and physical properties. The specific effects can vary depending on the material system and the intended application areas of the composite. However, in general, the particle size can influence properties such as strength, hardness, toughness, wear resistance, and thermal conductivity of the MMC (Gad et al., 2021; Cerit et al., 2008). According to previous studies and investigations the larger particles improves toughness by creating more crack deflection and bridging mechanisms, which can improve resistance to crack propagation; while the finer particles tend to improve the wear resisting properties of an MMCs by creating a harder surface and reducing abrasive wear. The fine particles can act as abrasive particles themselves and can also enhance the wear resistance of the matrix material.

Previous researches by Hosseini et al., (2010), exposed the tribological properties of Al6061 matrix composite reinforced with Al_2O_3 at particle sizes of 30nm, 1 μm and 60μm at an operating conditions of 20N load, 0.08 m/s speed and 1000 sliding distance which was fabricated through powder metallurgy process. Their result depicted that the primary wear mechanism was abrasion wear. Moreover, as the particle size increases; low density, low hardness and higher wear rate were obtained. In addition to this, (Hassan, 2006) investigated the effect of particle size on the Magnesium matrix composite reinforced with Al_2O_3/Y_2O_3, and ZrO_2 at different sizes (Nano, 0.66vol%; 0.3μm, 0.66vol%; 1μm, 0.66vol %). They obtained, as particle size decreased, the yield strength and ductility increased. Likewise, the fracture resistance has also improved significantly for smaller particle sizes.

4.4 Computational Results

The DEM numerical simulation results of the friction stir consolidation process offer a comprehensive understanding of FSC process. Employing the RSM Box-Behnken model with five influential factors namely load, rotational speed, thickness, time and composition. A total of 46 simulation experiments were carefully conducted. This approach enables a systematic exploration of the parametric effects on the porosity of a consolidated specimen. By analyzing the porosity results tabulated in the Table 4.6, valuable insights can be raised how variables such as applied load, rotational speed, workpiece thickness, process duration, and material composition collectively impact material flow dynamics and porosity of the consolidated structure.

Table 4. 6 Interaction among Different Particles

Interaction Number	Materials Interactions	Interaction Behaviors		
		Coefficient of restitution	Coefficient of Static Friction	Coefficient of Rolling Friction
1	AZ61Vs. AZ61	0.01	0.25	0.1
2	AZ61 Vs. D2	0.01	0.25	0.1
3	AZ61 Vs. SiC	0.01	0.25	0.1

4	AZ61 Vs. ZrO_2	0.01	0.25	0.1
5	D2 Vs. SiC	0.5	0.35	0.1
6	D2 Vs. ZrO_2	0.5	0.35	0.1
7	SiC Vs. SiC	0.5	0.35	0.1
8	SiC Vs. ZrO_2	0.5	0.35	0.1
9	ZrO_2 Vs. ZrO_2	0.5	0.35	0.1

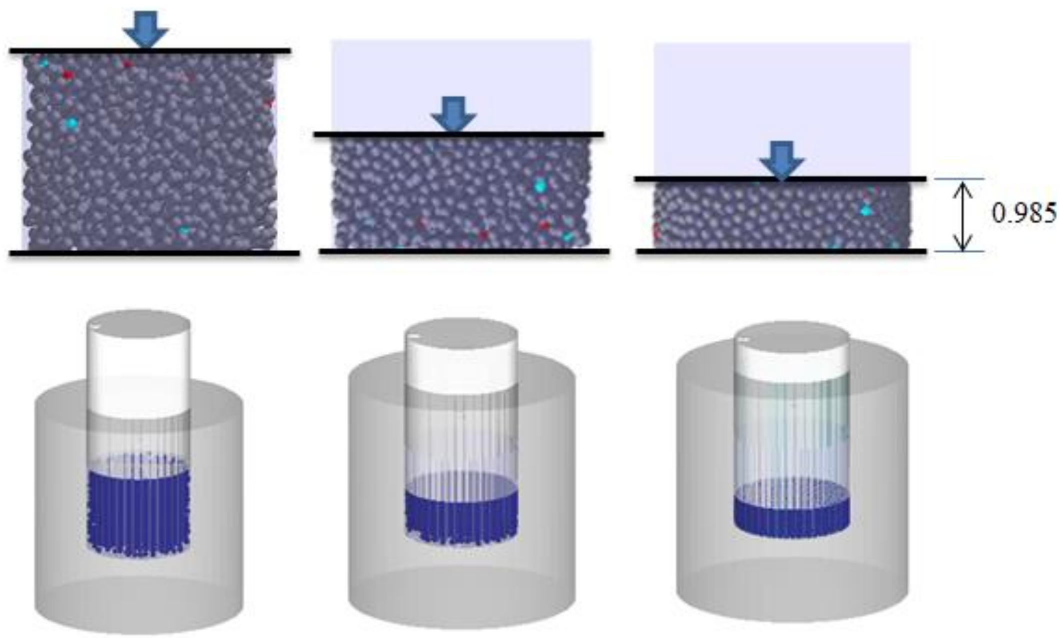

Figure 4. 7 Flow of DEM Simulation for Powder Compaction

From the DEM simulation, results such as height of consolidated powder and volume of powders before compaction were taken into Eq. 34 (described in methodology section) to calculate the porosity. The compaction steps are presented in Fig. 4.7.

$$\text{Porosity (\%)} = 1 - \frac{\text{volume of solid particles in the Die before compaction (at preprocess)}}{\text{volume of the chamber die after compaction (at postprocess)}} \times 100$$

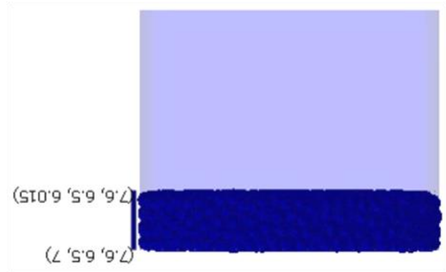

Figure 4.8 Consolidated Powder

The porosities of every simulation were theoretically calculated in such a way that: for instance for experiment number two which result was 1.71%.

The height after compaction was obtained from the DEM software was 0.985mm as shown in Fig. 4.8.

Height of powder after consolidation = 0.985mm = 0.0985cm; Radius of chamber was 2.5mm = 0.25cm; $A = \pi r^2 = (3.14)(0.25cm)^2$; A = (3.14)(0.0625 cm^2) = 0.19625 cm^2; Volume = $\pi r^2 h$; (0.19625 cm^2) (0.0985cm) = 0.019331 cm^3

$$\text{Porosity (\%)} = 1- \frac{\text{volume of solid particles in the Die before compaction (at preprocess)}}{\text{volume of the chamber die after compaction (at postprocess)}} \times 100$$

$$\text{Porosity (\%)} = 1- \frac{0.019}{0.019331} \times 100 = 1.71\ \%$$

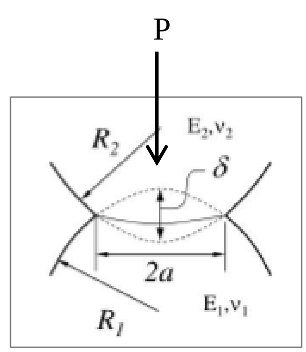

❖ ***Governing equation for DEM (Hertz Contact theory):***

$\delta = \left(\frac{3P}{4E^* R^{1/2}}\right)^{2/3}$ is Interference (Baxter and Bumby, 1995);

❖ ***Contact radius***

$a = \left(\frac{3PR}{4E^*}\right)^{1/3}$; is Contact Radius; $\frac{1}{E^*} = \frac{1-V_1^2}{E_1} + \frac{1-V_2^2}{E_2}$; is effective young's modulus

$\frac{1}{R} = \frac{1}{R_1} + \frac{1}{R_2}$; is effective Radius of curvature (Baxter and Bumby, 1995).

❖ ***Boundary condition:*** These conditions ensure that the spheres remain in contact and satisfy the appropriate force-displacement relationships (Baxter and Bumby, 1995).

- No interpenetration of spheres: $\boldsymbol{\delta \geq 0}$; No separation of spheres: $\boldsymbol{\delta = 0}$ when no contact force is applied, Coulomb friction law for tangential displacement: $\boldsymbol{|\Delta x| \leq \mu\delta}$

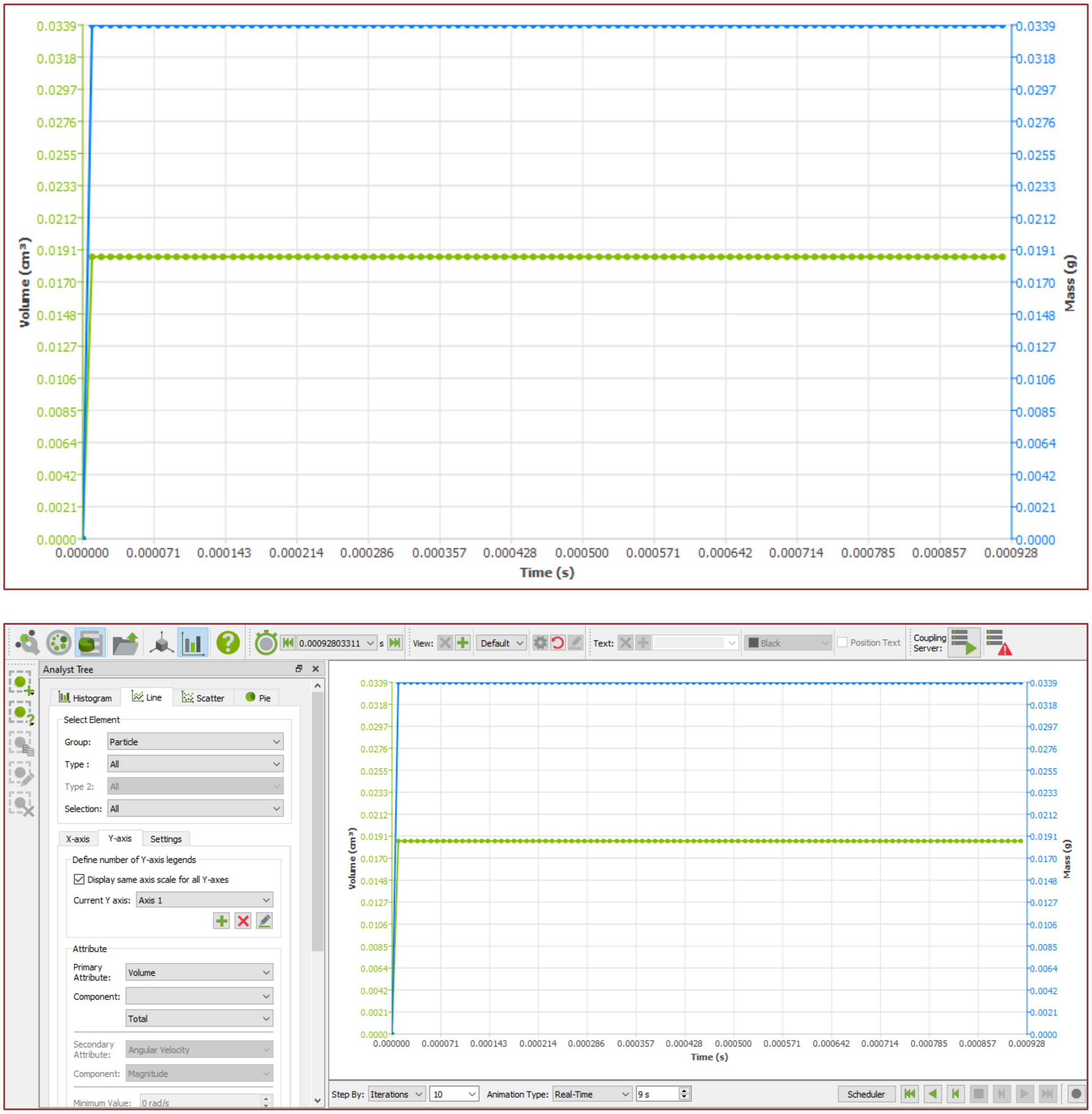

Figure 4. 9 DEM Result Showing Volume of Powders before FSC

The volume and the total weight of powder for every numerical simulation were taken from DEM results presented in the Fig. 4.9.

Table 4. 7 Altair EDEM Simulation Results of Porosity

S. No.	FACTORS					
	SPEED	**LOAD**	**THICKNESS**	**TIME**	**COMPOSITION**	**POROSITY**
1	500	500	16	6	10	0.81

2	500	400	12	5	10	1.71
3	800	450	16	5	5	1.39
4	500	450	20	4	10	2.06
5	500	450	16	4	15	1.56
6	500	500	16	5	15	1.11
7	500	500	20	5	10	1.34
8	200	450	16	4	10	1.92
9	200	400	16	5	10	2.35
10	500	400	16	5	15	1.75
11	500	450	16	6	15	1.15
12	500	400	16	6	10	1.79
13	500	400	16	5	5	1.95
14	500	450	20	5	15	1.54
15	200	450	16	5	5	1.57
16	200	450	20	5	10	1.98
17	500	450	20	6	10	1.61
18	500	400	16	4	10	2.24
19	500	450	12	5	15	1.25
20	500	450	16	5	10	1.40
21	200	450	16	5	15	1.56
22	500	450	16	5	10	1.59
23	500	450	16	6	5	1.24
24	500	450	20	5	5	1.92
25	500	450	16	4	5	1.88
26	800	450	16	5	15	1.31
27	500	400	20	5	10	2.51
28	500	450	16	5	10	1.59
29	500	450	16	5	10	1.68
30	500	450	12	4	10	1.54
31	800	500	16	5	10	1.18
32	200	450	16	6	10	1.54
33	200	500	16	5	10	1.23
34	500	450	16	5	10	1.61
35	800	450	16	6	10	1.28
36	800	450	16	4	10	1.77
37	200	450	12	5	10	1.52
38	500	450	12	5	5	1.22
39	800	400	16	5	10	1.96

40	500	450	16	5	10	1.48
41	500	450	12	6	10	1.22
42	500	500	16	4	10	1.49
43	500	500	16	5	5	1.20
44	800	450	12	5	10	1.27
45	800	450	20	5	10	1.89
46	500	500	12	5	10	0.98

Utilizing DEM numerical simulations, the friction stir consolidation process was comprehensively explored through a series of experiments guided by the RSM Box-Behnken model. Across a total of 46 simulations, a noteworthy finding emerged as the minimum porosity percentage of 0.81% was achieved under specific conditions as presented in Table 4.7. Notably, this minimum porosity obtained at a load of 500N, time duration of 6 minutes, a thickness of 16mm, a composition of 10%, and a rotational speed of 500RPM. These insights notify the potential of DEM simulations within the framework of the RSM Box-Behnken model to guide precise parameter adjustments for enhancing the consolidation process and minimizing porosity.

4.5 Optimizations and Model Validations

Following the determination of process parameters' levels, the initial phase of the study involved optimization using the RSM Box-Behnken design of experiment. This method allowed for a systematic optimization of process parameters, including composition, time, speed, load, and thickness. The primary objective was to minimize porosity, which was considered as the key target function. Through this structured experimentation, relationships between the parameters and porosity were established. This preliminary step laid the groundwork for subsequent model development and optimization strategies.

Following the RSM Box-Behnken design, the study validated the established model using an ANN through MATLAB 2014a. The neural network, a powerful computational tool, allowed for the validation and refinement of the established model. By effectively using the ANN, the accuracy and predictive capability of the model for porosity were rigorously assessed. This step was crucial in ensuring the reliability of the model and its capability to represent the complex relationships between the process parameters and objective function accurately. Upon implementing the verified model, additional optimization was necessary to enhance predictive accuracy and reach the global optimum porosity.

Once the model was rigorously validated, the study progressed to the optimization phase using a GA. This phase aimed to refine the model further and attain a superior predictive capability for minimum porosity. The genetic algorithm, a heuristic search and optimization technique inspired by the principles of natural selection, allowed for the exploration of a broader solution space. By iteratively evaluating and evolving potential solutions, the genetic algorithm tried to search to fine-tune the model, ultimately aiming for a more accurate prediction of minimum porosity and identifying the global optimum. This final optimization step intended to find the overall minimum porosity within the studied ranges of process parameters.

4.5.1 RSM Box-Behnken Process Parameter Optimization

The Response Surface Methodology (RSM) Box-Behnken technique represents a sophisticated approach to optimizing complex systems by systematically analyzing the relationships between variables. Its main advantage lies in efficiently exploring response surfaces while requiring fewer experimental runs than exhaustive methods. The Box-Behnken design consists of three levels for each factor, carefully chosen within a specified range. The approach involves major three-step process: Firstly, a set of experimental runs is designed based on the Box-Behnken matrix. Secondly, responses are measured and used to create a model that approximates the system’s behavior. Finally, this model is analyzed, optimized and verified to identify the factor settings that yield the optimal response. Generally, in the present optimization, the RSM procedure represented in Chapter three as Fig. 3.2 was implemented to reach on the final conclusion (Palanikumar & Davim, 2013).

4.5.1.1 Box-Behnken Response Surface Analysis and ANOVA Table

By removing the terms with low significance after evaluating the significance of the parameters, the model can be improved. For the final mathematical model can better describe the relationship between the five factors and response. Analysis of variance table indicates that the factors having probability value of less than 0.05 considered to be significant and greater probability value depicts that the factor is not significant. Table 4.8 indicates that the five factors are significantly affecting the porosity of the hybrid metal matrix composite.

Table 4. 8 Analysis of Variance Table

Source	DF	Seq SS	Contribution	Adj SS	Adj MS	F-Value	P-Value
Model	15	5.38508	92.91%	5.38508	0.35901	26.22	0.000
Linear	5	5.22140	90.09%	5.22140	1.04428	76.26	0.000
Speed	1	0.16403	2.83%	0.16403	0.16403	11.98	0.002
Load	1	2.99290	51.64%	2.99290	2.99290	218.57	0.000
Thickness	1	1.07122	18.48%	1.07123	1.07123	78.23	0.000
Time	1	0.91203	15.74%	0.91203	0.91203	66.61	0.000
Composition	1	0.08122	1.40%	0.08122	0.08122	5.93	0.021
2-Way Interaction	10	0.16367	2.82%	0.16367	0.01637	1.20	0.333
Speed*Load	1	0.02890	0.50%	0.02890	0.02890	2.11	0.157
Speed*Thickness	1	0.00640	0.11%	0.00640	0.00640	0.47	0.499
Speed*Time	1	0.00303	0.05%	0.00303	0.00303	0.22	0.642
Speed*Composition	1	0.00122	0.02%	0.00122	0.00122	0.09	0.767
Load*Thickness	1	0.04840	0.84%	0.04840	0.04840	3.53	0.070
Load*Time	1	0.01322	0.23%	0.01322	0.01322	0.97	0.334
Load*Composition	1	0.00303	0.05%	0.00302	0.00302	0.22	0.642
Thickness*Time	1	0.00422	0.07%	0.00422	0.00422	0.31	0.583
Thickness*Composition	1	0.04202	0.73%	0.04202	0.04202	3.07	0.090
Time*Composition	1	0.01322	0.23%	0.01322	0.01322	0.97	0.334
Error	30	0.41079	7.09%	0.41079	0.01369		
Lack-of-Fit	25	0.36010	6.21%	0.36010	0.01440	1.42	0.374
Pure Error	5	0.05068	0.87%	0.05068	0.01014		
Total	45	5.79586	100.00%	R^2 = 92.91% and R^2Adj = 89.37%			

The p-value of lack of fit should not be significant (less than 0.05) for the model to be fit with the data well (Abebe et al., 2023). The study of ANOVA table presented in Table 4.8, P-value for lack-of-fit, which is 0.374, reveals the insignificance and informs us that the model fits the data well (Lahlali et al., 2008b). ANOVA result showed that all the process parameters are significant with a p-value less 0.05. Likewise, based on the response optimization predicted by RSM analysis, the optimum parametric condition or setup for the minimum porosity of 0.62% is presented in the Table 4.9 and Figure 4.11. Furthermore, the ANOVA table witnessed that the load has the highest percentage contribution as high as 51.64% towards the response. This implies that the porosity result would be greatly affected by variations in load. Similarly, next to load, the thickness parameter contributed the second-highest percentage of 18.48%.

Conversely, the porosity was least affected by the composition, with a minimum impact of 1.40% contribution.

Table 4. 9 Optimum Parametric Setups Predicted by RSM

Factors				
Speed	Load	Thickness	Time	composition
800	500	12	6	5

The optimum parametric condition or setup predicted by RSM is indicated for each process parameter, shown in the Fig. 4.10. With the exception of speed, time and load, each variable's optimum process parameter level was chosen to be at its lowest possible value with the desirability value of d= 1.00000 (Nampi & Das, 2020). Where, d and y are desirability value and response respectively (Baloyi et al., 2022).

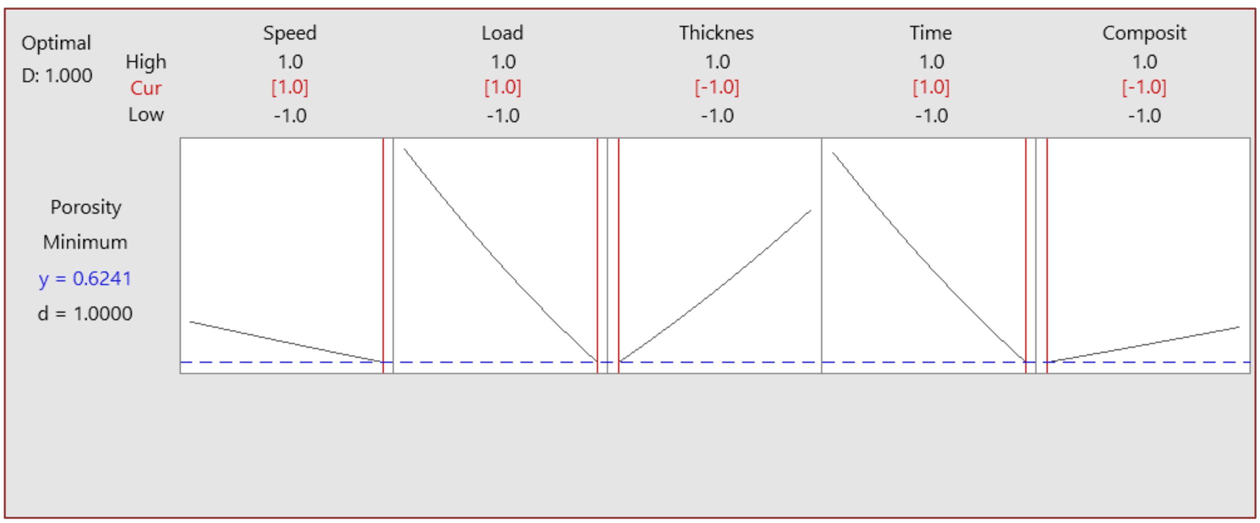

Figure 4. 10 Optimized Parametric Levels for Minimum Porosity

Each factor is varied between low (-1.0) and high (1.0) levels. The red lines marked "Cur" indicate the current settings for each factor, all set to their high values (1.0), except for Composition, which is at its low value (-1.0). For instance, Porosity Minimum (y = 0.6241) represents the minimum porosity achieved in the optimization process. Desirability (d = 1.0000) indicates that the optimal conditions for minimizing porosity have been achieved under the given settings. For instance as speed increases from -1.0 to 1.0, porosity decreases. The current level (1.0) seems optimal as it contributes to minimizing porosity.

Surface plots illustrate the relationship between two independent variables and the chosen dependent variable (Porosity) instead of referring to particular data points. The three major influencing parameters were selected for surface plot as provided in Fig. 4.11a, 4.11b and 4.11c. Surface plot of porosity versus time and load in Figure 4.11a clearly depicts the influence of load, which is when the load is at lower level the variation in porosity is higher regardless of the time whether it is at low, mid or higher levels. The porosity value remains largely between 1.5 and 2.00% at every levels of time and when the load kept constant at its lower level. However, at the higher level of load the porosity value shows below 1% at every specific levels of time. Generally, the surface plot witnessed minimum porosity value at higher levels of load and time. Similarly, Fig. 4.11b shows the surface plot of porosity vs thickness and load. The porosity value gets close to 2.5% at higher thickness value and lower value of load. Conversely, the porosity value estimated to be less than 1% at higher load and lower thickness this shows load and thickness has indirect relationship towards the response.

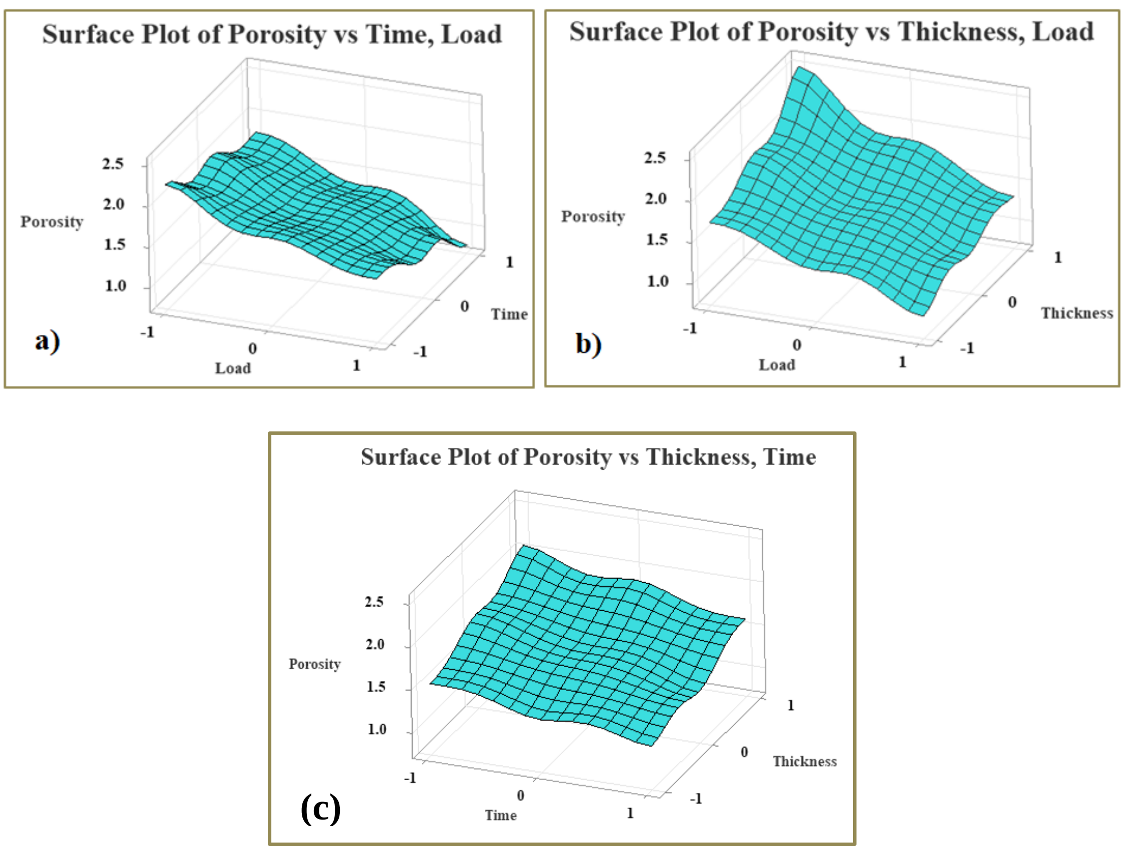

Figure 4. 11 Surface Interaction Plots of Porosity versus the Three Most Significant Factors a) Time and Load b) Thickness and Load c) Thickness and Time

The surface plot of porosity versus thickness and time presented in Fig. 4.11c shows the interrelation impact of thickness and time towards porosity. The lower level of thickness and higher level of time resulted in minimum porosity and vice versa. The slope of the edge of the surface to the side of thickness shows the impact of thickness is greater than time parameter.

Generally, the surface plot witnessed that the minimum porosity value could be found at higher level of time and higher level of load. In addition to this, lower thickness level combined with higher load level could also be preferable in achieving lesser porosity.

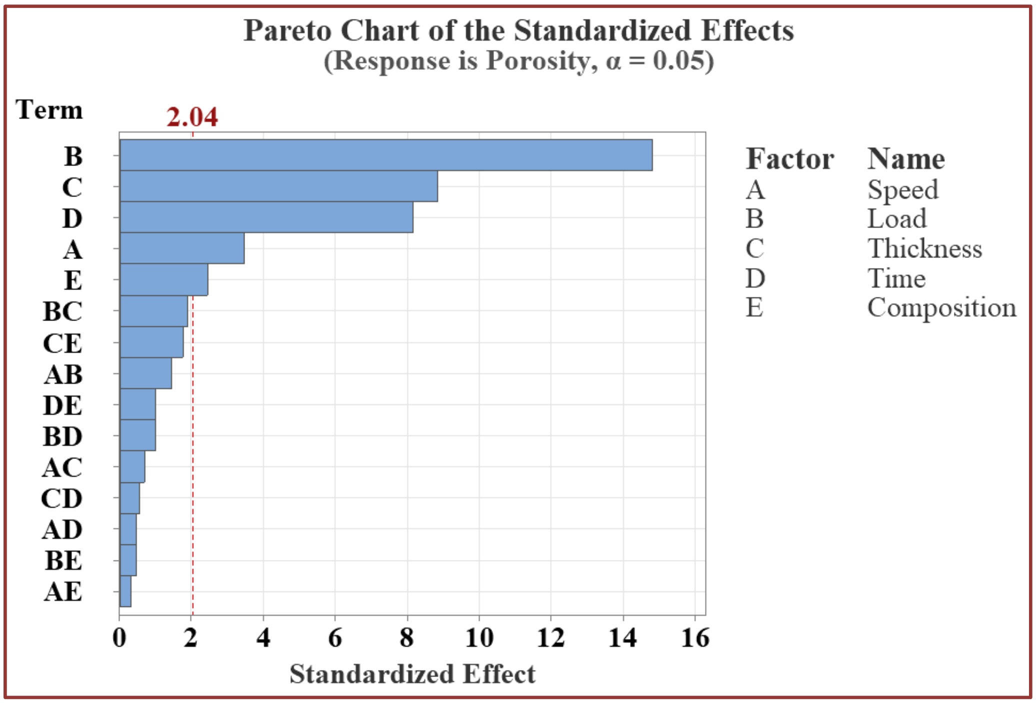

Figure 4.12 Pareto Chart of the Standardized Effects

The Pareto chart presented in Fig. 4.12 depicts the significance and insignificancy of the process parameters and the corresponding interaction effects on the Porosity. This strengthens the ANOVA table results which determined the significance of each process parameters. The bars past the hidden line at 2.04 indicate the significant contribution of the process parameters towards the Porosity statistically at 5% significance level (Nampi & Das, 2020; Minitab ® 21 Support, 2023).

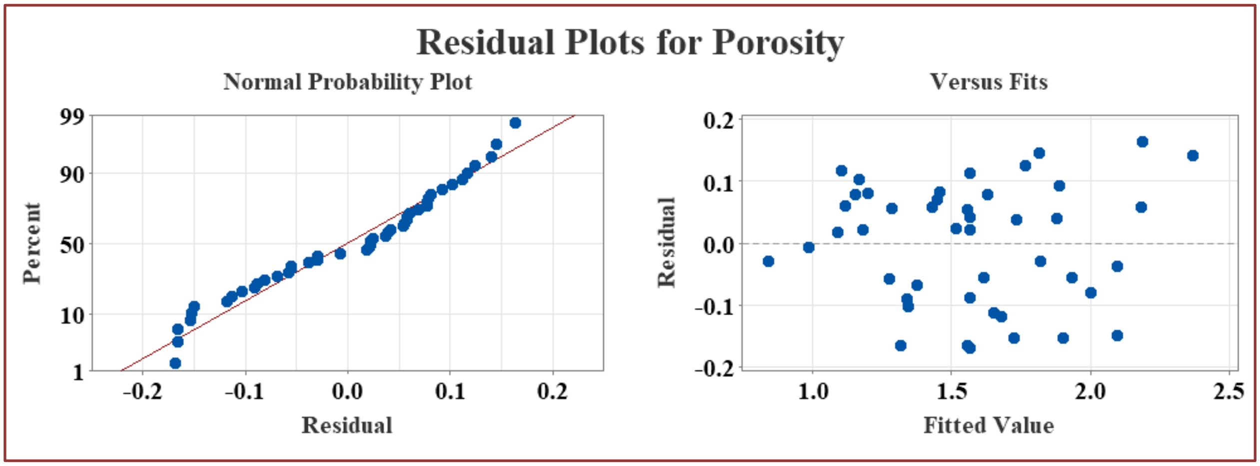

Figure 4.13 Residual Plot for Porosity

According to Das et al. (2018), the results shown in Figure 4.13 show that the probability plot of residuals remained noticeably close to the straight line, demonstrating the normal distribution of errors and the regression model's good fit to the observed results. Furthermore, with a result variation of between -0.18 and 0.18, Figure 4.13 demonstrated the excellent agreement between observed and fitted values.

4.5.1.2 Regression Model

The regression equation estimates how the input variables (Speed, Load, Thickness, Time and Composition) and response are related (porosity) (Abebe et al., 2023). The regression equation represented in Eq. 41 was obtained from RSM-BBD approach by statistical software MINITAB 19. Three distinct parametric combinations from RSM Box-Behnken were randomly selected in the verification experiment to confirm the accuracy of the developed regression model; these combinations were not present in the RSM-BBD experimental design matrix. With these three different and random experimental combinations experiments were conducted to verify the consistency of the regression model. Based on the findings of confirmation experiments in Table 4.10, the porosity obtained experimentally and those predicted using the regression model only differ considerably with a small margin. Error percentage of less than 5% obtained for all of the experiments, this shows that the developed regression model well predicted the porosity for the given ranges of experimental study.

$$\text{Porosity} = 1.5683 - 0.0712\, x_1 - 0.4325\, x_2 - 0.1013\, x_3 + 0.2588\, x_4 - 0.2388\, x_5 \qquad \text{eq. (41)}$$

Where, porosity is in %, x_1 is composition in %wt, x_2 is load in n and x_3 is speed in rpm, x_4 is thickness and x_5 is time. Verification experiment results showed in Table 10 depicted that the consistency and reliability of the regression model with error percentage of 4.17%, 1.92% and 3.7% for experiment number of 1, 2 and 3 respectively.

Table 4.10 Verification Experiment

Factors						**Verifications**		
S.No.	Speed	Load	Thicknes	Time	Comp.	Regression	Experimental	Error
1	800	500	16	6	15	0.72%	0.75±0.02	4.17%
2	200	400	12	4	10	2.08%	2.12±0.015	1.92%
3	500	450	20	5	5	1.89%	1.96±0.02	3.7%

The verified regression equation in the Table 4.10 stands as a witness to the precision and accuracy of the analytical process. Moreover, the identification of an error rate of merely 4.17% underscores the effectiveness of the analysis. This negligible margin of error attests to the robustness of both the methodology employed and the equation itself towards porosity determination. Figure 4.14 shows the FSC fabricated specimen based on optimum parametric setups predicted by RSM.

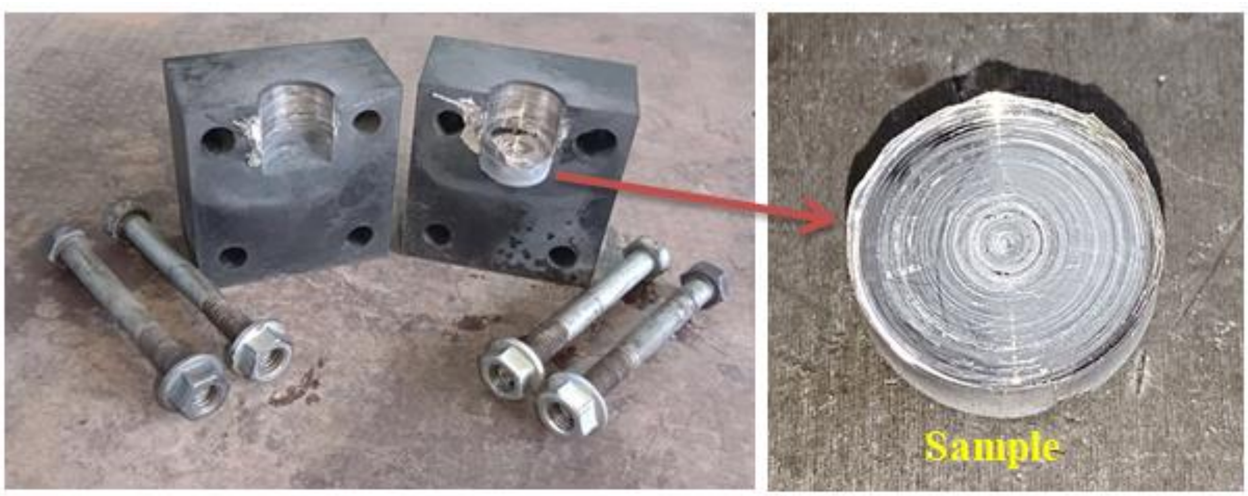

Figure 4.14 Friction Stir Consolidated Specimen Fabricated Based on Optimum Parametric Setups Predicted by RSM

The experimental verification results of the friction stir consolidation process have been consistently predicted by the regression model used in this study, which has shown to be significantly precise and reliable. The regression model validation was established by means of thorough verification, resulting in an exceptionally low error percentage of less than 5%. This result highlights the stability and suitability of the regression model for precisely predicting the experimental values related to the friction stir consolidation process. The performance of the regression model is quite impressive when considering the complex interaction of process parameters with one another. The effectiveness of the model to closely match the experimental results shows its efficiency in capturing the complex interaction between input process parameters and output responses (Porosity) in FSC process. Moreover, the use of advanced statistical methods and a large set of data can be attributed for the effectiveness of the regression. Similarly, the precision and reliability of the regression model have been enhanced through the integration of significant process parameters in conjunction with advanced optimization techniques. Likewise, achieving an error percentage below 5% highlights the robustness of the regression model practically or in real-world scenarios and shows its ability to generalize significantly beyond the training data or the design matrix. Previous researchers investigated experimentally and found verification experiment error of less than 5% and concluded as the extrapolation of the model as reliable (Bose, 2023).

The experimentally verified regression model uses as a valuable reference for researchers and engineers seeking to optimize and further investigate the FSC process. The model's precision, as demonstrated in the minimal error percentage (< 5%), strengthens its reliability and applicability, thereby opening the door for developments of materials in the field of materials processing techniques.

4.5.2 Artificial Neural Network Model Validation

The artificial neural network approach's basic concept is related to the manner in which the human brain functions (Altinkok & Koker, 2006). It is also environment-adaptive given the inputs and desired outputs, allowing it to react to various inputs parameters logically. The 10 hidden layers was filled with several neurons needed for enhancing the output value's prediction quality (Sanjeevi et al., 2020), as shown in Figure 4.15. Levenberg-Marquardt training was selected to determine the minimum of a function (Either linear or nonlinear) over a range of parameters ("CUDA for Machine Learning and Optimization," 2011). Levenberg-Marquardt training algorithm was used to randomly select 32 samples (70%) for training, 7 samples (15%) for validation and 7 samples (15%) for testing out of 46 samples.

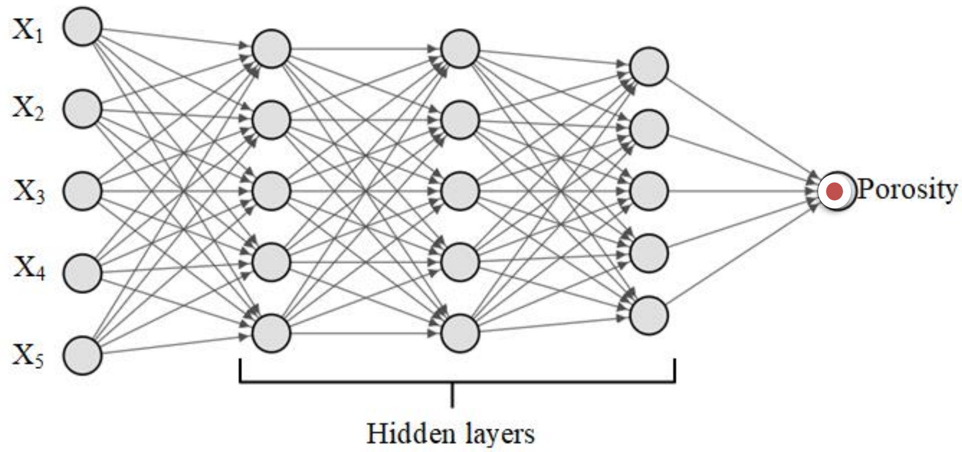

Figure 4.15 General Hidden Layer Architecture of ANN Showing Coded Input Variables and the Porosity Output

The results obtained from the RSM Box-Behnken optimization and model validation through MATLAB R20142a artificial neural network showed that friction stir consolidation is a promising technique for the fabrication of metal matrix composite with low porosity. The optimization of the FSC process parameters using RSM Box-Behnken design resulted in a significant reduction in the porosity of the MMCs. Figure 4.16 shows the schematic diagram of hidden layers where w (Weight) and b (Bias) affect the output of the process parameters.

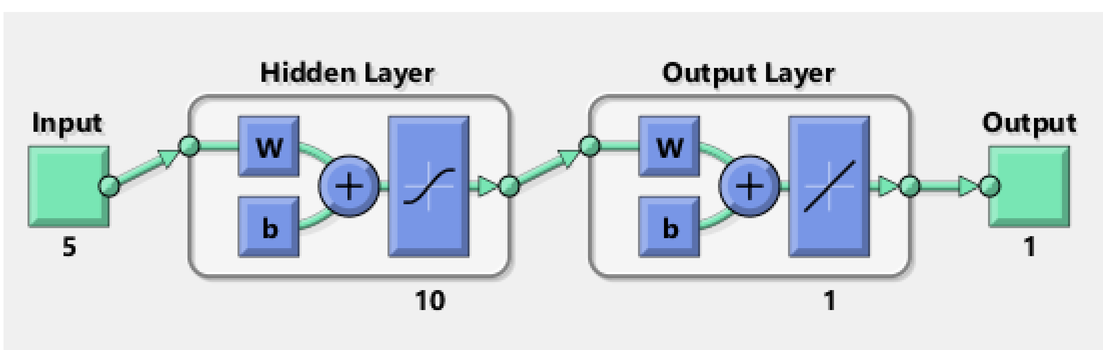

Figure 4.16 Schematic Representation of Hidden Layers

The validation of the RSM Box-Behnken model using the MATLAB R2014a artificial neural network showed that the model was accurate in predicting the porosity response of the MMCs to a higher correlation coefficient of R = 0.97333 as compared to RSM's R = 0.9291. This witnessed the fitness of the model towards the data. The regression plot in Fig. 4.17 demonstrated that the model had a high degree of accuracy to the unseen data with Training: R= 0.99356, Validation: R = 0.86149, Test: R = 0.89981 and the average over all: R = 0.97333 in predicting the porosity response of MMCs. This indicated that the FSC process can be used to produce MMCs with low porosity using optimized parameters additionally it insures to what extent the model developed was valid. The improvement in correlation coefficient from RSM's 0.9291 to ANN's 0.97333 indicates that the ANN model provides a more precise optimization framework for predicting and minimizing porosity in MMCs.

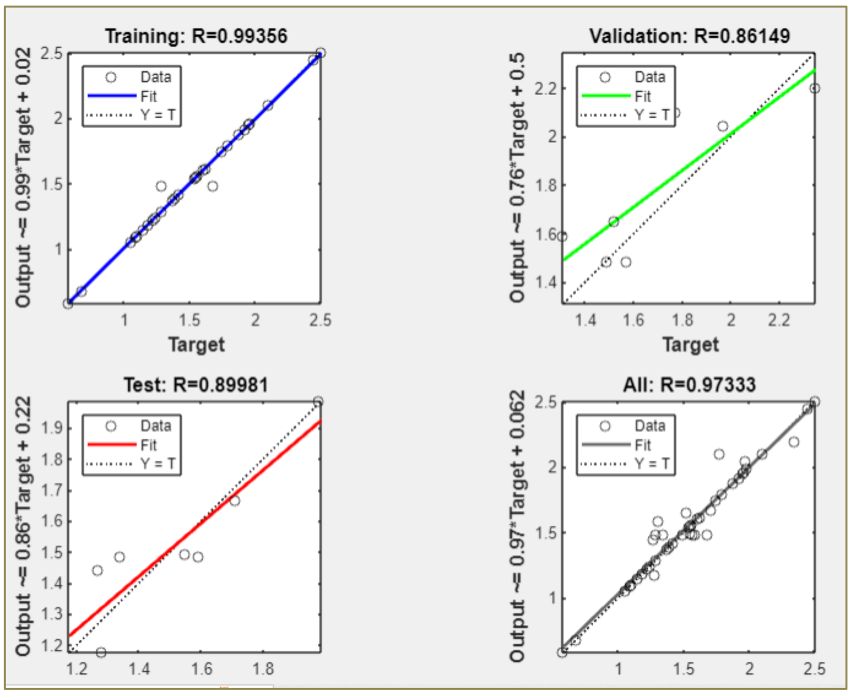

Figure 4.17 Regression Plot Training, Test and Validation performances

The Artificial Neural Network (ANN) model underwent validation to assess its performance, and the best validation performance was achieved at epoch 4, with a remarkably low value of 0.034183. This result holds significant implications and insights into the model's capability and behavior. The validation performance is often used as an indicator of how well the trained model generalizes to unseen data. Achieving a validation performance of 0.034183 in Fig. 4.18 suggests that the model is capable of making highly accurate predictions on new data samples.

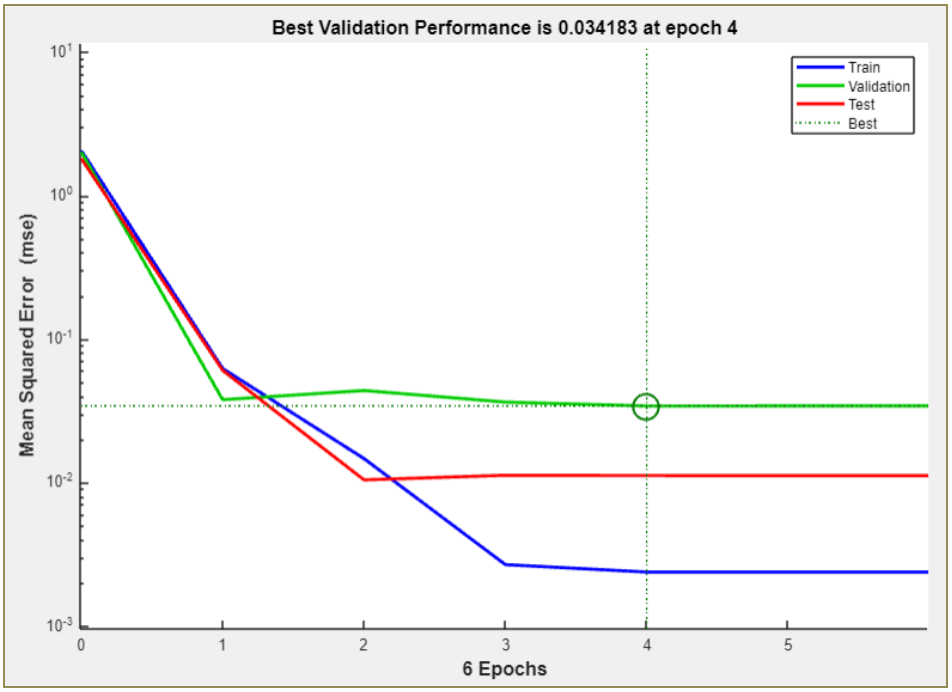

Figure 4.18 Validation Performance Plot

The fact that the best performance was achieved at epoch 4 indicates that the model was able to converge and achieve a strong level of generalization quite quickly. This suggests that the model's architecture and training process were well-suited for the dataset, enabling efficient learning of underlying patterns. While the model demonstrated impressive validation performance at Epoch 4, it is worth considering whether additional training epochs might lead to even better results. However, the rate of improvement beyond this point should also be evaluated, as excessive training could lead to over-fitting.

4.5.3 Genetic Algorithm Optimization

Genetic Algorithm stands as a robust optimization technique inspired by the principles of natural selection and genetics. At generation 221, the Genetic Algorithm shown in Figure 4.19 has converged to a solution with a fitness value of 0.469 with the parametric combinations given in Table 4.11. The fitness value represents the quantitative assessment of how well a solution performs with respect to the defined optimization criteria. The fitness function presented in Eq. 42 and the constraints taken for each process parameters are as follows:

Constraints: $5\%\text{wt} \leq X_2 \leq 15\%\text{wt}$

$400\text{N} \leq X_2 \leq 500\text{N}$

$200\text{RPM} \leq X_3 \leq 800\text{RPM}$

$12\text{mm} \leq X_4 \leq 20\text{mm}$

$4\text{min.} \leq X_4 \leq 6\text{min.}$

$$\textbf{\textit{Fitness Function}} = 1.5683 - 0.0712X_1 - 0.4325X_2 - 0.1013X_3 - 0.2588X_4 - 0.2388X_5 \quad \text{eq. (42)}$$

Table 4.11 Optimum Parametric Setups Predicted by GA

Factors				
Speed	Load	Time	Thickness	composition
800	500	6	12	15

In this study case, a lower fitness value indicates a better solution. The fitness value of 0.469% porosity suggests that the algorithm has made substantial progress in finding a solution that satisfies the objectives of the problem as compared to RSM's 0.62% porosity.

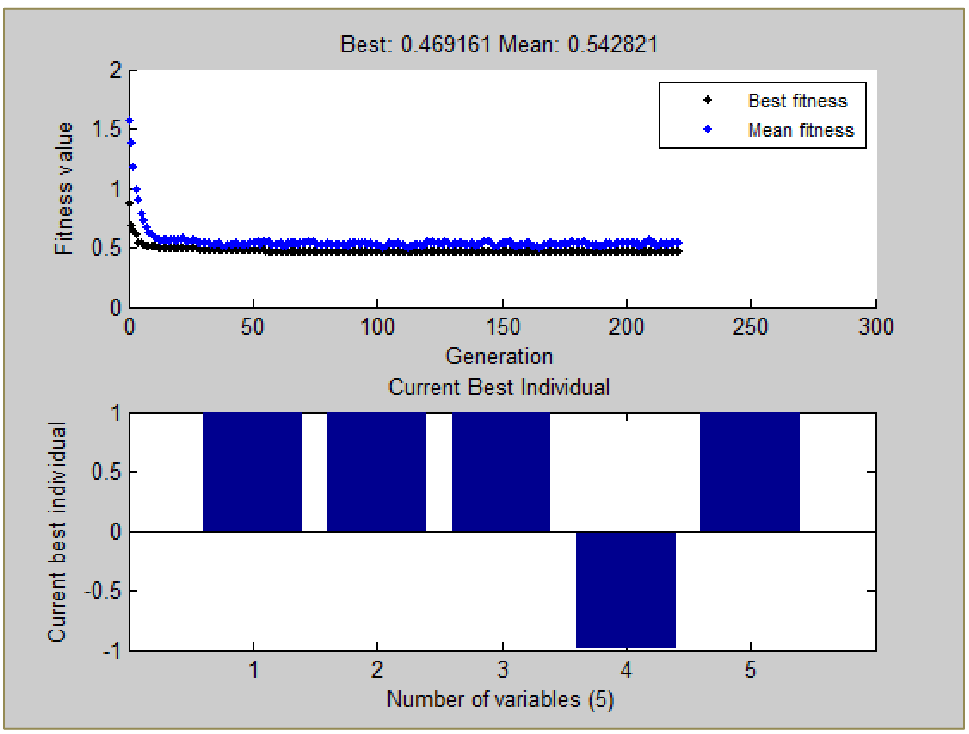

Figure 4.19 Genetic Algorithm Plots for Porosity

The convergence rate, as evidenced by reaching a fitness value of 0.469, is indicative of the algorithm's ability to explore and exploit the solution space effectively. At generation 221, the algorithm has refined in on a solution that significantly improves upon previous iterations. This implies that the algorithmic parameters, such as crossover, mutation, and population size, have been well-tuned to promote a balance between exploration of diverse solutions and exploitation of promising regions in the solution space.

4.5.4 Genetic Algorithm and RSM Optimum Conditions and Confirmation Tests

It is interesting to observe that both RSM and GA predicted the same optimal values for rotation speed, applied load, thickness, and time of consolidation for the porosity yield. This relationship would suggest that these parameters strongly affect the consolidation process and that the optimization scenario for these variables is preferably well-defined. However, there is a noticeable difference between the predicted optimal compositions from the two techniques. RSM suggests a composition of 5%, while GA suggests a composition of 15%. This could be attributed to the inherent differences between the two optimization methods. RSM relies on mathematical models and assumes a certain functional relationship between variables, whereas GA is more exploratory and can discover solutions that might not be apparent from the mathematical model alone. Optimum porosity predicted by RSM and GA are tabulated in Table 4.12.

Table 4.12 Optimum Porosity Predicted by RSM and GA

			Verification through		
S.No.	Techniques	Porosity	Regression	Experimental	Exp’tal variation
1	RSM	0.62	0.61	0.69±0.05	0.08
2	GA	0.469	0.21	0.51±0.04	0.041

It is crucial to understand that the optimal composition might depend on various factors such as the specific properties of the matrix material, the type of reinforcement, and the intended application of the composite. Both RSM and GA results should be carefully evaluated and validated through practical experimentation to determine the most suitable composition for achieving the desired mechanical and tribological properties of the final composite material.

The optimization of the friction stir consolidation process for metal matrix composites using RSM and GA provides valuable insights into the process parameters that influence the properties of the resulting materials. The similarities and inconsistencies between the predicted optima highlight the strengths and limitations of each optimization technique, emphasizing the importance of comprehensive experimentation for robust process optimization.

The consistency of regression equation was checked through different parametric set ups and found to be very consistent for most combinations. However, the consistency could not sustain for all the set ups. For instance, the optimum set up predicted by GA which was 0.469% of porosity, was miss predicted by regression equation lower to 0.21% of porosity. However, the experimental results revealed a porosity of 0.51% with variation of 0.041, demonstrating that we could not completely depend on the regression equation.

4.6 Synthesis, Testing and Characterization of Samples for the Optimum parametric combination

Numerically simulated and optimized sample was successfully fabricated through FSC process as shown in Fig. 4.20.

4.6.1 Fabrication of Samples

Samples were fabricated based on the prescribed parametric setup predicted by Genetic Algorithm. Additional elaborations have been made in (APPENDIX 8).

Figure 4.20 FSC Process on a Conventional Milling Machine

4.6.2 Testing of Optimized Sample

The final optimized sample was chosen for testing its compressive strength, tribological, and hardness properties. The tests that were chosen were thought to provide a thorough description of the current state of the FSC process. The hardness or scratch resisting property, the wear and resistance to compressive loads of the optimized sample underscores the process efficiency that the FSC process can stand in a certain way of roughly comparable with the existing dominant MMC processing when compared with previous works.

4.6.2.1 Analysis of Micro-Hardness Property of Optimized Sample

Four trials of microhardness (HV) were taken into consideration to analyze the average hardness values of an optimized sample. As the hardness results obtained in preliminary study, there was a minor variation in hardness at the top and bottom surfaces of the sample, the hardness values were taken at different cross-section of the sample i.e. two from the bottom half and two from the top half. During the preliminary experiments, the best hardness value obtained was 322.5 HV. However, after conducting Discrete Element Method (DEM) numerical simulations and optimization using an integrated approach of Response Surface Methodology (RSM), Box-Behnken Design (BBD), and Genetic Algorithms (GA), the hardness was significantly enhanced. The optimized process resulted in a hardness of 339 ± 1.5 HV (3324.6±14.7MPa), demonstrating the effectiveness of the combined optimization techniques in improving material properties. The hardness result of the optimized sample shown in Table 4.13. This shows that the obtained result witnesses the effectiveness and capability of the FSC process to produce parts with a favorable hardness property. An experimental study of hardness behavior of AZ31 reinforced with SiC, MoS_2 and ZrO_2 processed through powder metallurgy process shows the hardness range from 1007.957 MPa to 1497.64 MPa (Maryam et al., 2023). This witnesses that FSC produced samples showed prior hardness property. Another investigation by Sheelwant et al., (2021) witnessed the hardness behavior of a magnesium matrix composite reinforced with SiC and Al_2O_3 to be from 588.42MPa to 686.49MPa. In addition to this, Satish & Satish, (2018) investigated the hardness property of metal matrix hybrid composite through powder metallurgy process by taking Magnesium matrix reinforced with 15%SiC + 15%Al_2O_3 + 70% Mg and obtained hardness value of 385.22MPa. While their other composition of a metal matrix of 5%SiC + 5%Al_2O_3 + 90% Mg resulted in 417.19MPa. The hardness property of a magnesium alloy RZ5 reinforced with B_4C studied under stir casting and its hardness value obtained to have 1216.1MPa (Meher et al., 2019) which strongly supports the superiority of FSC process.

4.6.2.2 Analysis of Tribological Behavior

The tribological property of the GA optimized sample obtained as 0.0054 mg/m through pin-on-disc wear tester based on the ASTM/G-99 standards as presented in Table 4.13. The wear rate predicted by GA successfully converged on an optimized solution through multiple iterations at parametric combination of [350m, 220Rpm and 20N] which was experimentally validated wear rate of 0.00514 mg/m. The rolled-up debris, subsequent passage of abrasive particles delamination, shallow grooves and shallow ploughs were also observed, which indicated that the wear formation in the sample was abrasive wear (WIKIPEDIA, 2023). The values of wear rate witnessed the impact of the applied load that is the higher the load the higher the wear rate would be. An investigation by Siddhartha Prabhakar et al., (2014) testified the impact of applied load [10N, 20N and 30N] on the wear rate of Aluminum with 5 wt% of B_4C which was synthesized through stir casting which strongly support the proportionality of load against wear rate within the wear rate ranges from 0.001838 to 0.00353 mm^3/m. Similarly, Venkatesh et al., (2022) optimized the tribological property of a hybrid composite of AZ61 alloy reinforced with B_4C and ZrO_2 by considering the three common parameters of wear such as sliding speed [1m/s, 2m/s and 3m/s], sliding distance [1300m, 1500m and 1700m], Composition weight [4%, 8% and 12%] and load [30N, 40N and 50N] through stir casting process. The wear rate result of the investigation showed that a minimum of wear rate of 0.0018mm^3/m was obtained at parametric combination of [12%, 1m/s, 40N and 1500m] which witnessed the highest reinforcement composition bear the wear rate more. In the same way tribological behavior of Al reinforced with 20%wt of Al_2O_3 through powder metallurgy technique was investigated and wear rate of 0.025-0.03 mm^3/m was obtained witnessing the ranges of wear rate under powder metallurgy process.

4.6.2.3 Analysis of Compressive Strength Property

The compressive strength property of an optimized sample was tested and obtained as 170±2.6 MPa. Comparing this compressive yield strength result with previous studies which was fabricated through powder metallurgy process briefs the effectiveness of FSC process. Maclin et al., (2020), produced a metal matrix composite through powder metallurgy process and their compressive strength result obtained as ≈135 MPa. The parameters considered to reach on this specific compressive strength were 20 wt% of 48 micrometer Al_2O_3 reinforcement and sintering temperature of 500^oC for 90 minutes. This strongly supports the capability of FSC process that parts could be produced within short period of time as FSC does not require extended sintering time. Similarly, on another study by Senthil Murugan et al., (2023), the compressive strength of AA2024 metal matrix composite reinforced with 10 wt%(100mg) of fly ash and Graphite (5 wt%) which was produced through stir casting route resulted from 238 to 285 MPa.

Generally, the mechanical and tribological properties of the optimized sample has been tested and the values are presented in Table 4.13. The average Hardness value of the optimized sample was determined to be 339±1.5 HV (3,324.5 ± 14.7 MPa), this shows that, the effectiveness and comparable status of FSC process for Magnesium Matrix Composites fabrication.

Salih et al. (2019), have used friction stir welding process to investigate the mechanical properties of AA6092/SiC metal matrix composite, the result of their experimental study showed the hardness value ranging from 90-110HV at a lowest traverse speed of 25mm/min and speed ranging from 1500 to 2100rpm.

Table 4.13 Mechanical and Tribological Property of Optimum Specimen

Properties	Average Results
Hardness	339±1.5HV (3324.6±14.7MPa)
Compressive Yield Strength	170±2.6 MPa
Wear	0.00514 mg/m

As presented in Table 4.13, the wear rate of the optimized specimen is recorded at 0.00514mg/m at a sliding distance of 350 m, a sliding speed of 240 RPM and a load of 20 N.

4.6.2.4 Analysis of Fractography of the fractured Optimized Sample

Fractography is a vital technique used to investigate the failure behavior of materials by studying the surfaces of fractured specimens. In Figure 4.21, a Scanning Electron Microscope (SEM) image of a metal matrix composite material is examined to determine the fracture types and gain insights into the failure mechanisms (Hayes et al., 2015). The presence of micro void coalescence and dimples on the fracture surface indicates a significant ductile component in the fracture mechanism. The development of facets is a characteristic of localized plastic deformation (Krishna Sai & Tambe, 2022).

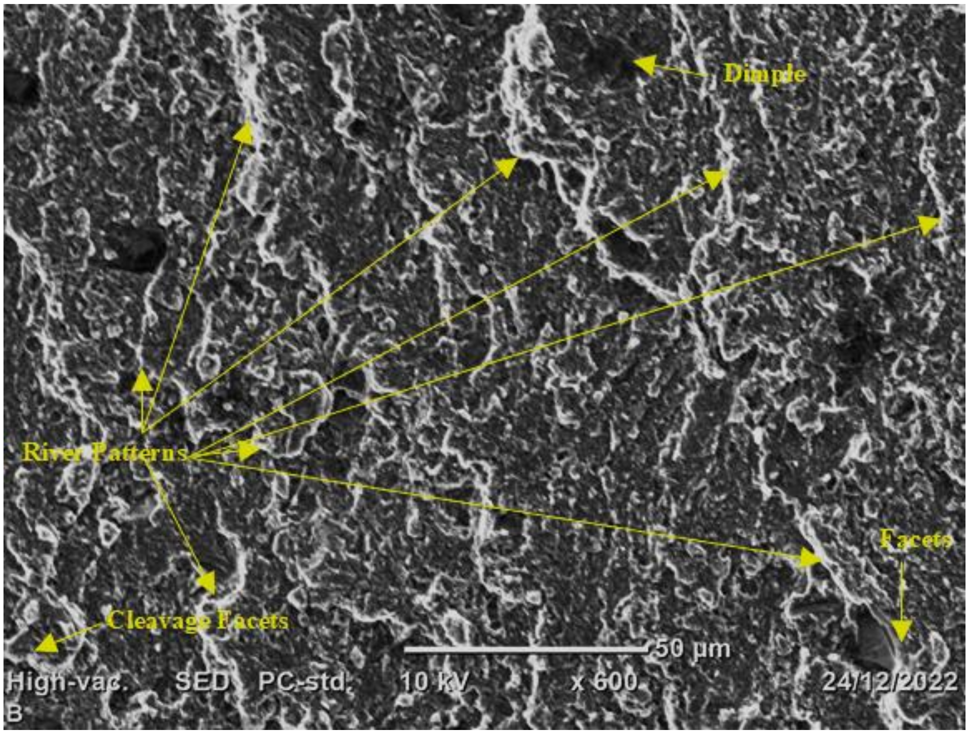

Figure 4.21 SEM Observation of Fractography of the Optimized Sample

The absence of significant plastic deformation suggests rapid crack propagation with little energy absorption. Cleavage facets and river-like patterns are observed, typical of brittle fractures (Chen & Cao, 2015). The presence of these features indicates that the material experienced sudden and catastrophic failure in certain regions. Generally, the presence of dimples, cleavage facets, and river-like patterns indicates that the material experienced different stress states and loading conditions. This comprehensive analysis highlights the material undergone a complex series of failure mechanism mostly favoring a brittle fracture.

4.6.3 Characterization of Optimum Sample

4.6.3.1 X-Ray Diffraction Phase Analysis

X-Ray diffraction is usually used to determine the phases of the materials; the intensity of the reflected X-Rays is measured as the detector and sample spin (Prasad et al., 2020). A phase analyzing equipment of (Model: XRD-7000 X-RAY DIFFRACTOMETER Maxima from Shimadzu Corporation Japan) was employed for the X-ray diffraction phase analysis in this investigation, which took angles ranging from 10^{o} to 80^{o} into consideration. XRD study reveals that all patterns reflect the existence of phase of AZ61 (Al, Zn, Mn, Ni, Cu, Fe, Si, Pb, Ca, Sn), SiC and ZrO_2 peaks forming a composite architecture of SiC, Zr, MgO, $CaCO_3$ and $MgCO_3$ with the miller indices shown in the Figure 4.22 as illustrated by Origin Pro2018 software. For instance, in sample number three (S-3) XRD results revealed the existence of $CaCO_3$ phase at a 2theta angle of 35.966^{o} which matches precisely with International Center for Diffraction Data (ICDD) reference code of 00-005-0586. The X'Pert HighScore software was utilized to analyze each sample’s major peak and corresponding miller indices. Consequently, all intensity peaks aligns with the ICDD standards; in which the major peak exhibits MgO at an angle of 36.96^{o}. Furthermore, researchers as well studied and found the existence of MgO at angles, 36.96, 38.02, 74.71 and 78.66 correspond to the planes (002),(202),(113) and (222) respectively (Balakrishnan et al., 2020). Formation of new phase ZnO has been detected which doesn’t exist in the unprocessed and matrix phase; this result found to be consistent with the previous investigation by Arefi & Rezaei-Zarchi, (2012). They found formation of ZnO wurtzite phase at (101) peak which matched with JCPDS data well. In addition to this, the newly emerged ZnO peak at 2theta angle of 35.60^{o} after FSC process again found to be aligned with previous investigation by Długosz et al., (2021).

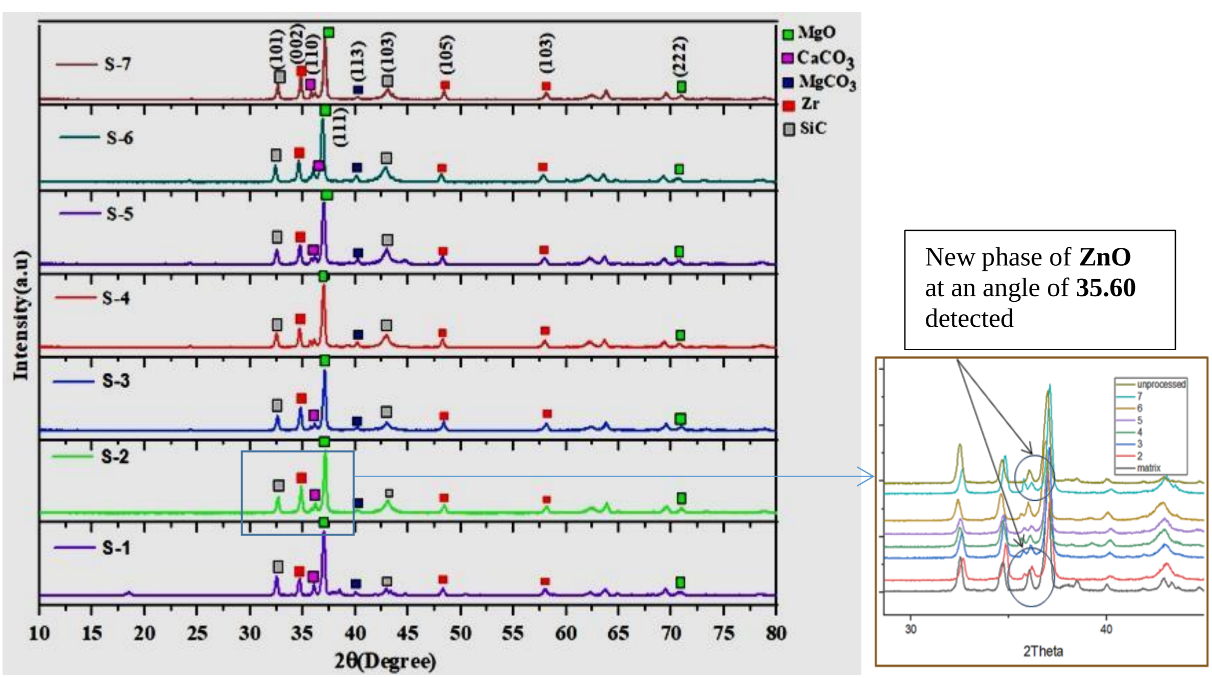

Figure 4.22 XRD Patterns of Sample

Previous research by John et al., (2020), found that the existence of ZnO phase led to an improved microhardness property. The impact of ZnO phase on the improvement of microhardness property of the composite materials strongly supported by Gómez-Esparza et al., (2019). In addition to this, with a slight fraction of 2 %wt, the micro-hardness performance showed a higher hardness improvement of 27.78% and a decrease in elastic modulus with 4.92% (Kumar et al., 2020).

4.6.3.2 Fractography of compressive deformation analysis of Optimized Sample

Fractography is a vital technique used to investigate the failure behavior of materials by studying the surfaces of fractured specimens. In Figure 4.23, a scanning electron microscope (SEM) image of a metal matrix composite material is examined to determine the fracture types and gain insights into the failure mechanisms (Hayes et al., 2015). The presence of micro void coalescence and dimples on the fracture surface indicates a significant ductile component in the fracture mechanism. The development of facets is a characteristic of localized plastic deformation (Krishna & Tambe, 2022).

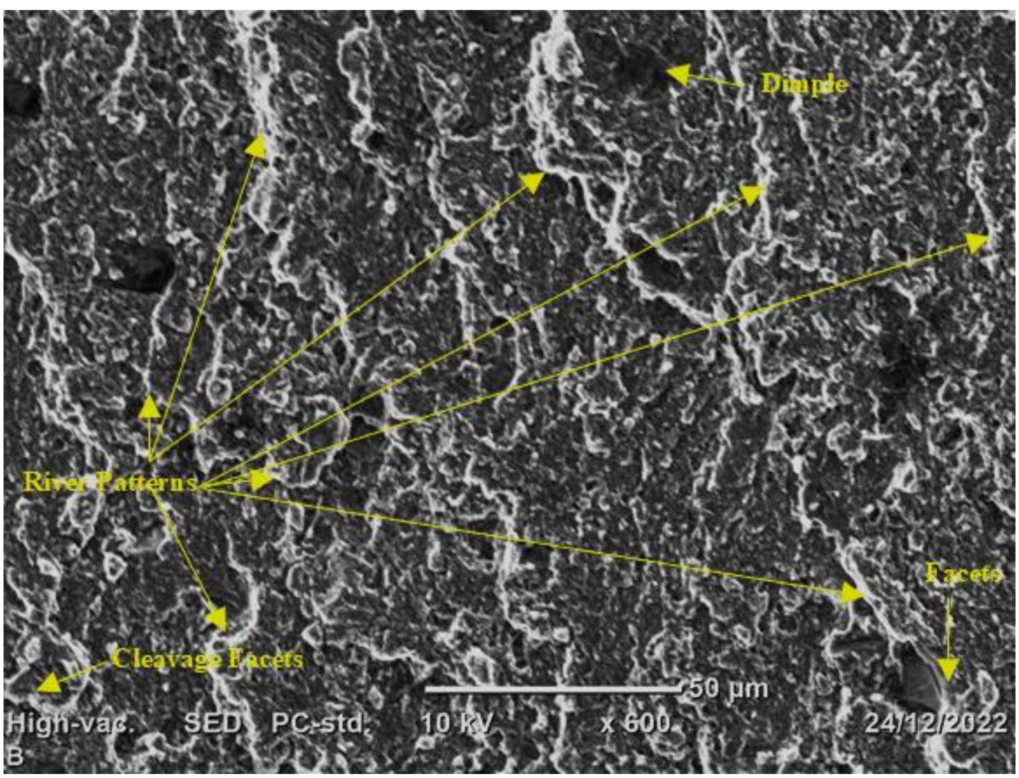

Figure 4.23 SEM Observation of Fractography of the Optimized Sample

The absence of significant plastic deformation suggests rapid crack propagation with little energy absorption. Cleavage facets and river-like patterns are observed, typical of brittle fractures (Chen & Cao, 2015). The presence of these features indicates that the material experienced sudden and catastrophic failure in certain regions. Generally, the presence of dimples, cleavage facets, and river-like patterns indicates that the material experienced different stress states and loading conditions. This comprehensive analysis highlights the material undergone a complex series of failure mechanism favoring a brittle fracture.

4.7 Wear Rate parametric optimization of a pre-Optimized Sample using RSM Box-Behnken Design

The Box-Behnken optimization technique was taken into consideration when designing the experiments. This experimental design approach enables efficient response surface modelling, factor interactions and quadratic effects analysis. It also offers a more thorough examination of the responses and permits optimization within the design space. Three independent process parameters such as load, sliding speed and sliding distance were chosen as the input parameters. Each variable was adjusted at three levels (-1, 0 and 1) based on their low, central and high values as presented in Table 4.14. The statistical software Minitab19 was then employed to evaluate the experimental data from the wear tests in order to create a model that would predict the wear rate in relation to the input process parameters. The model was optimized, in order to determine the optimal parametric combination for the lowest wear rate of MMHCs.

Table 4.14 Factors with Their Corresponding Levels

			Level	Level	level
Factors	Coded	Unit	-1	0	1
Load	X_1	N	20	30	40
Sliding Speed	X_2	Rpm	220	240	260
Sliding Distance	X_3	m	350	500	650

Similarly, as indicated in Table 4.15, a total of 15 experiments were conducted to cover the Box-Behnken design space and examine the impact of the input variables on the wear characteristics of the AZ61 magnesium alloy hybrid matrix composite.

Table 4.15 Box-Behnken Experimental Design

Run	Coded Factors			Actual Factors		
	X_1	X_2	X_3	Load	Sliding Speed	Sliding distance
1	-1	-1	0	20	220	500
2	0	-1	1	30	220	650
3	1	-1	0	40	220	500
4	0	0	0	30	240	500
5	-1	0	-1	20	240	350
6	0	0	0	30	240	500
7	1	0	1	40	240	650
8	1	1	0	40	260	500
9	0	-1	-1	30	220	350
10	0	1	1	30	260	650
11	1	0	-1	40	240	350
12	0	0	0	30	240	500
13	0	1	-1	30	260	350
14	-1	1	0	20	260	500
15	-1	0	1	20	240	650

Friction and wear are two important tribological phenomena that usually cause material degradation and energy loss when two solid surfaces move or slide one on the other (Omrani et al., 2016). Additionally, wear is the slow loss of material from one or both mating surfaces during sliding and caused on by mechanical and/or chemical processes (Sanjay et al., 2018). The results of the wear rate test showed that the highest wear rate of 0.181 mg/m was recorded at the parametric combination of 40N load, 260RPM speed, and 500m sliding distance, and the lowest wear rate of 0.008 mg/m was recorded for the testing parameters of 20N load, 240RPM sliding speed, and 350m sliding distance at room temperature. Table 4.16 presented the wear rate results for different loading condition [20, 30, 40N], sliding speed [220RPM, 240RPM, 260RPM] and sliding distance [350m, 500m, 650m].

Table 4.16 Box-Behnken Design and Wear Rate Results

Run	Coded			Actual Factors							Responses
	X_1	X_2	X_3	Load	Sliding Speed	Sliding distance	Weight before test (g)	Weight after test (g)	Weight Loss (g)	Conversion into mg	Wear rate (mg/m)
1	-1	-1	0	20	220	500	0.6428	0.6344	0.0084	8.4	0.0450
2	0	-1	1	30	220	650	0.6428	0.5873	0.0555	55.5	0.0854
3	1	-1	0	40	220	500	0.6427	0.5774	0.0653	65.3	0.1310

4	0	0	0	30	240	500	0.6427	0.59465	0.0661	48.4	0.0961
5	-1	0	-1	20	240	350	0.6428	0.6401	0.0027	2.7	0.0080
6	0	0	0	30	240	500	0.6427	0.6022	0.0405	40.5	0.0830
7	1	0	1	40	240	650	0.6429	0.5454	0.0975	97.5	0.1500
8	1	1	0	40	260	500	0.6429	0.5524	0.0905	90.5	0.1750
9	0	-1	-1	30	220	350	0.6428	0.625	0.0178	17.8	0.0480
10	0	1	1	30	260	650	0.6427	0.5623	0.0804	80.4	0.1240
11	1	0	-1	40	240	350	0.6428	0.5864	0.0546	56.4	0.1610
12	0	0	0	30	240	500	0.6427	0.5942	0.0665	48.5	0.0970
13	0	1	-1	30	260	350	0.6427	0.6280	0.0427	14.7	0.0510
14	-1	1	0	20	260	500	0.6428	0.6094	0.0334	33.4	0.0668
15	-1	0	1	20	240	650	0.6428	0.6024	0.0404	40.4	0.0623

Kumar et al., (2022), examined the wear properties of the AA8011/Boron Nitride metal matrix composite experimentally. Four parameters were selected for wear parameter optimization using Taguchi design: volume fraction of reinforcement (V) [7.5 10 12.5], load (L) [75 100 125N], time (T) [30 40 50min.], and speed (S) [200 220 240RPM]. Moreover, researchers found that, for a minimal wear of 70.12μm, the optimum parametric setup was V, L, S, and T at 12.5V, 75N, 200 RPM, and 30min, respectively. Through experimental investigation and optimization using Grey Relation Analysis, the effects of load [10 30 50N], sliding velocity (2 3 4 m/s), red mud weight percentage (3 4 5 wt.%), and counterpart material hardness (58 60 62 HRC) on the specific wear behavior and Coefficient of Friction (COF) of Red Mud Reinforced Aluminum Composites were investigated (Shanmugavel et al., 2016). The findings showed that the optimal parametric configuration was determined with the load at 10 N, sliding velocity at 3 m/s, red mud content of 5 wt%, and counterpart material hardness at 62 HRC. Comparatively, when researchers examined the tribological characteristics of AA6061 at 10, 20, and 30 N loads, reinforced with various ZrB_2 compositions fabricated via stir casting process, they discovered a wear rate of 0.0044mm^3/m. (Morampudi et al., 2022). This demonstrates that the samples made using the friction stir consolidation procedure possesses wear rate behavior that is adequate. Moreover, The various loading condition of wear rate investigation confirms and obeys the law of Archard's principle, which states that the wear rate and applied load are proportionate (Jojith

& Govindaraju, 2022). Wear is resisted at load ranges of 20N-40N by the SiC and ZrO_2 adequate bond with the AZ61 well. Similarly, at a maximum load of 40N, the sample pin encounters the highest stress at the interface of the rotating disc of the pin on the disc wear test instrument.

4.7.1 Analysis of Variance

Analyzing the model's reliability and accuracy can be accomplished by using the analysis of variance approach (Seeman et al., 2010). ANOVA is also helpful in examining the impacts of every parameter and the degree to which extent they can impact wear rate or the response. A significance level of 5% and a confidence level of 95% were taken into account when analyzing the wear rate results. The wear rate appeared to be most influenced by load (73.6%), followed by sliding distance (about 9.19%) and least influenced by speed (4.49%). A *p-value* of less than 0.05 suggests that the factors have significant effects on the wear rate or generally on the response. ANOVA results witnessed that sliding distance, load and speed were found to have significant effect on the wear rate. The *p-value* of the *lack-of-fit* is 0.174 which is insignificant; this indicates that how well the model fits the data (Umanath et al., 2021). R^2 and R^2 (Adj) accounted to about 96.80% and 91.03% respectively showing the fitness of the model as presented in Table 4.17. The interaction effects of two independent parameters on the wear rate are presented in Figure 4.25a) load and sliding speed, b) load and sliding distance, c) sliding speed and sliding distance; by holding the other parameter at medium level.

Table 4.17 Analysis of Variance for Wear Rate

Source	**DF**	**Adj SS**	**Adj MS**	**F-Value**	**P-Value**
Model	9	0.031095	0.003455	16.79	0.003
Linear	3	0.028037	0.009346	45.41	0.000
LOAD	1	0.023642	0.023642	114.87	0.000
SLIDING SPEED	1	0.001442	0.001442	7.01	0.046
DISTANCE	1	0.002953	0.002953	14.35	0.013
Square	3	0.001551	0.000517	2.51	0.173
LOAD*LOAD	1	0.000867	0.000867	4.21	0.095
SPEED*SPEED	1	0.000031	0.000031	0.15	0.713
DISTANCE*DISTANCE	1	0.000534	0.000534	2.60	0.168
2-Way Interaction	3	0.001506	0.000502	2.44	0.180
LOAD*SPEED	1	0.000123	0.000123	0.60	0.474
LOAD*DISTANCE	1	0.001066	0.001066	5.18	0.072

SPEED*DISTANCE	1	0.000317	0.000317	1.54	0.270
Error	5	0.001029	0.000206		
Lack-of-Fit	3	0.000906	0.000302	4.92	**0.174**
Pure Error	2	0.000123	0.000061		
Total	14	R^2 **= 96.80% and** R^2**(Adj) = 91.03%**			

Surface plots illustrated that the wear rate is higher at higher level of load and minimal at lower level of load. The surface plot result suggests that among the three process parameters tested, load has largest influence on the wear rate, while speed has the lowest effect as compared to sliding distance. This shows that the primary factor influencing wear rate was load, and that adjusting the load can have a major impact on wear rate variations. Furthermore, the surface plot analysis shows that the impact of load versus speed on wear rate is greater, indicating that the wear rate is significantly influenced by the combination of load and speed while sliding distance held at medium level. In particular, the analysis reveals that when higher levels of load and speed are combined, the wear rate found to be greater than 0.15 mg/m. This shows that while raising the load or speed alone would not have a big impact on wear rate, when both parameters are coupled at a greater level, wear rate increases significantly. Conversely, smaller sliding speeds and loads can produce wear rates that are far lower, down to 0.008 mg/m. Thus, reducing the wear rate was main objective of this study.

The higher levels of factors of sliding speed and load generated wear rate of slightly more than 0.15mg/m as illustrated in Fig. 4.24a. Conversely, surface plot of Fig. 4.24b indicates that minimum wear rate which was close to the optimum result was attained at minimum levels of both load and sliding distance. The two factors which had moderate percentage contribution on the wear rate, presented in Fig. 24c depicted a wear rate of 0.10 to 0.15mg/m at their highest level and generate wear rate of very close to 0.05 when their lower level met.

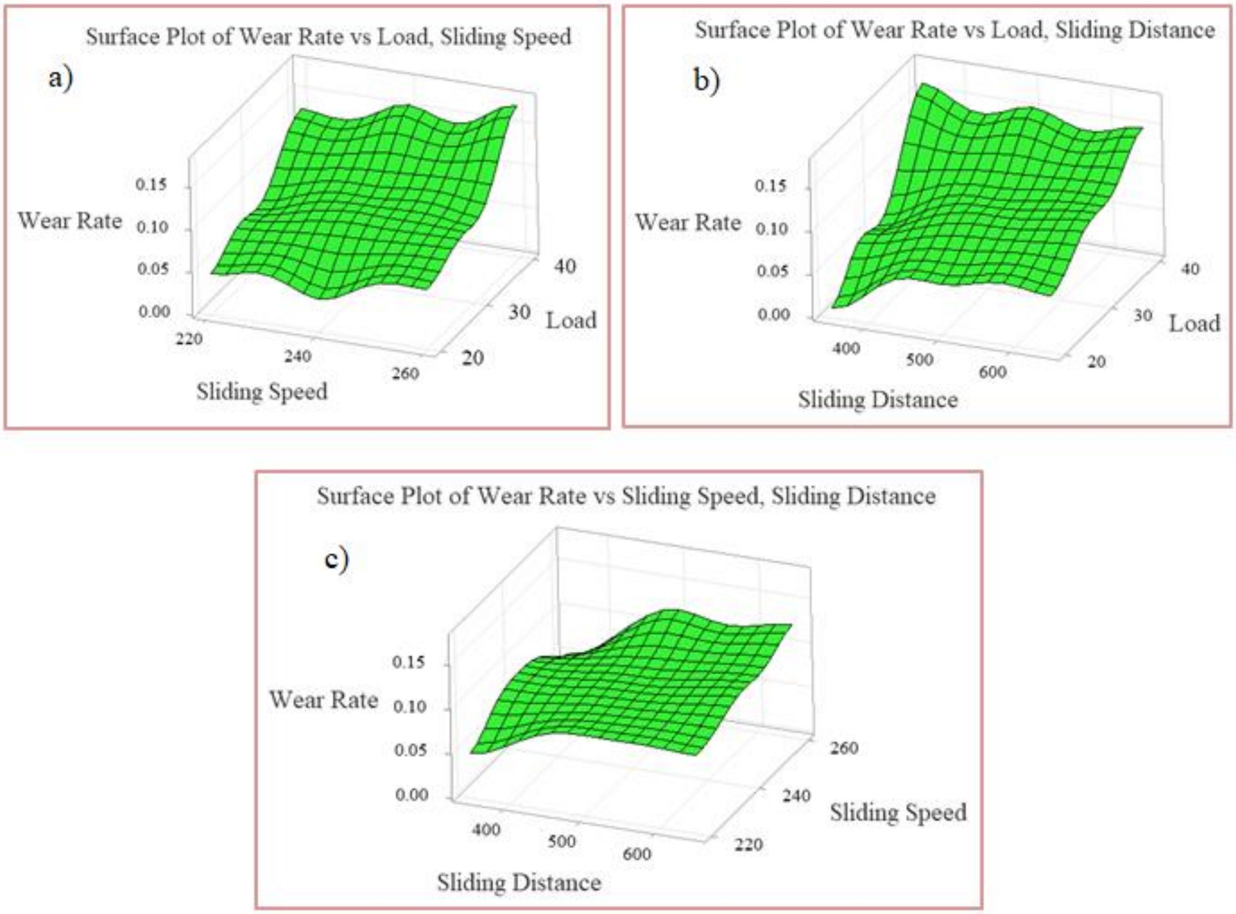

Figure 4.24 Response Surface Plots for a) Wear Rate Vs Load, Sliding Speed b) Wear Rate Vs Load, Sliding Distance c) Wear Rate Vs Sliding Speed, Sliding Distance

In a study by Uthayakumar et al., (2013), dry sliding parameters had been optimized on a metal matrix composite material of Fly Ash Reinforced AA-6351 by considering process parameters such as; Applied load [9.81 19.62 29.43 N], Sliding speed [1 2 3 m/s] and Percentage of fly ash [5 10 15 wt.%]. Their finding revealed that the optimum parametric combination for a minimum wear rate to be at; load at 19.62N sliding speed at 3m/s and fly ash at percentage of 5wt%. In addition to this, the result of their study depicted that applied load and sliding speed are the most influential. Researchers used the Taguchi technique to apply wear behavior parametric optimization of AA7075-Al_2O_3 Composites manufactured using stir casting, taking into account wear factors like applied load at 10 30 40N and sliding distance at 200 600 1200m (Baradeswaran et al., 2013). Their graphical and analytical results showed that a load at 10 N and a sliding distance of 400 m was the optimum parametric combination that could result the least amount of wear mass loss. The wear parameters, including normal load [5 15 25 35N], sliding distance [800 1600 2400 3200m], sliding speed [0.565 1.13 1.7 2.26 m/s], and reinforcement composition [0 2.5 5 7.5 wt%.], were taken into consideration and optimized using Taguchi design in another study on the wear properties of B_4C and MoS_2 reinforced Copper metal matrix composite. Their findings showed that the optimal combination of parameters for the least amount of wear loss was identified. Composition of 7.5 weight percent, load of 5 N, sliding distance of 1600 m, and sliding speed of 1.13 m/s (Gangwar et al., 2021).

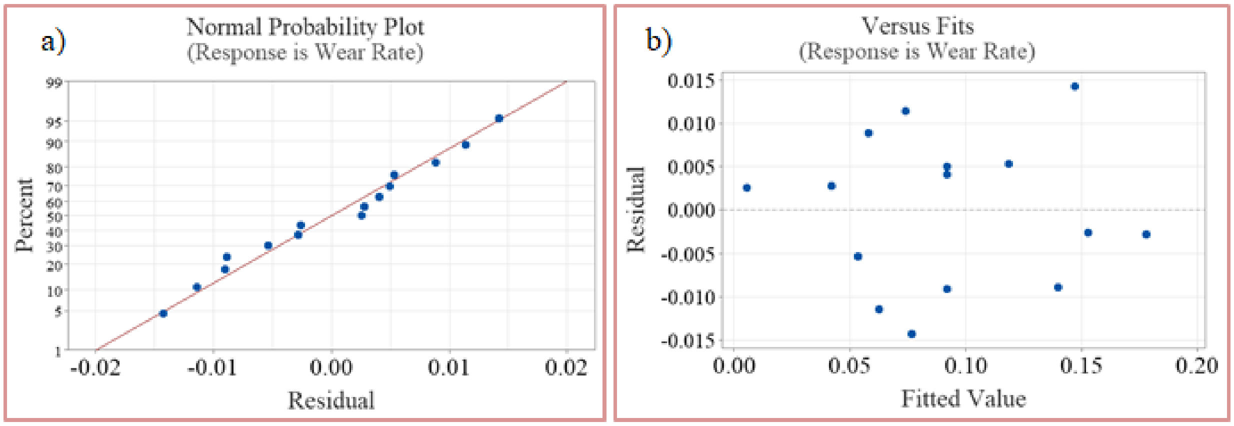

Figure 4.25 Normal Probability a) Plot of Residuals for Wear Rate and b) Residuals versus the Fitted Value for Wear Rate

Results portrayed in Figure 4.26a indicates that the probability plot of residuals kept distinctly close to the straight line confirming the normal distribution of errors and the well fitness of the regression model towards the obtained results (Das et al., 2018). Moreover, Figure 4.25b clearly proved the excellent relationship of observed and fitted values with result variation of between -0.15 and 0.15.

4.7.2 Pareto Chart of the Standardized Effect

The order or level of influence of process parameters is indicated by the Pareto chart in Figure 4.26. As indicated below the three process parameters such as speed, load and sliding distance have significant effect on the wear rate of the material regardless of their interaction effects. Certainly, from the Pareto chart it can be concluded that the load has the largest effect on the wear rate response while sliding speed has the lowest effect on the response. However, to what extent does the factors influence the response cannot be analyzed through Pareto Chart (Minitab ® 21 Support, 2023).

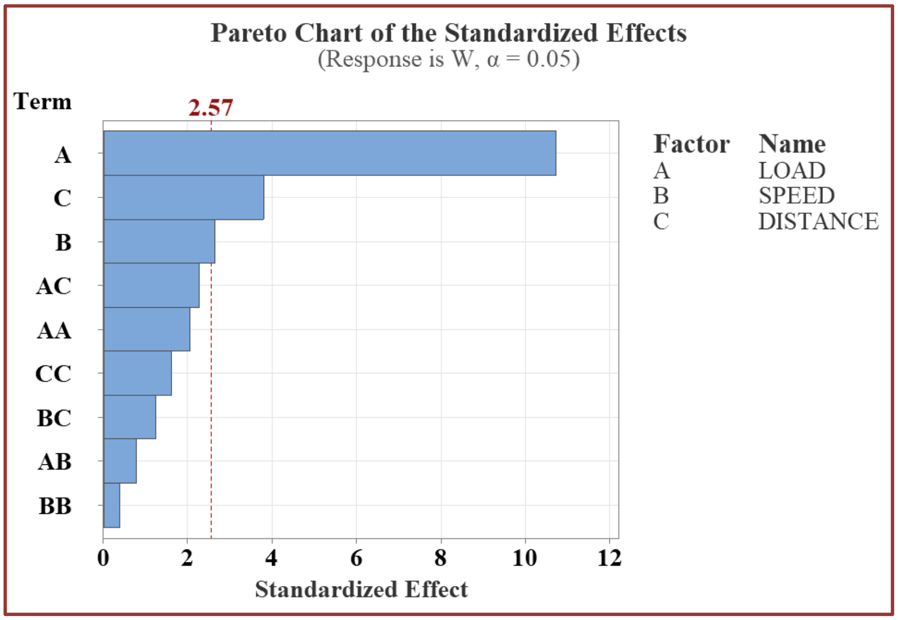

Figure 4.26 Pareto Chart of the Standardized Effect

Pareto chart witnessed the insignificancy of the interactions of the process parameters towards the wear rate as their standardized effect values are less than 2.57.

4.7.3 Optimized Process Parameters

The main effect plot of wear depicted the minimum wear rate could be found at parametric combination of Speed at 240 RPM, Load and Distance at their lower levels. The wear parametric optimization of main effect plot provides important information on how different parameters, such load, speed, and sliding distance, affect wear rate. With an objective on minimizing wear rate, the experimental parameters were predicted at 20N for load, 240RPM for sliding speed, and 350m for sliding distance. When all other variables are held constant, the main effect plot illustrates how speed affects wear rate. The wear rate is minor at 240 RPM, indicating that sliding speed is significant to minimize the wear rate. After this, deviating from the optimum sliding speed could cause the wear rate to increase especially at higher sliding speed. In the same way, the main effect plot shows how load affects wear rate while maintaining the same values of levels for other variables. The wear rate is minimized at 20N, suggesting that load is favorable for minimizing wear. The wear rate could increase or decrease depending on the loads exerted. The Figure 4.27 highlights how important load is to wear optimization and offers a point of reference for choosing load settings that result in a minimal amount of wear rate. A sliding distance of 350 meters results in the lowest wear rate, suggesting that this distance is optimal for reducing wear. Through the combination of the optimum sliding distance (350m), load (20N), and speed (240RPM) minimum wear rate was achieved.

4.7.4 Mathematical Model

The relationship between the response (wear rate) and the input factors (Load, Sliding Speed, and Sliding distance) could be predicted by the regression equation (Radhika & Sai Charan, 2017). The formula, referred in Equation 43, was developed using the statistical software MINITAB 19 based on RSM-BBD approach. To confirm the accuracy of the regression model that was developed, a verification experiment was carried out employing several parametric combinations that are not present in the RSM (Box-Behnken) design matrix. To confirm that the regression model was consistent, three distinct and random experimental combinations were carried out. The wear rates measured experimentally and those estimated using the regression model deviate only slightly, according to the results of confirmation experiments shown in Table 4.18. All of the experiments had an error percentage of less than 10%, which suggests that the regression model that was developed accurately predicted the wear rates for the specified experimental study ranges (Radhika & Sai, 2017).

$$W = -0.2960 + 0.005436\ X_1 + 0.000671\ X_2 + 0.000128\ X_3 \qquad \text{eq. (43)}$$

Where, W is wear rate in mg/m, X_1 is load in N and X_2 is speed in RPM and X_3 is sliding distance in m.

Table 4.18 Verification Experiment

	Factors					
S.No.	Load	Speed	Distance	Regression wear	Experimental wear	Error
1	40	260	650	0.18 mg/m	0.187	3.89%
2	30	260	500	0.11 mg/m	0.115	4.55%
3	30	220	350	0.059 mg/m	0.061	3.39%

The results of the verification experiments is presented in Table 4.18, which demonstrated the regression model's consistency and reliability with error percentages of 3.89%, 4.55%, and 3.39% for experiments number 1, 2, and 3, respectively.

4.7.5 Parametric Optimization Using Genetic Algorithm

Using MATLAB R2014a, GA was performed following RSM-Box-Behnken parametric optimization to achieve an even better wear rate result. The generation and population sizes were 100 and 50 respectively. The function Eq.43 was transformed into minimization problem in MATLAB to find the optimum result. The upper and lower constraints chosen are determined by the levels of each process parameter. The subsequent constraints along with Equation 43 were taken into account for the constraints and the Fitness function.

***Constraints*:** $20\text{N} \leq X_1 \leq 40\text{N}$

$220\text{RPM} \leq X_2 \leq 260\text{RPM}$

$350\text{m} \leq X_3 \leq 650\text{m}$

$$\boldsymbol{Fitness\ Function} = -0.296 - 0.005436X_1 - 0.000671X_2 - 0.000128X_3 \qquad \text{eq. (43)}$$

Table 4.19 Parameter Function Along with Their Values in GA

Parameter Function	**Parameter Value**
population size	50
Population type	Double vector
Creation Function	Constraint dependent
Fitness Scaling Function	Rank
Selection Function	Roulette
Reproduction: Elite Count	Default (0.05* Population size) = 2.5
Reproduction: Crossover Fraction	Default: 0.8
Mutation Function	Uniform: Rate at 0.15
Crossover Function	Constraint Dependent
Number of Generations	100
Function Tolerance	1e-6
Constraint Tolerance	1e-6

The demography was selected to be a double vector type of population (Panwar et al., 2020). Creation function of constraint dependent was set. Uniform mutation with a mutation function at rate of 0.15 was taken while crossover fraction was at 0.8 as illustrated in Table 4.19. Moreover, roulette parent selection was preferred (Panwar et al., 2020). The precise result of the minimum wear rate predicted by GA was 0.00514 mg/m at 51 iterations as shown in Figure 4.27.

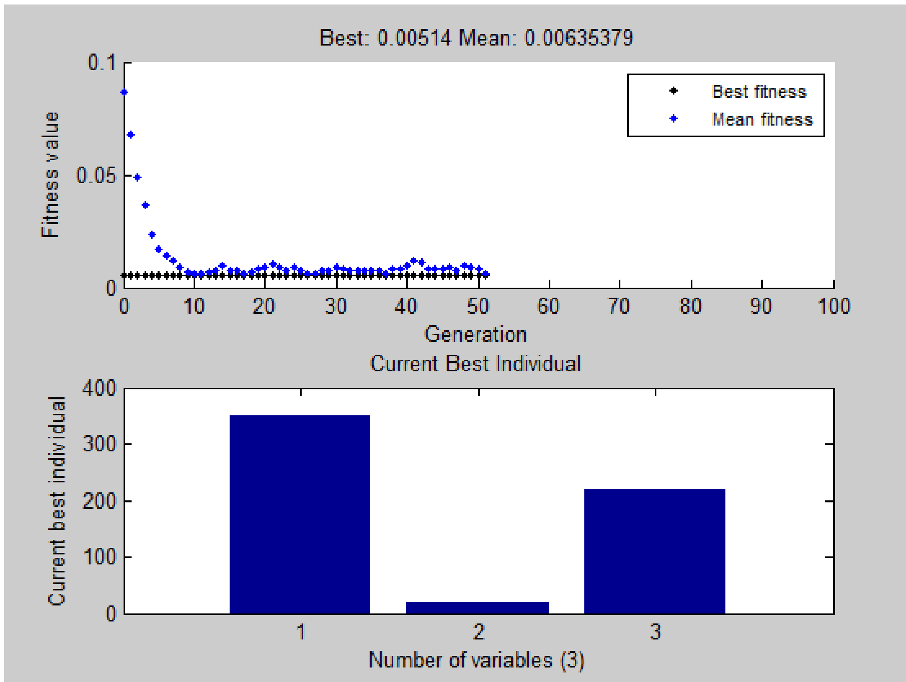

Figure 4.27 GA Plot for Wear Rate

Table 4.20 GA Predicted Best Individual for Minimum Wear Rate

Process parameters	Levels
Load	20N
Sliding Speed	220RPM
Sliding Distance	350m

The optimum parametric configuration with their corresponding levels for lowest wear rate was, Load, sliding speed and sliding distance at 20N, 220RPM and 350m respectively as illustrated in Table 4.20.

4.7.6 Verification Experiment for RSM and GA

The last stage was to confirm the efficiency of the model using the optimal levels of the design parameters for RSM (load, sliding speed and sliding distance at 20N, 240RPM and 350m respectively) and for GA (load, sliding speed and sliding distance at 20N, 220RPM and 350m respectively). Table 4.21 shows a comparison of the predicted and the actual experimental results of RSM and GA with their corresponding errors in percent. According to Table 4.21, the improvement on the response is noticed when the optimum conditions of GA was used.

Table 4.21 Confirmation Tests for RSM & GA for Optimized Process Parameters.

Method	Optimized parameters	Wear rate	S-1	S-2	S-3	Average WR
RSM	Load = 20N	Experiment	0.0085	0.0083	0.0084	0.0084
	Sliding Speed = 240RPM	Predicted	0.008	0.008	0.008	0.008
	Sliding distance = 350m	% Error	6.25	3.75	5	5%
GA	Load = 20N	Experiment	0.0054	0.00538	0.00532	0.00537
	Sliding Speed = 220RPM	Predicted	0.00514	0.00514	0.00514	0.00514
	Sliding distance = 350m	% Error	5.06	4.67	3.5	4.41%

The regression equation developed using the Box-Behnken design with a 5% error percentage was found to be persistent and reliable in the three replication confirmation or verification experiments shown in Table 4.21. On the other hand, an improved 4.41% error percentage was found in the GA prediction for the best parametric combination for the lowest wear rate.

4.7.7 Thermogravimetric Analysis of Optimized Composite

Thermogravimetry (TGA) is a thermal analysis technique where the material's weight loss or gain is measured over time at different temperatures ranges. The Friction stir consolidated sample was subjected to TGA testing in order to determine its applicability and temperature durability. Similarly, the temperature at which the sample begins to degrade or decompose over time is revealed by the TGA analysis. Figure 4.28 depicts the results of the optimal sample's thermal analysis.

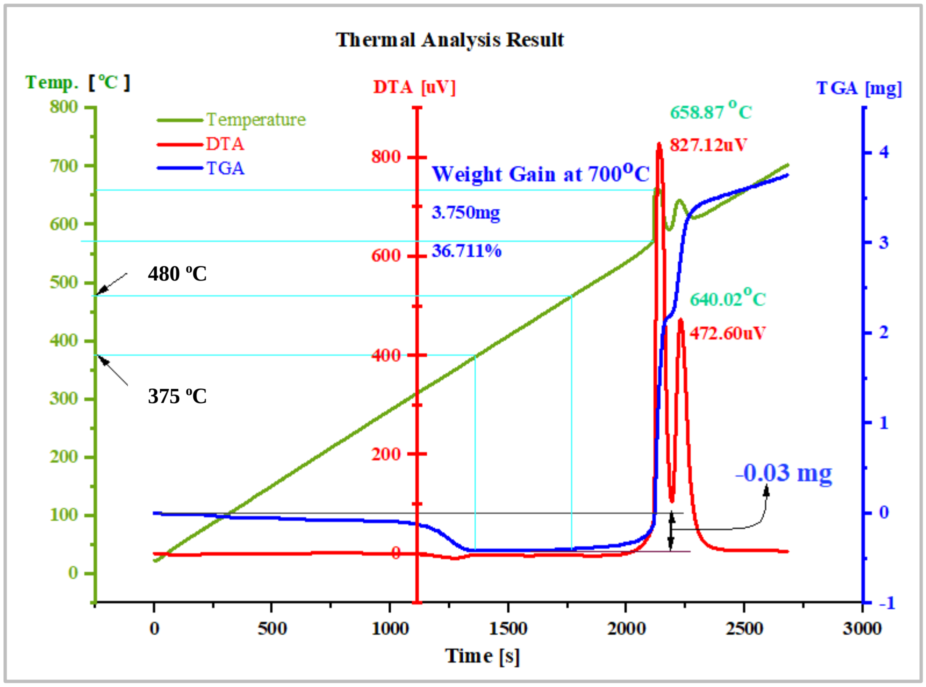

Figure 4.28 Thermogravimetric and Differential Thermal Analysis Curves for Optimized MMHC

Thermogravimetric Analysis (TGA) is a technique that is used to study the thermal decomposition of materials. Furthermore, Nasrollahzadeh et al., (2019), stated that TGA is a commonly employed method to examine specific characteristics of materials that exhibit mass gain or loss as a result of oxidation, decomposition, or volatile (moisture) loss. This study used a DTG-60H detector to perform a TGA of the optimum MMHC (85 %wt. AZ61-7.5 %wt. of ZrO_2-7.5 %wt. of SiC) of a sample weight of 10.215 mg. The temperature was heated at a rate of 15 ^{o}C per minute throughout a range of 15 to 700 ^{o}C in nitrogen gas at a flow rate of 50 ml/min. Results in the Figure 4.28 shows the temperature, TGA values, and DTA (Differential Thermal Analysis) data at different time intervals. The TGA curve result showed that weight loss increased very slightly until the temperature reached 375 degrees Celsius. This may have been caused by moisture escaping or the release of a volatile component (Lal et al., 2018). The MMHC exhibited thermal stability between 375 and 480 degrees Celsius with no weight gain or loss. Lal et al., (2018), has carried out thermal analysis for Al7075/SiC/Al_2O_3 hybrid composite and the TGA result showed that the composites had good thermal stability range from 400°C to 600°C. When the temperature surpasses 480 ^{o}C the material showed slight weight gain. However, when the temperature surpasses 570 ^{o}C the material starts to gain weight eminently up to 3.75mg and when the temperature surpassed 570 ^{o}C. The DTA exothermic peak occurred at temperature of 658.87 ^{o}C witnessing phase transition at that specific temperature (Ashebir et al., 2022). The DTA plot shows the existence of two exothermic peaks (at a temperature of 658.87 ^{o}C and 640.02 ^{o}C) and one endothermic peak at a 109.51 microvolt (temperature of 599.62 ^{o}C, and a weight loss of 2.23mg). The exothermic reaction at 658.87 ^{o}C may indicate combustion or oxidation because the temperature suddenly increased and then gradually returned to its consistently increasing pattern. Additionally, TGA revealed notable weight growth at that particular temperature. Overall, the findings indicate that the material begins to increase weight at higher temperatures but remains relatively stable at temperatures below 658.87 ^{o}C. The material could be decomposing through a complex series of reactions if the weight gain is sudden and continuous. TGA generally indicated that MMHC thermal stability ranged from 375 ^{o}C to 480 ^{o}C. Moreover, DTA revealed that the phase transition begins around 658.87 ^{o}C.

4.7.8 SEM Analysis of Worn Out Optimum Sample Predicted by GA

The hybrid composite's wear morphology was investigated by Scanning Electron Microscopy on the optimized worn-out samples. As the type of wear involved was dry sliding, wear mechanisms such as micro ploughing, grooves and delamination played a prominent role in defining the wear morphology as shown in Figure 4.29. Similar to this, the worn surface exhibited higher degrees of abrasive wear characteristics like ploughs (displacing material to the sides) because of mild abrasive wear, surface fatigue, and delamination (Jojith & Radhika, 2021). The debris is visible as broken pieces that are crushed between the test sample and rotating disc. Less wear is visible in the wear debris of graphite and ZrO_2-based composites, which contains tiny particles like pin fragments that have been pulled out. The extent of wear in composite material is determined by the size and shape of the debris (Kumar et al., 2021). Additionally, a study by Ram Kumar et al., (2018) investigated that, as the rubbing time rises, the ploughing effect occurs, this is evident that the shallow plough occurred due to minimum levels of sliding distance and sliding speed.

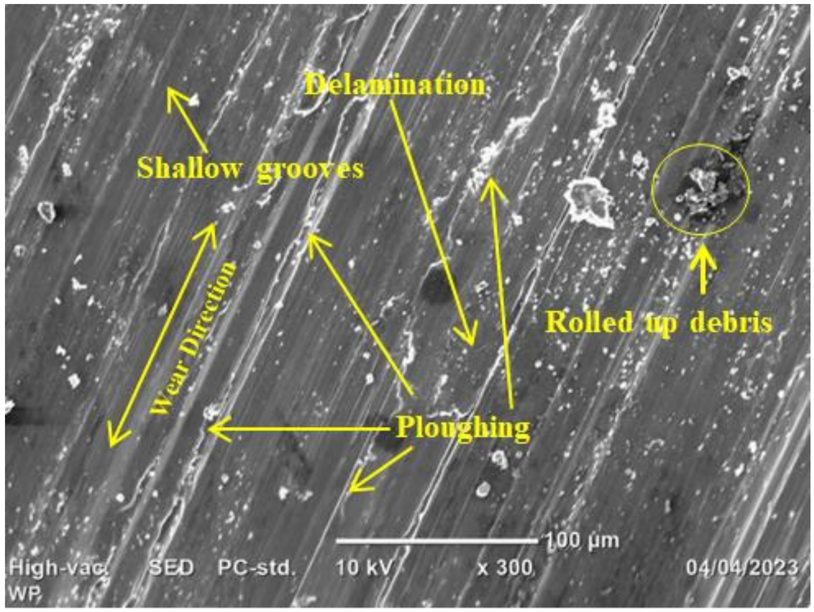

Figure 4.29 SEM Image of Wear Morphology of GA Optimized Sample (350m, 220RPM and 20N)

As the SEM observed surface image shown in Figure 4.29 minimum delamination and ploughing shows that the material has resistance to wear as investigated on study Ram K. et al., (Ram et al., 2018), witnessing the occurrence of anti-friction layer at the interface and which results in the lowering of the material's wear rate. Generally, as the loss of material caused by the movement of tough particles across a surface is known as abrasive wear (Alpas et al., 2017). The rolled up debris, delamination, shallow grooves and shallow ploughs also observed witnessing the wear formation on the sample is mostly abrasive wear.

4.7.9 Summary of Wear Property Optimization

In conclusion, wear rate parametric optimization of magnesium alloy hybrid composites (7.5%t of SiC, 7.5%wt of ZrO_2 as a reinforcement and 85% of AZ61 magnesium alloy) fabricated through FSC process were experimentally investigated. RSM (Box-Behnken) and GA were implemented in optimization. Thermal property was also studied. The Box-Behnken design allowed for the efficient exploration of the parameter space by systematically varying the input factors such as load, sliding speed and sliding distance. By running a minimum number of experiments, the Box-Behnken design efficiently attained the complex interactions between the independent variables, allowing for the development of mathematical model to describe the wear behavior. Generally, based on the obtained results the following conclusions can be drawn.

- ❖ Optimization through RSM, the optimum parametric setups for minimum wear rate was predicted to be at [350m, 240Rpm and 20N] and accounted experimentally verified wear rate of 0.008 mg/m.
- ❖ Optimization for minimum wear rate predicted by GA successfully converged on an optimized solution through multiple iterations at parametric combination of [350m, 220Rpm and 20N] which was experimentally verified wear rate of 0.00514 mg/m.
- ❖ Thermogravimetric results showed that, from the temperature 375 ^{o}C to 480 ^{o}C the MMHC showed thermal stability with no weight loss and gain.
- ❖ Results witnessed that FSC can be a promising fabrication method for magnesium alloy hybrid composites with a comparable wear resisting property of MMCs as compared to previous studies.

Furthermore, the implementation of GA optimization enhanced the Box-Behnken design by fine-tuning the independent variables such as, load, sliding speed and sliding distance to attain optimal wear rate.

5. CONCLUSIONS AND RECOMMENDATIONS

5.1 Conclusions

The comprehensive investigation into the physical, mechanical, and tribological behavior of metal matrix hybrid composites produced via the innovative FSC process, employing an integrated approach involving DEM simulation, RSM, ANN validation, and GA optimization, has yielded insightful findings.

The initial computational analysis using Altair EDEM software, based on a Box-Behnken design of experiments, considered five crucial process parameters: Load, Time, Thickness, Speed, and Composition. The optimization target, porosity, was successfully achieved at an impressive 0.62%. The subsequent validation of the RSM model using ANN provided a robust confirmation of the simulation results. Further refinement of the process parameters was pursued through Genetic Algorithm optimization, leading to a notable improvement in accuracy, with the optimized porosity reduced to 0.54%. Remarkably, the RSM analysis reiterated the significance of all five factors, emphasizing their crucial roles in influencing the fabrication process. Additionally, the regression model developed through RSM demonstrated exceptional reliability, exhibiting minimal error ranging from 3 to 5%, affirming its attractiveness for predicting outcomes in the fabrication process. This level of precision and predictability is crucial for the reproducibility and scalability of the Friction Stir Consolidation FSC process.

The mechanical properties of the AZ61 matrix hybrid composite reinforced with SiC and ZrO_2 produced through FSC exhibited a superior porosity level when contrasted with composites fabricated using conventional methods such as powder metallurgy and stir casting. This underscores the potential of FSC as an advanced and promising technique for enhancing the overall quality of metal matrix hybrid composites.

In light of these findings, the integration of DEM simulation, RSM optimization, ANN validation, and GA refinement in the study has not only provided a thorough understanding of the FSC process but has also demonstrated its superiority in achieving enhanced material properties. The outcomes of this research contribute valuable insights to the field, paving the way for further advancements in the fabrication of metal matrix hybrid composites. Therefore, it is recommended that future research endeavors continue to explore and exploit the full potential of the FSC process, considering its promising outcomes in terms of mechanical performance, porosity reduction, and overall material enhancement.

The GA-optimized sample was experimentally fabricated through FSC, resulting in mechanically attractive properties. This successful translation from simulation to practical application validates the effectiveness of the optimization techniques employed. The outcomes of this research not only contribute to the scientific understanding of FSC but also provide practical insights for the advancement of manufacturing processes, particularly in the realm of metal matrix hybrid composites.

5.1.1 DEM Simulation

The focus of this study was to comprehensively analyze the friction stir consolidation process computationally, followed by rigorous optimization and validation procedures. The numerical simulations using Altair EDEM software, particularly in the context of metal matrix composite powders, have proven to be highly successful. The DEM simulations were conducted with a keen emphasis on five crucial process parameters: Load, Time, Thickness, Speed, and Composition. The utilization of the RSM Box-Behnken design of experiments facilitated a systematic exploration of the parameter space, aiming to optimize the outcomes of the friction stir consolidation process.

One of the noteworthy achievements of this study is the exceptional accuracy demonstrated by the DEM simulation results when compared with the actual experimental validation. The porosity results obtained through DEM simulations were found to be in remarkable agreement with the experimental data, attesting to the credibility and reliability of the computational predictions.

5.1.2 Optimization and Model Validation

The journey of optimization results could lead to the following conclusions:

- ❖ The RSM optimization process, targeting five critical process parameters such as Load, Time, Thickness, Speed, and Composition led to the achievement of a highly optimized response, notably a reduced porosity of 0.62%.
- ❖ The validation of the RSM model through ANN underscored the robustness and accuracy of the developed model. The coefficient of determination values (R) obtained

during training (0.99356), validation (0.86149), test (0.89981), and overall (0.9733) phases highlighted the remarkable predictive capability of the model.

- To further enhance the precision and accuracy of the parameters, GA optimization was employed, resulting in an even lower porosity of 0.54%. The validation using RSM reiterated the significance of all five factors, as evidenced by p values less than 0.05. This reaffirms the importance of Load, Time, Thickness, Speed, and Composition in influencing the porosity of the metal matrix hybrid composite.
- The regression model developed through the RSM optimization was found to be highly attractive, boasting a minimal error ranging from 3 to 5% (based on verification experiment). This level of accuracy is crucial for ensuring the reliability of the model in predicting and optimizing the fabrication process. The success of the developed regression model not only highlights the significance of the chosen parameters but also emphasizes the robustness and applicability of the integrated DEM simulation with optimization techniques.
- The regression model was developed as (Porosity = 1.5683- 0.0712 x_1 - 0.4325 x_2 - 0.1013 x_3 + 0.2588 x_4 - 0.2388 x_5); Where, porosity is in %, x_1 is composition in %wt, x_2 is load in n and x_3 is speed in rpm, x_4 is thickness and x_5 is time. Verification experiment results depicted that the consistency and reliability of the regression model with error percentage of 4.17%, 1.92% and 3.7% for experiment three random experiments.

5.1.3 Characterizations and Test Results

Optimization of parameters using Genetic Algorithm aimed at enhancing accuracy resulted in a refined porosity of 0.54%. This iterative optimization process showcases the dynamic adaptability of the computational framework in fine-tuning the FSC process for optimal outcomes. The computational efforts ended in the actual fabrication of GA-optimized MMHC samples for thorough testing and characterization.

- The obtained results underscore the success of the computational predictions, revealing a compressive yield strength of 170±2.6 MPa, a hardness of 339±1.5 HV (3324.6±14.7 MPa), and a minimal wear rate of 0.00514 mg/m.

- Fractography analysis via Scanning Electron Microscopy (SEM) unveiled a complex form of fracture favoring brittle form of fracture, while wear morphology, as observed in SEM images, pointed towards abrasive wear characteristics.
- Thermogravimetric Analysis demonstrated the thermal stability of the MMHC, revealing no discernible weight gain or loss in the temperature range from 375°C to 480°C.

5.2 Recommendations

5.2.1 Technical Recommendations

Basing from the understandings gained from the FSC process experiment, the following recommendations are few technical suggestions that are considered to be useful in helping next researcher avoid having to start from scratch.

- Two-way rotating die is recommendable as there was noticed infinitesimal variation in hardness property at the top and bottom surface of the sample.
- Although split dies coupled with bolt-nuts were used in this experimental investigation, it is advised to couple dies with pins instead of bolt-nuts since this saves time while removing samples.

5.2.2 Future Works

In establishing the way for future research inspirations, the investigation into the "Physical, Mechanical, and Tribological Behavior of Metal Matrix Hybrid Composite Fabricated via Friction Stir Consolidation Process" has opened ways for further exploration and refinement. Depending on the foundation established by this research, several key areas emerge as promising directions for future research:

- **Optimization of Additional Parameters:** While the current study delved into five critical process parameters, there exists an opportunity to extend the investigation by considering additional factors that might influence the FSC process. Exploring a broader parameter space could unveil nuanced insights and enhance the overall understanding of the fabrication process.

- **Advanced Simulation Techniques:** The use of DEM simulation has proven effective in this research. However, the incorporation of other advanced simulation techniques, such as finite element analysis or computational fluid dynamics, may offer a more comprehensive understanding of the material behavior during FSC. Combining these methods could provide a holistic view of the consolidation process.

- **Material Characterization beyond Porosity:** While porosity is a crucial factor, future research could delve into a more nuanced examination of material properties. Investigating other mechanical, thermal, and tribological properties of the metal matrix hybrid composites fabricated through FSC would contribute to a more thorough understanding of their overall performance.

- **Microstructural Analysis:** Conduct a detailed microstructural analysis to delve deeper into the grain structure and phase distribution within the composite material, providing insights into the relationship between microstructure and mechanical properties.

- **Multi-scale Modeling:** Employing multi-scale modeling approaches could enable a more accurate representation of the FSC process, considering the interactions at both macro and micro levels. Integrating different modeling scales could provide a more detailed and accurate prediction of material behavior, aiding in the optimization of the fabrication process.

- **Multi-Objective Optimization:** Explore multi-objective optimization approaches to simultaneously enhance multiple material properties, such as strength, hardness, and wear resistance, to achieve a well-rounded performance profile.

- **Environmental and Sustainability Considerations:** Future research could also explore the environmental impact and sustainability aspects of the FSC process. Assessing the energy consumption, carbon footprint, and recyclability of materials produced through FSC would contribute valuable insights in the context of advancing environmentally conscious manufacturing practices.

- **Validation Techniques Diversity:** While the current study validated the RSM model through ANN and GA, exploring alternative validation techniques or combining multiple methods could enhance the robustness of the models developed. This could involve experimental validations, statistical analyses, or other machine learning approaches.

- **Real-world Applications and Industrial Scale-Up:** Transitioning from laboratory-scale experiments to real-world applications and industrial-scale production is a crucial step. Future research could focus on bridging this gap, addressing challenges and optimizing the FSC process for practical implementation in manufacturing settings.
- **Comparative Analysis:** In order to fully define the status of FSC, a detail comparative analysis of FSC process with the pre-existing dominant methods of metal matrix fabrication techniques such as stir casting and powder metallurgy could be recommendable. Optimizations and MMC fabrications through stir casting as well as powder metallurgy are important to fully describe the FSC process.

By addressing these areas for future research, the next researcher can continue to advance the understanding of the Friction Stir Consolidation process and contribute to the development of innovative, efficient, and sustainable manufacturing practices for metal matrix hybrid composites.

REFERENCES

Abbasi, M., Bagheri, B., Dadaei, M., Omidvar, H. R., & Rezaei, M. (2015). The effect of FSP on mechanical, tribological, and corrosion behavior of composite layer developed on magnesium AZ91 alloy surface. *International Journal of Advanced Manufacturing Technology*, *77*(9–12), 2051–2058. https://doi.org/10.1007/s00170-014-6577-x

Abebe, S. K., Beri, H., Sinha, D. K., Rajhi, A. A., Hossain, N., Duhduh, A. A., Zainuddin, S., & Ahmed, G. M. S. (2023). Wear Behavior of AZ61 Matrix Hybrid Composite Fabricated via Friction Stir Consolidation: A Combined RSM Box–Behnken and Genetic Algorithm Optimization. *Journal of Composites Science*, *7*(7), 1–18. https://doi.org/10.3390/jcs7070275

Abreu, C. M., Acuña, R., Cabeza, M., Cristóbal, M. J., Merino, P., & Verdera, D. (2017). Microstructure and mechanical properties of Al/SiC composite surface layer produced by friction stir processing. *Ciencia e Tecnologia Dos Materiais*, *29*(1), e82–e86. https://doi.org/10.1016/j.ctmat.2016.07.001

Ajay Guru, N., Swaminathan, G., Prasanna Venkatesh, P. R., & Aravind, P. (2018). Experimental Investigation on Hardness and Thermal Conductivity of D2 Steel Alloyed with Copper. *Materials Today: Proceedings*, *5*(14), 27673–27679. https://doi.org/10.1016/j.matpr.2018.10.001

Alizadeh, M., Alizadeh, M., & Amini, R. (2013). Structural and mechanical properties of Al/B4C composites fabricated by wet attrition milling and hot extrusion. *Journal of Materials Science and Technology*, *29*(8), 725–730. https://doi.org/10.1016/j.jmst.2013.04.015

Alpas, A. T., Bhattacharya, S., & Hutchings, I. M. (2017). Wear of particulate metal matrix composites. In *Comprehensive Composite Materials II* (Vol. 4). Elsevier Ltd. https://doi.org/10.1016/B978-0-12-803581-8.09965-3

Altinkok, N., & Koker, R. (2006). Modelling of the prediction of tensile and density properties in particle reinforced metal matrix composites by using neural networks. *Materials and Design*, *27*(8), 625–631. https://doi.org/10.1016/j.matdes.2005.01.005

Álvarez, M. J., Ilzarbe, L., Viles, E., & Tanco, M. (2009). The Use of Genetic Algorithms in Response Surface Methodology. *Quality Technology & Quantitative Management*, *6*(3), 295–307. https://doi.org/10.1080/16843703.2009.11673201

Amancio-Filho, S. T., Bueno, C., dos Santos, J. F., Huber, N., & Hage, E. (2011). On the feasibility of friction spot joining in magnesium/fiber-reinforced polymer composite hybrid structures. *Materials Science and Engineering: A*, *528*(10–11), 3841–3848. https://doi.org/10.1016/j.msea.2011.01.085

Anggara, B. S., Fahdiran, R., Marpaung, M. A., & Soegijono, B. (2019). Silicon carbide (SiC) effect on mechanical properties and corrosion rates on composite Al/SiC and Al-Cu/SiC. *AIP Conference Proceedings*, *2169*(October 2016). https://doi.org/10.1063/1.5132691

Annigeri, U. K., & Veeresh Kumar, G. B. (2017). Method of stir casting of Aluminum metal matrix Composites: A review. *Materials Today: Proceedings*, *4*(2), 1140–1146. https://doi.org/10.1016/j.matpr.2017.01.130

Ardebili, H., & Pecht, M. G. (2009). Defect and Failure Analysis Techniques for Encapsulated Microelectronics. *Encapsulation Technologies for Electronic Applications*, 287–350. https://doi.org/10.1016/b978-0-8155-1576-0.50010-3

Arefi, M. R., & Rezaei-Zarchi, S. (2012). Synthesis of zinc oxide nanoparticles and their effect on the compressive strength and setting time of self-compacted concrete paste as cementitious composites. *International Journal of Molecular Sciences*, *13*(4), 4340–4350. https://doi.org/10.3390/ijms13044340

Arora, H. S., Singh, H., & Dhindaw, B. K. (2012). Composite fabrication using friction stir processing - A review. *International Journal of Advanced Manufacturing Technology*, *61*(9–12), 1043–1055. https://doi.org/10.1007/s00170-011-3758-8

Asadi, P., Faraji, G., & Besharati, M. K. (2010). Producing of AZ91/SiC composite by friction stir processing (FSP). *International Journal of Advanced Manufacturing Technology*, *51*(1–4), 247–260. https://doi.org/10.1007/s00170-010-2600-z

Ashebir, D. A., Mengesha, G. A., & Sinha, D. K. (2022). The Role of Tetra Hybrid Reinforcements on the Behavior of Aluminum Metal Matrix Composites. *Journal of Nanomaterials*, *2022*. https://doi.org/10.1155/2022/1988293

Aslantas, K., Danish, M., Hasçelik, A., Mia, M., Gupta, M., Ginta, T., & Ijaz, H. (2020). investigations on surface roughness and toolwear characteristics in micro-turning of Ti-6Al-4V alloy. *Materials*, *13*(13), 1–20. https://doi.org/10.3390/ma13132998

Avettand-Fènoël, M. N., & Simar, A. (2016). A review about Friction Stir Welding of metal matrix composites. *Materials Characterization*, *120*, 1–17. https://doi.org/10.1016/j.matchar.2016.07.010

Avinash, L., Kumar, H., Parthasarathy, A., Varun Kumar, K. N., & Sajjan, B. (2017). The Effect of Ceramic Reinforcement on the Microstructure, Mechanical Properties and Tribological Behavior of Al-7.5%Si-0.5%Mg Alloy. *Applied Mechanics and Materials*, *867*, 3–9. https://doi.org/10.4028/www.scientific.net/amm.867.3

Azevedo, L., Kashaev, N., Horstmann, C., Ventzke, V., Furtado, C., Moreira, P. M. G. P., & Tavares, P. J. (2022). Fatigue behaviour of laser shock peened AISI D2 tool steel. *International Journal of Fatigue*, *165*, 107226. https://doi.org/10.1016/J.IJFATIGUE.2022.107226

Aziz, I., & Bedien, R. (2020). Effect of ZrO2 Addition on Microstructure and Mechanical Properties of Al-Zn-Mg Alloy Matrix Composite. *Engineering and Technology Journal*, *38*(12), 1751–1757. https://doi.org/10.30684/etj.v38i12a.336

Babu, J., Anjaiah, M., & Mathew, A. (2018). Experimental studies on Friction stir processing of AZ31 Magnesium alloy. *Materials Today: Proceedings*, *5*(2), 4515–4522. https://doi.org/10.1016/j.matpr.2017.12.021

Babu, S., Elangovan, K., Balasubramanian, V., & Balasubramanian, M. (2009). Optimizing friction stir welding parameters to maximize tensile strength of AA2219 aluminum alloy joints. *Metals and Materials International*, *15*(2), 321–330. https://doi.org/10.1007/s12540-009-0321-3

Bahloul, R., Arfa, H., & Belhadjsalah, H. (2014). *A study on optimal design of process parameters in single point incremental forming of sheet metal by combining Box – Behnken design of experiments , response surface methods and genetic algorithms*. 163–185. https://doi.org/10.1007/s00170-014-5975-4

Bajakke, P. A., Malik, V. R., & Deshpande, A. S. (2019). Particulate metal matrix composites and their fabrication via friction stir processing–a review. *Materials and Manufacturing Processes*, *34*(8), 833–881. https://doi.org/10.1080/10426914.2019.1605181

Balakrishnan, G., Velavan, R., Mujasam Batoo, K., & Raslan, E. H. (2020). Microstructure, optical and photocatalytic properties of MgO nanoparticles. *Results in Physics*, *16*(February), 103013. https://doi.org/10.1016/j.rinp.2020.103013

Baloyi, N. P., Nseke, J. M., & Makhatha, M. E. (2022). Application of Response Surface Methodology (RSM) for Simultaneous Optimization of Kinetic Parameters Affecting Gold Leaching in Thiosulfate Based Media: A Statistical Approach. *Journal of Chemistry*, *2022*. https://doi.org/10.1155/2022/8348167

Baradeswaran, A., Elayaperumal, A., & Franklin Issac, R. (2013). A statistical analysis of optimization of wear behaviour of Al- Al 2O3 composites using taguchi technique. *Procedia Engineering*, *64*, 973–982. https://doi.org/10.1016/j.proeng.2013.09.174

Baxter, J. W., & Bumby, J. R. (1995). *Proceedings of the Institution of Mechanical Engineers , Part I : Journal of Systems and Control Engineering*. https://doi.org/10.1243/PIME

Behera, M. P., Dougherty, T., & Singamneni, S. (2019). Conventional and additive manufacturing with metal matrix composites: A perspective. *Procedia Manufacturing*, *30*, 159–166. https://doi.org/10.1016/j.promfg.2019.02.023

Ben-Nissan, B., Cazalbou, S., & Choi, A. H. (2019). Bioceramics. *Encyclopedia of Biomedical Engineering*, *1–3*, 16–33. https://doi.org/10.1016/B978-0-12-801238-3.99867-2

Bhadouria, N., Kumar, P., Thakur, L., Dixit, S., & Arora, N. (2017). A Study on Micro-hardness and Tribological Behaviour of Nano-WC–Co–Cr/Multi-walled Carbon Nanotubes Reinforced AZ91D Magnesium Matrix Surface Composites. *Transactions of the Indian Institute of Metals*, *70*(9), 2477–2483. https://doi.org/10.1007/s12666-017-1111-0

Bhardwaj, N., Narayanan, R. G., Dixit, U. S., Petrov, M., & Petrov, P. (2020). ScienceDirect ScienceDirect ScienceDirect An Inverse Approach Towards Determination of Friction in Friction Stir An Inverse Approach Towards Determination of Friction in Friction Stir Spot Welding Spot Welding. *Procedia Manufacturing*, *47*(2019), 839–846. https://doi.org/10.1016/j.promfg.2020.04.261

Boac, J. M., Casada, M. E., & Maghirang, R. G. (2010). *M i p s g o m d p*. *53*(4), 1201–1216.

Bose, N. B. P. S. C. (2023). Optimizing the Wear Behaviour of AA7178 Metal Matrix Composites Reinforced with SiC and - TiO 2 Nanoparticles : A Comparative Study Using Evolutionary and Statistical Methods. *Silicon*, *0123456789*. https://doi.org/10.1007/s12633-023-02395-6

Bourithis, L., Papadimitriou, G. D., & Sideris, J. (2006). Comparison of wear properties of tool steels AISI D2 and O1 with the same hardness. *Tribology International*, *39*(6), 479–489. https://doi.org/10.1016/j.triboint.2005.03.005

Cao, X., Li, Z., Zhou, X., Luo, Z., & Duan, J. (2021). Modeling and optimization of resistance spot welded aluminum to Al-Si coated boron steel using response surface methodology and genetic algorithm. *Measurement: Journal of the International Measurement Confederation*, *171*(November 2020), 108766. https://doi.org/10.1016/j.measurement.2020.108766

Cardoso-jaime, V., Broderick, N. A., & Maya-maldonado, K. (2022). Jo ur n al Pr pr oo. *Current Opinion in Insect Science*, 100924. https://doi.org/10.1016/j.jalmes.2023.100002

Cerit, A. A., Karamiş, M. B., Fehmi, N., & Kemal, Y. (2008). Effect of reinforcement particle size and volume fraction on wear behaviour of metal matrix composites. *Tribology in Industry*, *30*(3–4), 31–36.

Chaira, D. (2021). Powder Metallurgy Routes for Composite Materials Production. In *Encyclopedia of Materials: Composites* (Vol. 2, Issue 1). Elsevier Ltd. https://doi.org/10.1016/B978-0-12-803581-8.11703-5

Chanakyan, C., Sivasankar, S., Meignanamoorthy, M., Ravichandran, M., Alagarsamy, S. V., Kumar, S. D., & Sakthivelu, S. (2020). Friction stir processing (FSP) of numerical study based on design of experiment-review. *Materials Today: Proceedings*, *27*(xxxx), 748–751. https://doi.org/10.1016/j.matpr.2019.12.035

Chandradass, J., Thirugnanasambandham, T., Jawahar, P., & Kannan, T. T. M. (2020). Effect of silicon carbide and silicon carbide/alumina reinforced aluminum alloy (AA6061) metal matrix composite. *Materials Today: Proceedings*, *45*, 7147–7150. https://doi.org/10.1016/j.matpr.2021.02.143

Chawla, N., & Chawla, K. K. (2010). *Metal-Matrix Composites in Ground Transportation*.

2004–2007.

Chen, J. H., & Cao, R. (2015). Introduction. *Micromechanism of Cleavage Fracture of Metals*, 1–54. https://doi.org/10.1016/b978-0-12-800765-5.00001-0

Chen, X., & Miedema, S. A. (2007). Porosity calculation in discrete element modeling of sand cutting process. *18th World Dredging Congress 2007, WODCON 2007, June 2013*, 942–955.

Christian, J. L., & Campbell, M. D. (1973). Mechanical and Physical Properties of Several Advanced Metal-Matrix Composite Materials. *Advances in Cryogenic Engineering*, 175–183. https://doi.org/10.1007/978-1-4684-3111-7_21

CUDA for Machine Learning and Optimization. (2011). *CUDA Application Design and Development*, 33–61. https://doi.org/10.1016/B978-0-12-388426-8.00002-1

Danish, M., Ginta, T. L., Habib, K., Carou, D., Rani, A. M. A., & Saha, B. B. (2017). Thermal analysis during turning of AZ31 magnesium alloy under dry and cryogenic conditions. *International Journal of Advanced Manufacturing Technology*, *91*(5–8), 2855–2868. https://doi.org/10.1007/s00170-016-9893-5

Danninger, H., & Gierl-Mayer Dr, C. (2013). Advanced powder metallurgy steel alloys. In *Advances in Powder Metallurgy: Properties, Processing and Applications*. https://doi.org/10.1533/9780857098900.2.149

Das, A., Sarkar, S., Karanjai, M., & Sutradhar, G. (2018). RSM Based Study on the Influence of Sintering Temperature on MRR for Titanium Powder Metallurgy Products using Box-Behnken Design. *Materials Today: Proceedings*, *5*(2), 6509–6517. https://doi.org/10.1016/j.matpr.2018.01.137

Dehabadi, V. M., Ghorbanpour, S., & Azimi, G. (2016). Application of artificial neural network to predict Vickers microhardness of AA6061 friction stir welded sheets. *Journal of Central South University*, *23*(9), 2146–2155. https://doi.org/10.1007/s11771-016-3271-1

Deswal, S., Narang, R., & Chhabra, D. (2019). Modeling and parametric optimization of FDM 3D printing process using hybrid techniques for enhancing dimensional preciseness. *International Journal on Interactive Design and Manufacturing*, *13*(3), 1197–1214. https://doi.org/10.1007/s12008-019-00536-z

Dinaharan, I., & Akinlabi, E. T. (2018). Low cost metal matrix composites based on aluminum, magnesium and copper reinforced with fly ash prepared using friction stir processing. *Composites Communications*, *9*(November 2017), 22–26. https://doi.org/10.1016/j.coco.2018.04.007

Dinaharan, I., Zhang, S., Chen, G., & Shi, Q. (2022). Assessment of Ti-6Al-4V particles as a reinforcement for AZ31 magnesium alloy-based composites to boost ductility incorporated through friction stir processing. *Journal of Magnesium and Alloys*, *10*(4), 979–992. https://doi.org/10.1016/j.jma.2020.09.026

Długosz, O., Szostak, K., Krupiński, M., & Banach, M. (2021). Synthesis of Fe3O4/ZnO nanoparticles and their application for the photodegradation of anionic and cationic dyes. *International Journal of Environmental Science and Technology*, *18*(3), 561–574. https://doi.org/10.1007/s13762-020-02852-4

Dolatkhah, A., Golbabaei, P., Besharati Givi, M. K., & Molaiekiya, F. (2012). Investigating effects of process parameters on microstructural and mechanical properties of Al5052/SiC metal matrix composite fabricated via friction stir processing. *Materials and Design*, *37*, 458–464. https://doi.org/10.1016/j.matdes.2011.09.035

El-Sabbagh, A., Soliman, M., Taha, M., & Palkowski, H. (2012). Hot rolling behaviour of stir-cast Al 6061 and Al 6082 alloys - SiC fine particulates reinforced composites. *Journal of Materials Processing Technology*, *212*(2), 497–508. https://doi.org/10.1016/j.jmatprotec.2011.10.016

Elatharasan, G., & Kumar, V. S. S. (2012). Modelling and optimization of friction stir welding parameters for dissimilar aluminium alloys using RSM. *Procedia Engineering*, *38*, 3477–3481. https://doi.org/10.1016/j.proeng.2012.06.401

Fan, M., Li, T., Hu, J., Cao, R., Wei, X., Shi, X., & Ruan, W. (2017). Artificial neural network modeling and genetic algorithm optimization for cadmium removal from aqueous solutions by reduced graphene oxide-supported nanoscale zero-valent iron (nZVI/rGO) composites. *Materials*, *10*(5). https://doi.org/10.3390/ma10050544

Feng, Y. T., Han, K., Owen, D. R. J., & Loughran, J. (2009). On upscaling of discrete element models: Similarity principles. *Engineering Computations (Swansea, Wales)*, *26*(6), 599–

609. https://doi.org/10.1108/02644400910975405

Feng, Y. T., & Owen, D. R. J. (2014). Discrete element modelling of large scale particle systems—I: exact scaling laws. *Computational Particle Mechanics*, *1*(2), 159–168. https://doi.org/10.1007/s40571-014-0010-y

Fenghong, C., Chang, C., Zhenyu, W., Muthuramalingam, T., & Anbuchezhiyan, G. (2019). Effects of Silicon Carbide and Tungsten Carbide in Aluminium Metal Matrix Composites. *Silicon*, *11*(6), 2625–2632. https://doi.org/10.1007/s12633-018-0051-6

Gad, S. I., Attia, M. A., Hassan, M. A., & El-Shafei, A. G. (2021). Predictive computational model for damage behavior of metal-matrix composites emphasizing the effect of particle size and volume fraction. *Materials*, *14*(9). https://doi.org/10.3390/ma14092143

Gangwar, S., Sharma, S., & Pathak, V. K. (2021). Preliminary Evaluation and Wear Properties Optimization of Boron Carbide and Molybdenum Disulphide Reinforced Copper Metal Matrix Composite Using Adaptive Neuro-fuzzy Inference System. *Journal of Bio- and Tribo-Corrosion*, *7*(1), 1–19. https://doi.org/10.1007/s40735-020-00444-w

Gethin, D. T., Lewis, R. W., & Ransing, R. S. (2003). A discrete deformable element approach for the compaction of powder systems. *Modelling and Simulation in Materials Science and Engineering*, *11*(1), 101–114. https://doi.org/10.1088/0965-0393/11/1/308

Ghasemi-Kahrizsangi, A., Kashani-Bozorg, S. F., Moshref-Javadi, M., & Sharififar, M. (2015). Friction Stir Processing of Mild Steel/Al2O3 Nanocomposite: Modeling and Experimental Studies. *Metallography, Microstructure, and Analysis*, *4*(2), 122–130. https://doi.org/10.1007/s13632-015-0193-5

Gómez-Esparza, C. D., Duarte-Moller, A., López-Díaz de León, C., Martínez-Sánchez, R., Hernández-Paz, J. F., & Rodríguez-González, C. A. (2019). Influence of ZnO nanoparticles on the microstructure of a CoCrFeMoNi matrix via powder metallurgy. *International Journal of Minerals, Metallurgy and Materials*, *26*(11), 1467–1476. https://doi.org/10.1007/s12613-019-1863-0

Haja Syeddu Masooth, P., Bharathiraja, G., Jayakumar, V., & Palani, K. (2022). Microstructure and mechanical characterisation of ZrO2reinforced Ti6Al4V metal matrix composites by powder metallurgy method. *Materials Research Express*, *9*(2).

https://doi.org/10.1088/2053-1591/ac5352

Han, B. Q., & Chan, K. C. (1996). Superplastic deformation mechanisms of particulate reinforced aluminum matrix composites. *Materials Science and Engineering: A*, *212*(2), 256–264. https://doi.org/10.1016/0921-5093(96)10208-2

Hashim, J., Looney, L., & Hashmi, M. S. J. (1999). *Metal matrix composites : production by the stir casting method*. *93*, 1–7.

Hassan, S. F. (2006). Creation of new magnesium-based material using different types of reinforcements. *Thesis*.

Hayes, M. D., Edwards, D. B., & Shah, A. R. (2015). Introduction. *Fractography in Failure Analysis of Polymers*, 1–5. https://doi.org/10.1016/b978-0-323-24272-1.00001-5

Heat, T., Equation, C., Resistance, T., Conduction, T., Factor, S., & Conduction, U. (2007). *Heat conduction*. 1–42.

Horabik, J., & Molenda, M. (2016). Parameters and contact models for DEM simulations of agricultural granular materials: A review. *Biosystems Engineering*, *147*, 206–225. https://doi.org/10.1016/j.biosystemseng.2016.02.017

Hosseini, N., Karimzadeh, F., Abbasi, M. H., & Enayati, M. H. (2010). Tribological properties of Al6061-Al2O3 nanocomposite prepared by milling and hot pressing. *Materials and Design*, *31*(10), 4777–4785. https://doi.org/10.1016/j.matdes.2010.05.001

Hu, Z., Wu, Z., Luo, S., Wang, X., Nian, Q., Chen, Y., & Nagaumi, H. (2023). Large scale production of graphene aluminum composites by stir casting: Process, microstructure and properties. *Journal of Materials Research and Technology*, *27*, 681–691. https://doi.org/10.1016/j.jmrt.2023.09.298

JANBOZORGI, M., SHAMANIAN, M., SADEGHIAN, M., & SEPEHRINIA, P. (2017). Improving tribological behavior of friction stir processed A413/SiCp surface composite using MoS2 lubricant particles. *Transactions of Nonferrous Metals Society of China (English Edition)*, *27*(2), 298–304. https://doi.org/10.1016/S1003-6326(17)60034-7

Ji, X., Li, S., Zhang, X., Liu, L., Li, S., Gao, L., Li, X., & Wang, S. (2023). Influence of characteristic parameters of SiC reinforcements on mechanical properties of AlSi10Mg matrix composites by powder metallurgy. *Journal of Materials Research and Technology*, *24*, 6843–6853. https://doi.org/10.1016/j.jmrt.2023.04.262

Jiang, M. J., Yu, H. S., & Harris, D. (2005). A novel discrete model for granular material incorporating rolling resistance. *Computers and Geotechnics*, *32*(5), 340–357. https://doi.org/10.1016/j.compgeo.2005.05.001

John Joshua, K., Vijay, S. J., Ramkumar, P., & Mohanasundaram, S. (2020). Effect of ZnO particles on microstructure, microhardness and wear behaviour of AA7068 metal matrix composites synthesized by powder metallurgy. *Materials Science Forum*, *979 MSF*, 68–73. https://doi.org/10.4028/www.scientific.net/MSF.979.68

Johnson, K. L. (2013a). Normal contact of elastic solids – Hertz theory. *Contact Mechanics*, 84–106. https://doi.org/10.1017/cbo9781139171731.005

Johnson, K. L. (2013b). Rolling contact of elastic bodies. In *Contact Mechanics*. https://doi.org/10.1017/cbo9781139171731.009

Jojith, R., Radhika, N., & Govindaraju, M. (2022). *Reciprocating Wear Behavioural Analysis of Heat-treated Aluminium ZrO2/Al7Si0.3Mg Functionally Graded Composite Through Taguchi's Optimization Method*. https://doi.org/https://doi.org/10.1007/s12633-022-01862-w

Jojith, R., & Radhika, N. (2021). Reciprocal dry sliding wear of SiCp/Al–7Si-0.3 Mg functionally graded composites: Influence of T6 treatment and process parameters. *Ceramics International*, *47*(21), 30459–30470. https://doi.org/10.1016/j.ceramint.2021.07.225

Juliyana, S. J., Prakash, J. U., Salunkhe, S., Hussein, H. M. A., & Gawade, S. R. (2022). Mechanical Characterization and Microstructural Analysis of Hybrid Composites (LM5/ZrO2/Gr). *Crystals*, *12*(9). https://doi.org/10.3390/cryst12091207

Kaczmar, J. W., & Kainer, K. U. (1992). Effect of alumina fibre content on properties of pm 6061 aluminium alloy based composite materials. *Powder Metallurgy*, *35*(2), 133–136. https://doi.org/10.1179/pom.1992.35.2.133

Kalashnikov, K. N., Kalashnikova, T. A., Chumaevskii, A. V., Tarasov, S. Y., Rubtsov, V. E., Ivanov, A. N., & Kolubaev, E. A. (2017). High-strength friction stir processed dispersion hardened Al-Cu-Mg alloy. *AIP Conference Proceedings*, *1909*, 1–5. https://doi.org/10.1063/1.5013757

Kane, S. N., Mishra, A., & Dutta, A. K. (2016). Preface: International Conference on Recent Trends in Physics (ICRTP 2016). *Journal of Physics: Conference Series*, *755*(1). https://doi.org/10.1088/1742-6596/755/1/011001

Karkalos, N. E., Galanis, N. I., & Markopoulos, A. P. (2016). Surface roughness prediction for the milling of Ti-6Al-4V ELI alloy with the use of statistical and soft computing techniques. *Measurement: Journal of the International Measurement Confederation*, *90*, 25–35. https://doi.org/10.1016/j.measurement.2016.04.039

Katiyar, J. K., Hammad, J. Al, & Mohammed, A. S. (2021). Tribological Properties of Light Metal Matrix Composites. In *Encyclopedia of Materials: Composites* (Vol. 1, Issue 1). Elsevier Ltd. https://doi.org/10.1016/B978-0-12-819724-0.00104-X

Khajeh, M. (2009). Application of Box-Behnken design in the optimization of a magnetic nanoparticle procedure for zinc determination in analytical samples by inductively coupled plasma optical emission spectrometry. *Journal of Hazardous Materials*, *172*(1), 385–389. https://doi.org/10.1016/j.jhazmat.2009.07.025

Khalid, M. Y., Umer, R., & Khan, K. A. (2023). Review of recent trends and developments in aluminium 7075 alloy and its metal matrix composites (MMCs) for aircraft applications. *Results in Engineering*, *20*(August). https://doi.org/10.1016/j.rineng.2023.101372

Khodabakhshi, F., Simchi, A., Kokabi, A. H., Švec, P., Simančík, F., & Gerlich, A. P. (2015). Effects of nanometric inclusions on the microstructural characteristics and strengthening of a friction-stir processed aluminum-magnesium alloy. *Materials Science and Engineering: A*, *642*, 215–229. https://doi.org/10.1016/j.msea.2015.06.081

Kleijnen, J. P. C. (1995). Sensitivity analysis and optimization in simulation: design of experiments and case studies. *Winter Simulation Conference Proceedings*, *i*, 133–140. https://doi.org/10.1109/wsc.1995.478715

Kosky, P., Balmer, R., Keat, W., & Wise, G. (2021). Chapter 14 - Mechanical Engineering. *Exploring Engineering (Fifth Edition)*, 317–340. https://doi.org/10.1016/B978-0-12-415891-7.00012-1

Krishna Sai, B. L. N., & Tambe, P. (2022). Fracture mechanism and scratch behaviour of MWNTs reinforced 70/30 (wt/wt) PC/ABS blends and their nanocomposites. *Advanced Industrial and Engineering Polymer Research*, *5*(3), 183–197. https://doi.org/10.1016/j.aiepr.2022.02.002

Kumar, A., Vichare, O., Debnath, K., & Paswan, M. (2020). Fabrication methods of metal matrix composites (MMCs). *Materials Today: Proceedings*, *46*(xxxx), 6840–6846. https://doi.org/10.1016/j.matpr.2021.04.432

Kumar, B. S. P., Shobha, K. R., Singh, M. K., Rinawa, M. L., Madhavarao, S., Wadhawa, G. C., Alrebdi, T. A., & Christopher, D. (2022). Optimization and Wear Properties for the Composites of Metal Matrix AA8011/Boron Nitride Using Taguchi Method. *Journal of Nanomaterials, 2022*. https://doi.org/10.1155/2022/6957545

Kumar Bhoi, N., Singh, H., & Pratap, S. (2020). Synthesis and characterization of zinc oxide reinforced aluminum metal matrix composite produced by microwave sintering. *Journal of Composite Materials*, *54*(24), 3625–3636. https://doi.org/10.1177/0021998320918646

Kumar, N., Sharma, A., Manoj, M. K., & Ahn, B. (2023). Taguchi optimization of tribological properties and corrosion behavior of self-lubricating Al–Mg–Si/MoS2 composite processed by powder metallurgy. *Journal of Materials Research and Technology*, *26*, 1185–1197. https://doi.org/10.1016/j.jmrt.2023.07.215

Kumar Parida, A., & Maity, K. (2019). Modeling of machining parameters affecting flank wear and surface roughness in hot turning of Monel-400 using response surface methodology (RSM). *Measurement: Journal of the International Measurement Confederation*, *137*, 375–381. https://doi.org/10.1016/j.measurement.2019.01.070

Kumar, R., Deshpande, R. G., Gopinath, B., Harti, J., Nagaral, M., & Auradi, V. (2021). Mechanical Fractography and Worn Surface Analysis of Nanographite and ZrO2-Reinforced Al7075 Alloy Aerospace Metal Composites. *Journal of Failure Analysis and Prevention*, *21*(2), 525–536. https://doi.org/10.1007/s11668-020-01092-5

Lahlali, R., Massart, S., Serrhini, M. N., & Jijakli, M. H. (2008a). A Box-Behnken design for predicting the combined effects of relative humidity and temperature on antagonistic yeast population density at the surface of apples. *International Journal of Food Microbiology*, *122*(1–2), 100–108. https://doi.org/10.1016/j.ijfoodmicro.2007.11.053

Lahlali, R., Massart, S., Serrhini, M. N., & Jijakli, M. H. (2008b). *A Box-Behnken design for predicting the combined effects of relative humidity and temperature on antagonistic yeast population density at the surface of apples*. *122*, 100–108. https://doi.org/10.1016/j.ijfoodmicro.2007.11.053

Lai, S., & Chung, D. D. L. (1996). *Consumption of S i c whiskers by the AI-Sic reaction in aluminium-matrix S i c whisker composites*. *6*(3), 469–477.

Lal, S., Kumar, S., & Khan, Z. A. (2018). Microstructure evaluation, thermal and mechanical characterization of hybrid metal matrix composite. *IEEE Journal of Selected Topics in Quantum Electronics*, *25*(6), 1187–1196. https://doi.org/10.1515/secm-2017-0210

Lee, C. J., Huang, J. C., & Hsieh, P. J. (2006). Mg based nano-composites fabricated by friction stir processing. *Scripta Materialia*, *54*(7), 1415–1420. https://doi.org/10.1016/j.scriptamat.2005.11.056

Li, X., Baffari, D., & Reynolds, A. P. (2018). Friction stir consolidation of aluminum machining chips. *International Journal of Advanced Manufacturing Technology*, *94*(5–8), 2031–2042. https://doi.org/10.1007/s00170-017-1016-4

Li, Y., Xu, Y., & Thornton, C. (2005). A comparison of discrete element simulations and experiments for “sandpiles” composed of spherical particles. *Powder Technology*, *160*(3), 219–228. https://doi.org/10.1016/j.powtec.2005.09.002

Liu, B., Jin, W., Lu, A., Liu, K., Wang, C., & Mi, G. (2020). Optimal design for dual laser beam butt welding process parameter using artificial neural networks and genetic algorithm for SUS316L austenitic stainless steel. *Optics and Laser Technology*, *125*(November 2019), 106027. https://doi.org/10.1016/j.optlastec.2019.106027

Liu, F., Li, Y., Sun, Z., & Ji, Y. (2021). Corrosion resistance and tribological behavior of particles reinforced AZ31 magnesium matrix composites developed by friction stir processing. *Journal of Materials Research and Technology*, *11*, 1019–1030. https://doi.org/10.1016/j.jmrt.2021.01.071

Liu, G., Gao, X., Peng, C., Huang, Y., Fang, H., Zhang, Y., You, D., & Nanfeng, Z. (2020). Optimization of laser welding of DP780 to Al5052 joints for weld width and lap-shear force using response surface methodology. *Optics and Laser Technology*, *126*(November 2019), 106072. https://doi.org/10.1016/j.optlastec.2020.106072

Liu, H. J., Zhang, H. J., Huang, Y. X., & Yu, L. (2010). Mechanical properties of underwater friction stir welded 2219 aluminum alloy. *Transactions of Nonferrous Metals Society of China (English Edition)*, *20*(8), 1387–1391. https://doi.org/10.1016/S1003-6326(09)60309-5

Lone, N. F., Bajaj, D., Gangil, N., Mohammed, S. M. A. K., Chen, D., & Siddiquee, A. N. (2022). A Novel Study on the Effect of Tool Offset in Friction Stir Processing for Mg-NiTi Composite. *Crystals*, *12*(11), 1–11. https://doi.org/10.3390/cryst12111651

Luo, A. A. (2013). Magnesium casting technology for structural applications. *Journal of Magnesium and Alloys*, *1*(1), 2–22. https://doi.org/10.1016/j.jma.2013.02.002

Luo, X. C., Kang, L. M., Liu, H. L., Li, Z. J., Liu, Y. F., Zhang, D. T., & Chen, D. L. (2020). Enhancing mechanical properties of AZ61 magnesium alloy via friction stir processing: Effect of processing parameters. *Materials Science and Engineering: A*, *797*(August). https://doi.org/10.1016/j.msea.2020.139945

Lupo, M., Barletta, D., Sofia, D., & Poletto, M. (2021). *Spreading Process*.

M, S. K., S, R. B., M, V., & K, N. S. R. (2020). Applying visualization techniques to study the fluid flow pattern and the particle distribution in the casting of metal matrix composites. *Journal of Manufacturing Processes*, *58*(June), 668–676. https://doi.org/10.1016/j.jmapro.2020.08.044

Ma, Z. Y. (2008). Friction stir processing technology: A review. *Metallurgical and Materials Transactions A: Physical Metallurgy and Materials Science*, *39 A*(3), 642–658. https://doi.org/10.1007/s11661-007-9459-0

Maclin John Vasanth, K., Lokendar Ram, P. S., Pon Anand, V., Prabu, M., & Rahul, S. (2020). Experimental investigation of mechanical and tribological properties of Aluminium metal matrix composites fabricated by powder metallurgy route - A review. *Materials Today: Proceedings*, *33*(xxxx), 1058–1072. https://doi.org/10.1016/j.matpr.2020.07.057

Manjunatha, L. H., Yunus, M., Alsoufi, M. S., & Dinesh, P. (2017). Development and Comparative Studies of Aluminum-Based Carbon Nano Tube Metal Matrix Composites using Powder Metallurgy and Stir Casting Technology Deep cryogenic treatment View project novel post processing techniques and Genetic Programming in Forecastin. *Article in International Journal of Scientific and Engineering Research*, *8*(2). http://www.ijser.org

Martin, A. R., Moore, C. P., Finlay, W. H., Martin, A. R., Moore, C. P., & Models, W. H. F. (2018). Ac ce us. *Expert Opinion on Drug Delivery*, 1. https://doi.org/10.1080/17425247.2018.1544616

Maryam, B. H., Sinha, D. K., Kefyalew, S., Gautam, S. S., Kumar, S., & Pande, S. (2023). AZ31-Mg metal matrix composite in metallurgical and testing approaches. *Advances in Mechanical Engineering*, *15*(7), 1–21. https://doi.org/10.1177/16878132231184199

Maurya, M., Kumar, S., & Maurya, N. K. (2020). Composites prepared via friction stir processing technique: A review. *Revue Des Composites et Des Materiaux Avances*, *30*(3–4), 143–151. https://doi.org/10.18280/rcma.303-404

Meher, A., Mahapatra, M. M., Samal, P., Vundavilli, P. R., & Madavan, S. P. (2019). Synthesis, microstructure and mechanical properties of magnesium matrix composites fabricated by stir casting. *Materials Today: Proceedings*, *18*, 4034–4041. https://doi.org/10.1016/j.matpr.2019.07.346

Minitab ® 21 Support. (2023). *Interpretation*. Pareto Chart. https://support.minitab.com/en-us/minitab/21/help-and-how-to/statistical-modeling/doe/how-to/factorial/analyze-factorial-design/interpret-the-results/all-statistics-and-graphs/effects-plots

Mir, F. A., Khan, N. Z., Siddiquee, A. N., & Parvez, S. (2022). Joining of aluminium matrix composites using friction stir welding: A review. *Proceedings of the Institution of Mechanical Engineers, Part L: Journal of Materials: Design and Applications*, *236*(5), 917–932. https://doi.org/10.1177/14644207211069616

Miracle, D. B. (2005). Metal matrix composites - From science to technological significance. *Composites Science and Technology*, *65*(15-16 SPEC. ISS.), 2526–2540. https://doi.org/10.1016/j.compscitech.2005.05.027

Mishra, R. S., Ma, Z. Y., & Charit, I. (2003). Friction stir processing: A novel technique for fabrication of surface composite. *Materials Science and Engineering A*, *341*(1–2), 307–310. https://doi.org/10.1016/S0921-5093(02)00199-5

Moradkhani, A., & Baharvandi, H. (2018). Effects of additive amount, testing method, fabrication process and sintering temperature on the mechanical properties of Al2O3/3Y-TZP composites. *Engineering Fracture Mechanics*, *191*, 446–460. https://doi.org/10.1016/j.engfracmech.2017.12.033

Morampudi, P., Venkata Ramana, V. S. N., Vikas, K. S., Rahul, & Prasad, C. (2022). Enhancing wear properties of Al6061 metal-matrix composites by reinforcement of ZrB2 nano particles. *Materials Today: Proceedings*, *59*, A45–A51. https://doi.org/10.1016/j.matpr.2022.04.865

Muhammad, F., & Jalal, S. (2021). A Comparative Study of the Impact of the Stirrer Design in the Stir Casting Route to Produce Metal Matrix Composites. *Advances in Materials Science and Engineering*, *2021*. https://doi.org/10.1155/2021/4311743

Muthu Krishnan, M., Maniraj, J., Deepak, R., & Anganan, K. (2018). Prediction of optimum welding parameters for FSW of aluminium alloys AA6063 and A319 using RSM and ANN. *Materials Today: Proceedings*, *5*(1), 716–723. https://doi.org/10.1016/j.matpr.2017.11.138

N, V., Lakshmikanthan, A., Patel GC, M., Selvan, C. P., S Jain, V. K., Srinivasan, S. A., & hm, H. (2022). Mechanical, Microstructure and Wear properties of Al 6113 Fly Ash reinforced Composites: Comparison of as-cast and Heat-treated Conditions. *Advances in Materials and Processing Technologies*, *8*(3), 2603–2618. https://doi.org/10.1080/2374068X.2021.1927649

Nampi, T., & Das, S. (2020). Materials Today : Proceedings Optimization of tribological parameters of AA7075 / SiC metal matrix composites. *Materials Today: Proceedings*, *xxxx*. https://doi.org/10.1016/j.matpr.2020.02.470

Nasrollahzadeh, M., Atarod, M., Sajjadi, M., Sajadi, S. M., & Issaabadi, Z. (2019). Plant-Mediated Green Synthesis of Nanostructures: Mechanisms, Characterization, and Applications. In *Interface Science and Technology* (1st ed., Vol. 28). Elsevier Ltd. https://doi.org/10.1016/B978-0-12-813586-0.00006-7

Nayak, K. C., Rane, K. K., Date, P. P., & Srivatsan, T. S. (2022). Synthesis of an Aluminum Alloy Metal Matrix Composite Using Powder Metallurgy: Role of Sintering Parameters.

Applied Sciences (Switzerland), *12*(17). https://doi.org/10.3390/app12178843

Olani, M., Kumar, D., & Asrat, G. (2023). Mechanical and corrosion properties of Fe–SiC–ZrO2 hybrid composite fabricated through powder metallurgy process. *Results in Engineering*, *17*(December 2022), 100866. https://doi.org/10.1016/j.rineng.2022.100866

Omrani, E., Moghadam, A. D., Menezes, P. L., & Rohatgi, P. K. (2016). Influences of graphite reinforcement on the tribological properties of self-lubricating aluminum matrix composites for green tribology, sustainability, and energy efficiency—A review. *International Journal of Advanced Manufacturing Technology*, *83*(1–4), 325–346. https://doi.org/10.1007/s00170-015-7528-x

Ozben, T., Kilickap, E., & Çakir, O. (2008). Investigation of mechanical and machinability properties of SiC particle reinforced Al-MMC. *Journal of Materials Processing Technology*, *198*(1–3), 220–225. https://doi.org/10.1016/j.jmatprotec.2007.06.082

p = 600 kPa. (2016). 1–8.

Padhy, G. K., Wu, C. S., & Gao, S. (2018). Friction stir based welding and processing technologies - processes, parameters, microstructures and applications: A review. *Journal of Materials Science and Technology*, *34*(1), 1–38. https://doi.org/10.1016/j.jmst.2017.11.029

Palanikumar, K., & Davim, J. P. (2013). Electrical discharge machining: study on machining characteristics of WC/Co composites. In *Machining and machine-tools*. Woodhead Publishing Limited. https://doi.org/10.1533/9780857092199.135

Panwar, V., Kumar Sharma, D., Pradeep Kumar, K. V., Jain, A., & Thakar, C. (2020). Experimental investigations and optimization of surface roughness in turning of en 36 alloy steel using response surface methodology and genetic algorithm. *Materials Today: Proceedings*, *46*(xxxx), 6474–6481. https://doi.org/10.1016/j.matpr.2021.03.642

Parray, M. R., Khan, N. Z., & Maqbool, A. (2020). Fabrication and characterization of magnesium based surface composites with hybrid reinforcements by friction stir processing: A review. *Materials Today: Proceedings*, *46*(xxxx), 6507–6512. https://doi.org/10.1016/j.matpr.2021.03.694

Patel, R. D., & Bhavsar, S. N. (2019). Experimental investigation during end milling of AISI

D2 tool steel using AlCrN coated tool. *Materials Today: Proceedings*, *22*, 2647–2656. https://doi.org/10.1016/j.matpr.2020.03.396

Peng, J., Zhang, Z., Huang, J., Guo, P., Li, Y., Zhou, W., & Wu, Y. (2019). The effect of the inhomogeneous microstructure and texture on the mechanical properties of AZ31 Mg alloys processed by friction stir processing. *Journal of Alloys and Compounds*, *792*, 16–24. https://doi.org/10.1016/j.jallcom.2019.04.014

Periyasamy, P., Mohan, B., Balasubramanian, V., Rajakumar, S., & Venugopal, S. (2013). Multi-objective optimization of friction stir welding parameters using desirability approach to join Al/SiCp metal matrix composites. *Transactions of Nonferrous Metals Society of China (English Edition)*, *23*(4), 942–955. https://doi.org/10.1016/S1003-6326(13)62551-0

Prasad, V. J., Rao, K. N., & Babu, N. K. (2020). Mechanical and tribological characterization of aluminum metal matrix composite reinforced with micro ceramic particles (TiB2/SiC). *Materials Today: Proceedings*, *23*(xxxx), 637–641. https://doi.org/10.1016/j.matpr.2019.05.446

Prater, T., Strauss, A., Cook, G., Gibson, B., & Cox, C. (2013). A comparative evaluation of the wear resistance of various tool materials in friction stir welding of metal matrix composites. *Journal of Materials Engineering and Performance*, *22*(6), 1807–1813. https://doi.org/10.1007/s11665-012-0468-9

Premnath, A. A., Alwarsamy, T., & Rajmohan, T. (2012). Experimental investigation and optimization of process parameters in milling of hybrid metal matrix composites. *Materials and Manufacturing Processes*, *27*(10), 1035–1044. https://doi.org/10.1080/10426914.2012.677911

Purohit, R., Dewang, Y., Rana, R. S., Koli, D., & Dwivedi, S. (2018). Fabrication of magnesium matrix composites using powder metallurgy process and testing of properties. *Materials Today: Proceedings*, *5*(2), 6009–6017. https://doi.org/10.1016/j.matpr.2017.12.204

Puviyarasan, M., & Senthil Kumar, V. S. (2015). An Experimental Investigation for Multi-Response Optimization of Friction Stir Process Parameters During Fabrication of AA6061/B4Cp Composites. *Arabian Journal for Science and Engineering*, *40*(6), 1733–1741. https://doi.org/10.1007/s13369-015-1654-5

Qiao, K., Zhang, T., Wang, K., Yuan, S., Zhang, S., Wang, L., Wang, Z., Peng, P., Cai, J., Liu, C., & Wang, W. (2021). Mg/ZrO2 Metal Matrix Nanocomposites Fabricated by Friction Stir Processing: Microstructure, Mechanical Properties, and Corrosion Behavior. *Frontiers in Bioengineering and Biotechnology*, *9*(March), 1–16. https://doi.org/10.3389/fbioe.2021.605171

Radhakrishnan, G., Anirudh, P. V., & Anujan Kumar, S. (2019). Mechanical behavior of nanoparticulate TiO2 reinforced magnesium matrix composite. *IOP Conference Series: Materials Science and Engineering*, *574*(1). https://doi.org/10.1088/1757-899X/574/1/012006

Radhika, N., & Sai Charan, K. (2017). Experimental Analysis on Three Body Abrasive Wear Behaviour of Stir Cast Al LM 25/TiC Metal Matrix Composite. *Transactions of the Indian Institute of Metals*, *70*(9), 2233–2240. https://doi.org/10.1007/s12666-017-1061-6

Rajakumar, S., & Balasubramanian, V. (2012). Predicting grain size and tensile strength of friction stir welded joints of AA7075-T 6 aluminium alloy. *Materials and Manufacturing Processes*, *27*(1), 78–83. https://doi.org/10.1080/10426914.2011.557123

Rajeswari, B., & Amirthagadeswaran, K. S. (2018). Study of machinability and parametric optimization of end milling on aluminium hybrid composites using multi-objective genetic algorithm. *Journal of the Brazilian Society of Mechanical Sciences and Engineering*, *40*(8), 1–15. https://doi.org/10.1007/s40430-018-1293-3

Rajmohan, T., & Palanikumar, K. (2013). Application of the central composite design in optimization of machining parameters in drilling hybrid metal matrix composites. *Measurement: Journal of the International Measurement Confederation*, *46*(4), 1470–1481. https://doi.org/10.1016/j.measurement.2012.11.034

Ram Kumar, S., Gowtham, S., & Radhika, N. (2018). Fabrication of Cu-Sn/SiC Metal Matrix Composites and Investigation of its Mechanical and Dry Sliding Wear Properties. *Materials Today: Proceedings*, *5*(5), 12757–12771. https://doi.org/10.1016/j.matpr.2018.02.260

Ramírez-Aragón, C., Ordieres-Meré, J., Alba-Elías, F., & González-Marcos, A. (2018). Comparison of Cohesive models in EDEM and LIGGGHTS for simulating powder compaction. *Materials*, *11*(11). https://doi.org/10.3390/ma11112341

Rangrej, S., Mehta, V., Ayar, V., & Sutaria, M. (2020). Effects of stir casting process parameters on dispersion of reinforcement particles during preparation of metal composites. *Materials Today: Proceedings*, *43*, 471–475. https://doi.org/10.1016/j.matpr.2020.11.1002

Rao, C. V. S., Rao, Y. S., Marimuthu, P., Jeyapaul, R., Chakravarthy, N. S. K., & Murugesan, P. (2021). Optimisation of Drilling Parameters of Metal Matrix Composites using Genetic Algorithm in the Taguchi Method. *IOP Conference Series: Materials Science and Engineering*, *1126*(1), 012035. https://doi.org/10.1088/1757-899x/1126/1/012035

Rao, J. S., & Kumar, B. (2012). 3D Blade root shape optimization. In *Institution of Mechanical Engineers - 10th International Conference on Vibrations in Rotating Machinery*.Woodhead Publishing Limited. https://doi.org/10.1533/9780857094537.4.173

Rathee, S., Maheshwari, S., Siddiquee, A. N., & Srivastava, M. (2018). A Review of Recent Progress in Solid State Fabrication of Composites and Functionally Graded Systems Via Friction Stir Processing. *Critical Reviews in Solid State and Materials Sciences*, *43*(4), 334–366. https://doi.org/10.1080/10408436.2017.1358146

Reddy, K. S. T., Manohar, H. S., Mungara, S. R., & Anand, S. A. (2020). Studies on mechanical properties of graphite reinforced AA7475 metal matrix composites. *Materials Today: Proceedings*, *45*(xxxx), 307–310. https://doi.org/10.1016/j.matpr.2020.10.654

Remacle, J., Lambrechts, J., & Seny, B. (2012). Blossom-Quad: A non-uniform quadrilateral mesh generator using a minimum-cost perfect-matching algorithm. *International*, *February*, 1102–1119. https://doi.org/10.1002/nme

Roebuck, B., Gorley, T. A. E., & McCartney, L. N. (1989). Mechanical property test procedures for metal matrix composites. *Materials Science and Technology (United Kingdom)*, *5*(2), 105–117. https://doi.org/10.1179/mst.1989.5.2.105

Rojek, J., Nosewicz, S., Jurczak, K., Chmielewski, M., Bochenek, K., & Pietrzak, K. (2016). Discrete element simulation of powder compaction in cold uniaxial pressing with low pressure. *Computational Particle Mechanics*, *3*(4), 513–524. https://doi.org/10.1007/s40571-015-0093-0

Rojek, J., Nosewicz, S., Pietrzak, K., & Chmielewski, M. (2015). *Discrete element modelling* *of powder metallurgy processes*. *73*(2011), 71–78.

Rong, Y., Zhang, Z., Zhang, G., Yue, C., Gu, Y., Huang, Y., Wang, C., & Shao, X. (2015). Parameters optimization of laser brazing in crimping butt using Taguchi and BPNN-GA. *Optics and Lasers in Engineering*, *67*, 94–104. https://doi.org/10.1016/j.optlaseng.2014.10.009

Sagar, P., & Handa, A. (2020a). A comprehensive review of recent progress in fabrication of magnesium base composites by friction stir processing technique—A review. *AIMS Materials Science*, *7*(5), 684–704. https://doi.org/10.3934/matersci.2020.5.684

Sagar, P., & Handa, A. (2020b). Role of tool rotational speed on the tribological characteristics of magnesium based az61a/tic composite developed via friction stir processing route. *Journal of Achievements in Materials and Manufacturing Engineering*, *101*(2), 60–75. https://doi.org/10.5604/01.3001.0014.4921

Salehi, M., Saadatmand, M., & Aghazadeh Mohandesi, J. (2012). Optimization of process parameters for producing AA6061/SiC nanocomposites by friction stir processing. *Transactions of Nonferrous Metals Society of China (English Edition)*, *22*(5), 1055–1063. https://doi.org/10.1016/S1003-6326(11)61283-1

Salih, O. S., Ou, H., Wei, X., & Sun, W. (2019). Microstructure and mechanical properties of friction stir welded AA6092/SiC metal matrix composite. *Materials Science and Engineering: A*, *742*(November 2018), 78–88. https://doi.org/10.1016/j.msea.2018.10.116

Samuel, M. (2003). A new technique for recycling aluminium scrap. *Journal of Materials Processing Technology*, *135*(1), 117–124. https://doi.org/10.1016/S0924-0136(02)01133-0

Sanjay, M. R., Madhu, P., Jawaid, M., Senthamaraikannan, P., Senthil, S., & Pradeep, S. (2018). Characterization and properties of natural fiber polymer composites: A comprehensive review. In *Journal of Cleaner Production* (Vol. 172). Elsevier B.V. https://doi.org/10.1016/j.jclepro.2017.10.101

Sanjeevi, R., Nagaraja, R., & Krishnan, B. R. (2020). Vision-based surface roughness accuracy prediction in the CNC milling process (Al6061) using ANN. *Materials Today: Proceedings*, *37*(Part 2), 245–247. https://doi.org/10.1016/j.matpr.2020.05.122

Sankhla, A. M., Patel, K. M., Makhesana, M. A., Giasin, K., Pimenov, D. Y., Wojciechowski, S., & Khanna, N. (2022). Effect of mixing method and particle size on hardness and compressive strength of aluminium based metal matrix composite prepared through powder metallurgy route. *Journal of Materials Research and Technology*, *18*, 282–292. https://doi.org/10.1016/j.jmrt.2022.02.094

SarsIlmaz, F., & Çaydaş, U. (2009). Statistical analysis on mechanical properties of friction-stir-welded AA 1050/AA 5083 couples. *International Journal of Advanced Manufacturing Technology*, *43*(3–4), 248–255. https://doi.org/10.1007/s00170-008-1716-x

Sathiskumar, R., Murugan, N., Dinaharan, I., & Vijay, S. J. (2014). Prediction of mechanical and wear properties of copper surface composites fabricated using friction stir processing. *Materials and Design*, *55*, 224–234. https://doi.org/10.1016/j.matdes.2013.09.053

Satish, J., & Satish, K. G. (2018). Preparation of magnesium metal matrix composites by powder metallurgy process. *IOP Conference Series: Materials Science and Engineering*, *310*(1). https://doi.org/10.1088/1757-899X/310/1/012130

Schmidt, J., Boehling, M., Burkhardt, U., & Grin, Y. (2007). Preparation of titanium diboride TiB2 by spark plasma sintering at slow heating rate. *Science and Technology of Advanced Materials*, *8*(5), 376–382. https://doi.org/10.1016/j.stam.2007.06.009

Seeman, M., Ganesan, G., Karthikeyan, R., & Velayudham, A. (2010). Study on tool wear and surface roughness in machining of particulate aluminum metal matrix composite-response surface methodology approach. *International Journal of Advanced Manufacturing Technology*, *48*(5–8), 613–624. https://doi.org/10.1007/s00170-009-2297-z

Selvan, C. P., Girisha, L., Koti, V., Madgule, M., Davanageri, M. B., Lakshmikanthan, A., & Chandrashekarappa, M. P. G. (2023). Optimization of stir casting and drilling process parameters of hybrid composites. *Journal of Alloys and Metallurgical Systems*, *3*(March), 100023. https://doi.org/10.1016/j.jalmes.2023.100023

Senthil Murugan, S., Vigneshkumar, M., John Iruthaya Raj, M., Selvaraju, S., Vinayaka, N., Murugan, S., Vijayan, V., & Mekonnen, A. (2023). Stir Casting Processing, Mechanical, and Wear Behavior of AA2024 +10 wt. % Flyash +5 wt. % Graphite Hybrid Composite. *Advances in Materials Science and Engineering*, *2023*.

https://doi.org/10.1155/2023/9089620

Shahraki, S., Khorasani, S., Abdi Behnagh, R., Fotouhi, Y., & Bisadi, H. (2013). Producing of AA5083/ZrO2 nanocomposite by friction stir processing (FSP). *Metallurgical and Materials Transactions B: Process Metallurgy and Materials Processing Science*, *44*(6), 1546–1553. https://doi.org/10.1007/s11663-013-9914-9

Shang, Q., Ni, D. R., Xue, P., Xiao, B. L., Wang, K. S., & Ma, Z. Y. (2019). An approach to enhancement of Mg alloy joint performance by additional pass of friction stir processing. *Journal of Materials Processing Technology*, *264*, 336–345. https://doi.org/10.1016/j.jmatprotec.2018.09.021

Shanmugavel, R., Sundaresan, T. K., Marimuthu, U., & Manickaraj, P. (2016). Process Optimization and Wear Behavior of Red Mud Reinforced Aluminum Composites. *Advances in Tribology*, *2016*. https://doi.org/10.1155/2016/9082593

Sharma, V., Prakash, U., & Kumar, B. V. M. (2015). Surface composites by friction stir processing: A review. *Journal of Materials Processing Technology*, *224*, 117–134. https://doi.org/10.1016/j.jmatprotec.2015.04.019

Sheelwant, A., Jadhav, P. M., & Narala, S. K. R. (2021). ANN-GA based parametric optimization of Al-TiB2 metal matrix composite material processing technique. *Materials Today Communications*, *27*(March), 102444. https://doi.org/10.1016/j.mtcomm.2021.102444

Shivalingaiah, K., Nagarajaiah, V., Selvan, C. P., Kariappa, S. T., Chandrashekarappa, N. G., Lakshmikanthan, A., Chandrashekarappa, M. P. G., & Linul, E. (2022). Stir Casting Process Analysis and Optimization for Better Properties in Al-MWCNT-GR-Based Hybrid Composites. *Metals*, *12*(8). https://doi.org/10.3390/met12081297

Siddhartha Prabhakar, N., Radhika, N., & Raghu, R. (2014). Analysis of tribological behavior of aluminium/B4C composite under dry sliding motion. *Procedia Engineering*, *97*, 994–1003. https://doi.org/10.1016/j.proeng.2014.12.376

Sivanesh Prabhu, M., Elaya Perumal, A., Arulvel, S., & Franklin Issac, R. (2019). Friction and wear measurements of friction stir processed aluminium alloy 6082/CaCO3 composite. *Measurement: Journal of the International Measurement Confederation*, *142*, 10–20.

https://doi.org/10.1016/j.measurement.2019.04.061

Sonmez, F., Basak, H., & Baday, S. (2017). *The mechanical strength of aluminum alloys which are joined with friction stir welding modelling with artificial neural networks*. 1–4. https://doi.org/10.1109/idap.2017.8090325

Sreenivasan, K. S., Satish Kumar, S., & Katiravan, J. (2019). Genetic algorithm based optimization of friction welding process parameters on AA7075-SiC composite. *Engineering Science and Technology, an International Journal*, *22*(4), 1136–1148. https://doi.org/10.1016/j.jestch.2019.02.010

Srinivasa Rao, M., & Ramanaiah, N. (2018). Optimization of process parameters for FSW of Al-Mg-Mn-Sc-Zr alloy using CCD and RSM. *Strojnicky Casopis*, *68*(3), 195–224. https://doi.org/10.2478/scjme-2018-0035

Srinivasan, S., Thirumurugaveerakumar, S., Nagarajan, N., Mohammed Raffic, N., & Ganesh Babu, K. (2020). A review of optimization techniques in machining of composite materials. *Materials Today: Proceedings*, *47*(xxxx), 6811–6814. https://doi.org/10.1016/j.matpr.2021.05.136

Subramani, M., Huang, S. J., & Borodianskiy, K. (2022). Effect of SiC Nanoparticles on AZ31 Magnesium Alloy. *Materials*, *15*(3), 1–12. https://doi.org/10.3390/ma15031004

Sun, K., Shi, Q. Y., Sun, Y. J., & Chen, G. Q. (2012). Microstructure and mechanical property of nano-SiCp reinforced high strength Mg bulk composites produced by friction stir processing. *Materials Science and Engineering: A*, *547*, 32–37. https://doi.org/10.1016/j.msea.2012.03.071

Sun, N., & Apelian, D. (2011). Friction stir processing of aluminum cast alloys for high performance applications. *Jom*, *63*(11), 44–50. https://doi.org/10.1007/s11837-011-0190-3

Sunil, B. R., Reddy, G. P. K., Patle, H., & Dumpala, R. (2016). Magnesium based surface metal matrix composites by friction stir processing. *Journal of Magnesium and Alloys*, *4*(1), 52–61. https://doi.org/10.1016/j.jma.2016.02.001

Tang, L., Gao, C., Huang, J., Zhang, H., & Chang, W. (2013). Dry sliding friction and wear behaviour of hardened AISI D2 tool steel with different hardness levels. *Tribology*

International, *66*, 165–173. https://doi.org/10.1016/j.triboint.2013.05.006

Tangri, H., Guo, Y., & Curtis, J. S. (2017). Packing of cylindrical particles: DEM simulations and experimental measurements. *Powder Technology*, *317*, 72–82. https://doi.org/10.1016/j.powtec.2017.03.058

Thangarasu, A., Murugan, N., Dinaharan, I., & Vijay, S. J. (2015). Synthesis and characterization of titanium carbide particulate reinforced AA6082 aluminium alloy composites via friction stir processing. *Archives of Civil and Mechanical Engineering*, *15*(2), 324–334. https://doi.org/10.1016/j.acme.2014.05.010

Thiagarajan, C., Sivaramakrishnan, R., & Somasundaram, S. (2012). Modeling and optimization of cylindrical grinding of Al/SiC composites using genetic algorithms. *Journal of the Brazilian Society of Mechanical Sciences and Engineering*, *34*(1), 32–40.

Tosun, G., & Kurt, M. (2019). The porosity, microstructure, and hardness of Al-Mg composites reinforced with micro particle SiC/Al2O3 produced using powder metallurgy. *Composites Part B: Engineering*, *174*(May 2019), 106965. https://doi.org/10.1016/j.compositesb.2019.106965

Umanath, K., Palanikumar, K., Sankaradass, V., & Uma, K. (2021). Materials Today : Proceedings Optimization of wear properties on AA7075 / Sic / Mos 2 hybrid metal matrix composite by response surface methodology. *Materials Today: Proceedings*, *xxxx*. https://doi.org/10.1016/j.matpr.2021.02.541

Uthayakumar, M., Kumaran, S. T., & Aravindan, S. (2013). Dry sliding friction and wear studies of fly ash reinforced AA-6351 metal matrix composites. *Advances in Tribology*, *2013*. https://doi.org/10.1155/2013/365602

V.K. Parikh, A.D. Badgujar, N. D. G. (2022). Effect of Friction stir processing parameters on microstructure and microhardness of aluminium based Metal matrix composites. *Materials Today: Proceedings*, *62*(Part 14), 7455–7460. https://doi.org/https://doi.org/10.1016/j.matpr.2022.03.386.

Vafaeesefat, A. (2011). Optimization of composite pressure vessels with metal liner by adaptive response surface method. *Journal of Mechanical Science and Technology*, *25*(11), 2811–2816. https://doi.org/10.1007/s12206-011-0721-4

Venkatesh, R., Kannan, C. R., Manivannan, S., Vivekanandan, M., Krishna, J. P., Mezni, A., Islam, S., & Rajkumar, S. (2022). Synthesis and Experimental Investigations of Tribological and Corrosion Performance of AZ61 Magnesium Alloy Hybrid Composites. *Journal of Nanomaterials*, *2022*. https://doi.org/10.1155/2022/6012518

Verma, A. S., Cheema, M. S., Kant, S., & Suri, N. M. (2019). Porosity Study of Developed Al–Mg–Si/Bauxite Residue Metal Matrix Composite Using Advanced Stir Casting Process. *Arabian Journal for Science and Engineering*, *44*(2), 1543–1552. https://doi.org/10.1007/s13369-018-3613-4

Vijayakumar, S., Satheesh Kumar, P. S., Sampath Kumar, P., Manickam, S., Ramaiah, G. B., & Pydi, H. P. (2022). The Effect of Stir-Squeeze Casting Process Parameters on Mechanical Property and Density of Aluminum Matrix Composite. *Advances in Materials Science and Engineering*, *2022*. https://doi.org/10.1155/2022/3741718

Vijayavel, P., Balasubramanian, V., & Sundaram, S. (2014). Effect of shoulder diameter to pin diameter (D/d) ratio on tensile strength and ductility of friction stir processed LM25AA-5% SiCp metal matrix composites. *Materials and Design*, *57*, 1–9. https://doi.org/10.1016/j.matdes.2013.12.008

Wakchaure, K. N., Thakur, A. G., Gadakh, V., & Kumar, A. (2018). Multi-Objective Optimization of Friction Stir Welding of Aluminium Alloy 6082-T6 Using hybrid Taguchi-Grey Relation Analysis- ANN Method. *Materials Today: Proceedings*, *5*(2), 7150–7159. https://doi.org/10.1016/j.matpr.2017.11.380

Wang, Y., Huang, Y., Meng, X., Wan, L., & Feng, J. (2017). Microstructural evolution and mechanical properties of Mg[sbnd]Zn[sbnd]Y[sbnd]Zr alloy during friction stir processing. *Journal of Alloys and Compounds*, *696*, 875–883. https://doi.org/10.1016/j.jallcom.2016.12.068

Węglowski, M. S. (2018). Friction stir processing – State of the art. *Archives of Civil and Mechanical Engineering*, *18*(1), 114–129. https://doi.org/10.1016/j.acme.2017.06.002

Wiacek, J., Molenda, M., Horabik, J., & Ooi, J. Y. (2012). Influence of grain shape and intergranular friction on material behavior in uniaxial compression: Experimental and DEM modeling. *Powder Technology*, *217*, 435–442.

https://doi.org/10.1016/j.powtec.2011.10.060

WIKIPEDIA. (2023). *Abrasive Wear*. Wear Types and Mechanisms. https://en.wikipedia.org/wiki/Wear (MatWeb, 2024)

Yilmaz, O., & Buytoz, S. (2001). Abrasive wear of Al2O3-reinforced aluminium-based MMCs. *Composites Science and Technology*, *61*(16), 2381–2392. https://doi.org/10.1016/S0266-3538(01)00131-2

Yu, K., & Tafti, D. (2016). Impact model for micrometer-sized sand particles. *Powder Technology*, *294*, 11–21. https://doi.org/10.1016/j.powtec.2016.02.014

Zamani, S. M. M., Behdinan, K., Razfar, M. R., Fatmehsari, D. H., & Mohandesi, J. A. (2021). Studying the effects of process parameters on the mechanical properties in friction stir welding of Al-SiC composite sheets. *International Journal of Advanced Manufacturing Technology*, *113*(11–12), 3629–3641. https://doi.org/10.1007/s00170-021-06852-7

Zhang, X., & Tan, M. J. (1997). Selection of particulate reinforcement in P/M metal matrix composites. *Journal of Materials Processing Technology*, *63*(1–3), 913–917. https://doi.org/10.1016/S0924-0136(96)00013-1

Zykova, A. P., Chumaevskiy, A. V, & Kolubaev, E. A. (2020). Metallic Materials : Process , Properties , and Methods. *Mdpi*.

APPENDICES

APPENDIX 1: WEAR TESTING APPARATUS AND SAMPLE

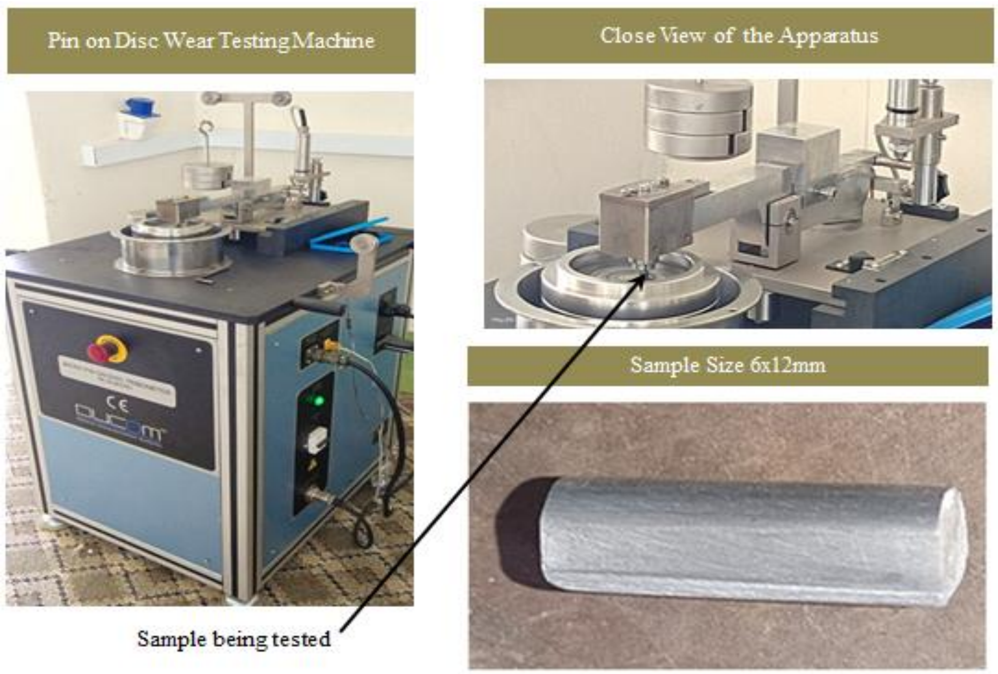

Figure I wear testing apparatus

APPENDIX 2: MACHINES USED FOR DIE MANUFACTURING

Figure II machines used for die manufacturing a) Millin b) Milling DECKEL CNC c) Lathe machine (Harrison M460)

APPENDIX 3: POWDERS MEASURED FOR SAMPLE FABRICATION

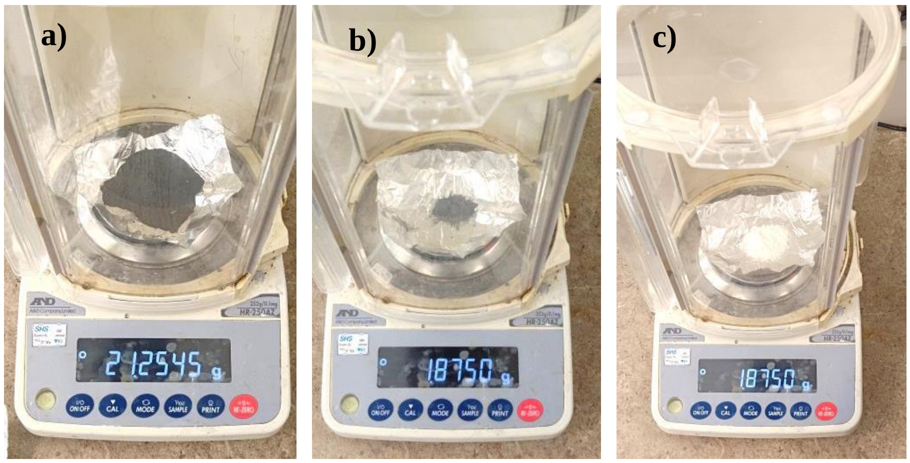

Figure III weight percentage measurement of the a) AZ61 b) SiC c) ZrO_2

APPENDIX 4: FSC PROCEDURES

Figure IV FSC experimental setup and procedure on a conventional milling machine

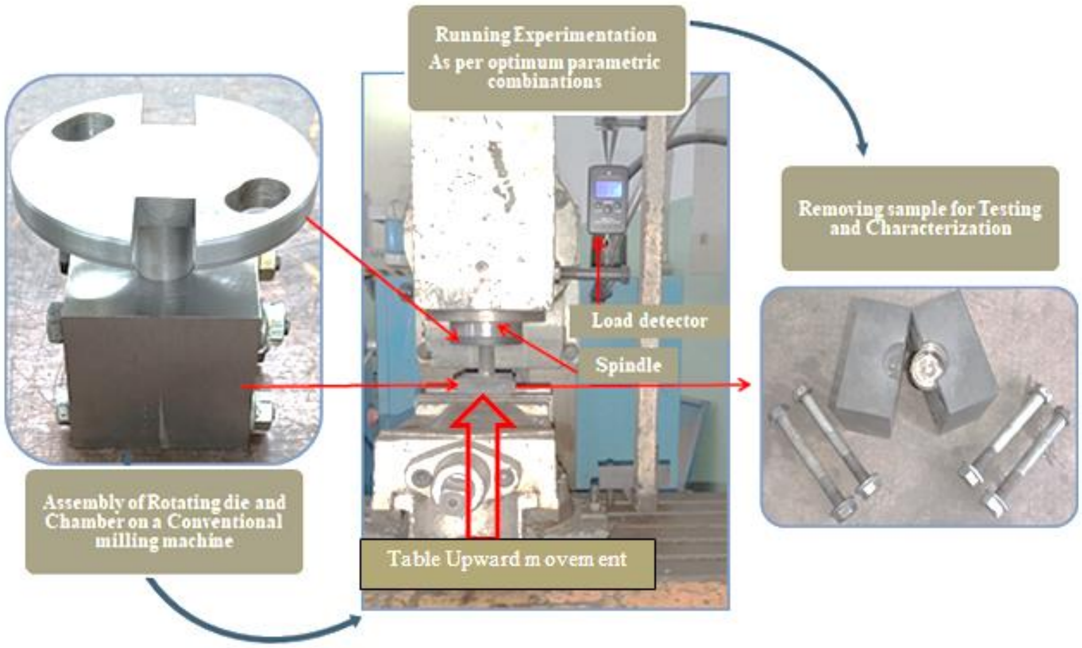

Figure V Specimens preparation through FSC process on a conventional milling machine

APPENDIX 5: DEM SIMULATIONS DIES

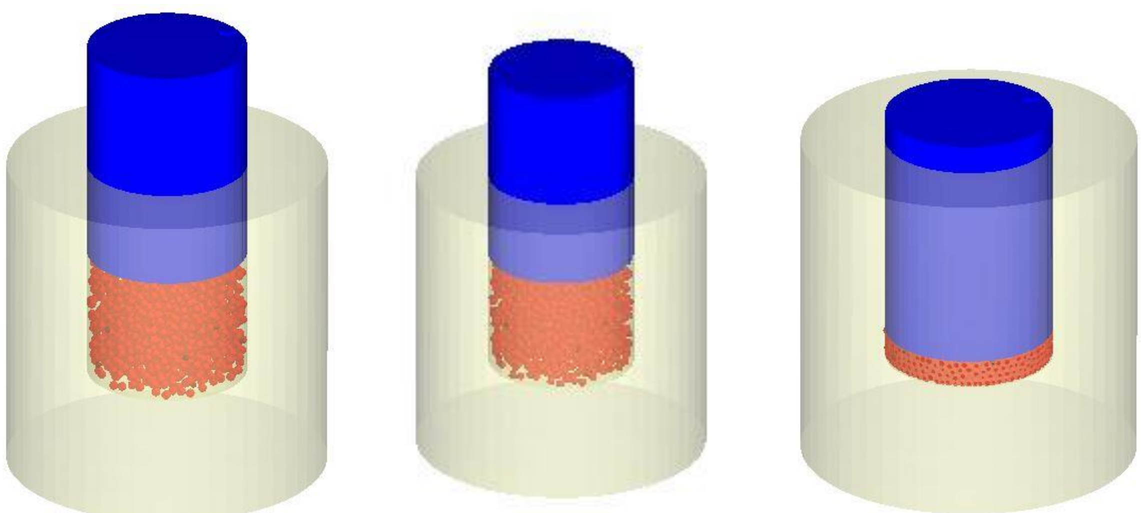

Figure VI Dies and simulation in DEM

APPENDIX 6: WEAR TEST CONVERSION PARAMETERS

It was necessary to convert running time into sliding distance because the wear test or pin on disc apparatus (Model: DUCOM TR-20 instrument (Pvt. Ltd. Company in Peenya Industrial Area, Bangalore, India) does not include the sliding distance parameter. To get the required sliding distance, the conversion technique below was used. For instance, 500m sliding distance conversion calculation presented as follows.

- ❖ To calculate the time required to travel 500m when the RPM is 260 with a circumference of the disc at pin contact of 157.08mm the following steps were followed

    1. Conversion of the circumference from mm to m:

Circumference = $\frac{157.058\text{mm}}{1000}$ = 0.15708m

    2. Calculation of the distance covered in one revolution:

Distance per Revolution = Circumference * 1 Revolution = 0.15708m * 1 = 0.15708m

    3. Calculate the number of revolutions required to travel 500m:

Total revolutions = $\frac{500\text{m}}{\text{Distance Per Revolution}} = \frac{500\text{m}}{0.15708\text{m}}$ = 3179.19 Revolutions

    4. Calculation of the time required in minutes;

Time = $\frac{\text{Total Revolutions}}{\text{RPM}} = \frac{3179.19\text{ Revolution}}{260\text{RPM}}$ = <u>12.23 minutes</u>

Therefore, when traveling a distance of 500m with a circumference of 157.08mm and rotating at 260rpm, it would take 12.23 minutes.

The following minutes tabulated in table I was used for each experimental run.

Table I Correlation of sliding distance and time

	Actual Factors			
Run	Load	Sliding Speed	Sliding Distance	Minutes Required
1	20	220	500	14.45
2	30	220	650	18.89
3	40	220	500	14.45
4	30	240	500	13.25
5	20	240	350	9.28
6	30	240	500	13.25
7	40	240	650	17.24
8	40	260	500	12.23
9	30	220	350	10.13

10	30	260	650	15.91
11	40	240	350	9.28
12	30	240	500	13.25
13	30	260	350	8.56
14	20	260	500	12.23
15	20	240	650	17.24

➢ Wear Test Procedure and Adjustments

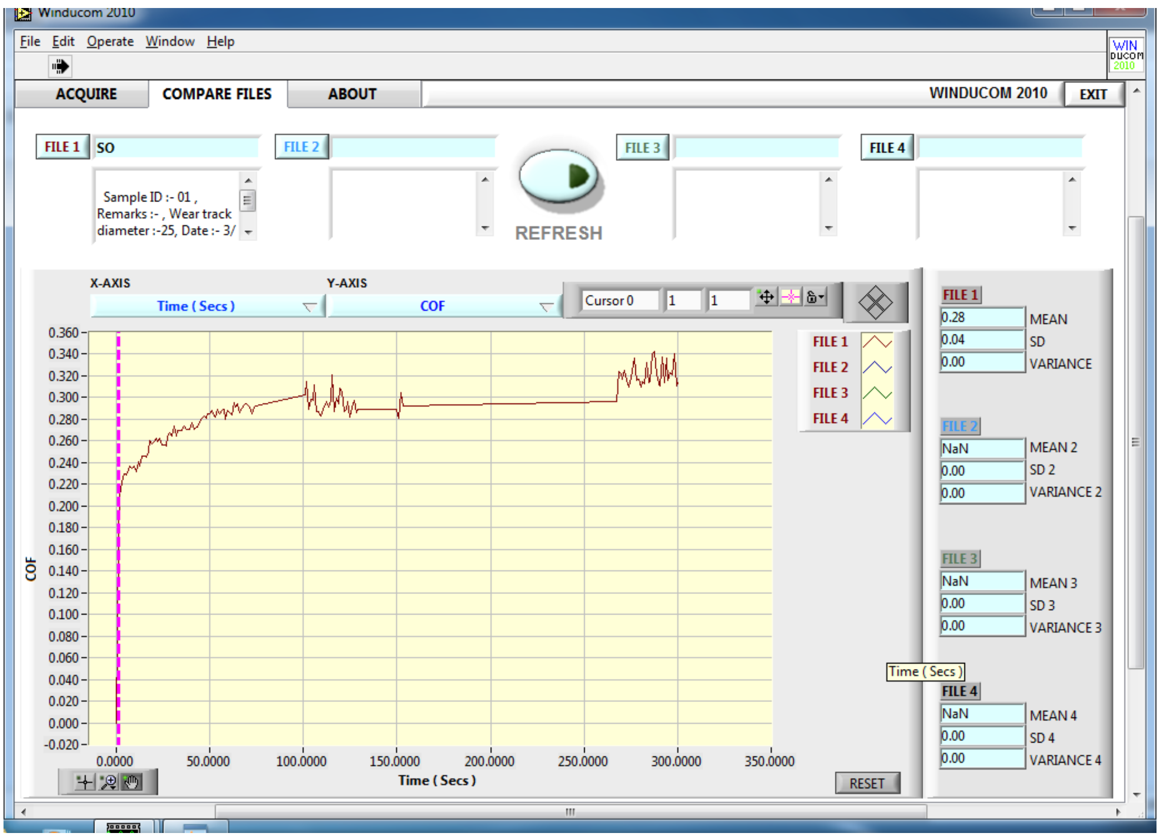

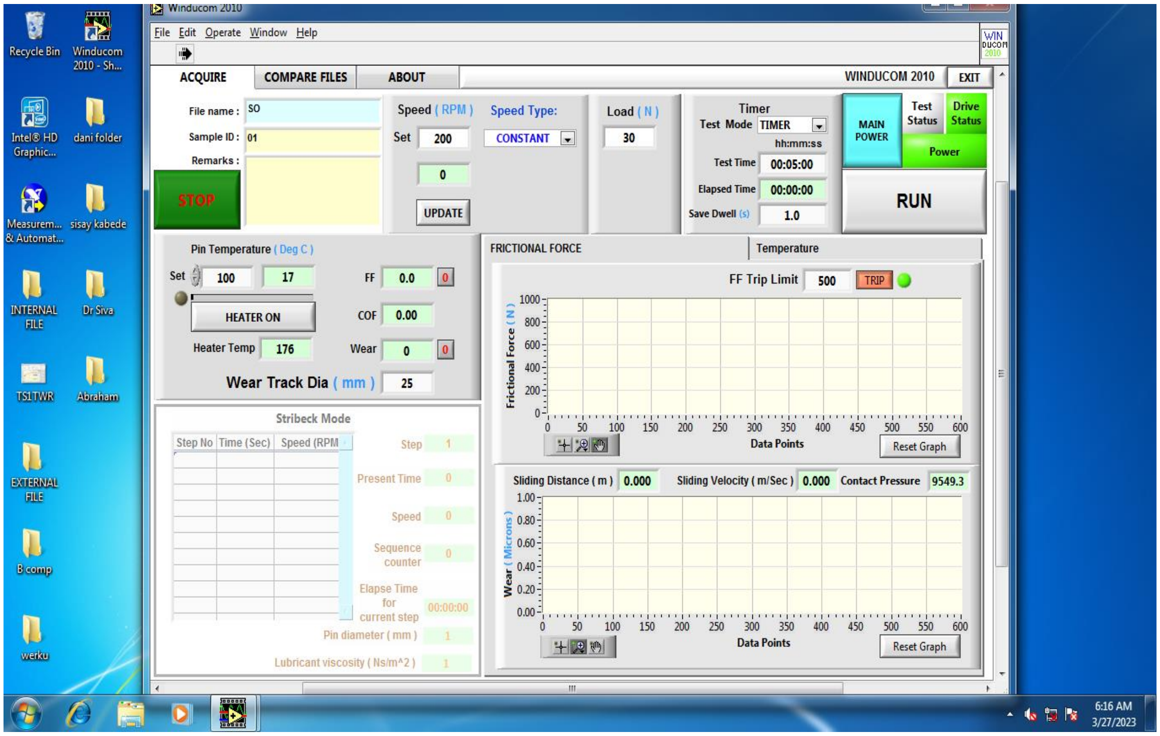

Figure VII Wear test parametric adjustment

APPENDIX 7: HARDNESS MACHINES USED

Figure VIII Hardness property testing machine

APPENDIX 8: COMPRESSIVE MACHINES USED

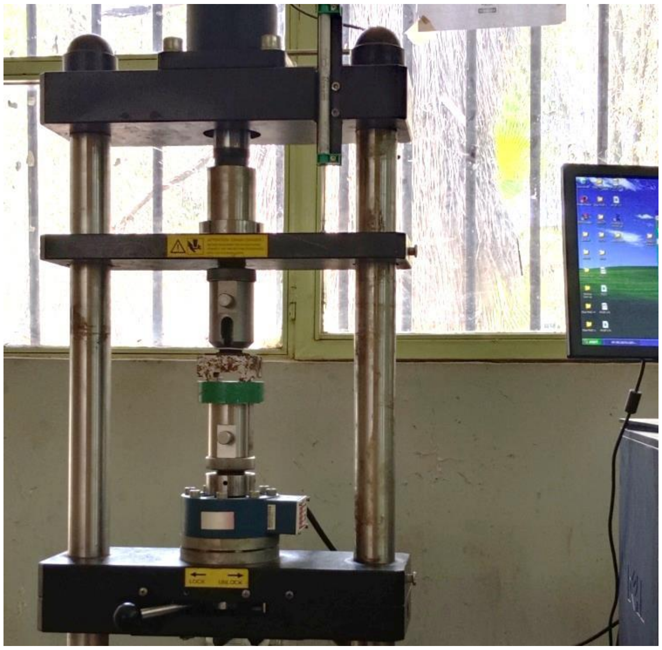

Figure IX Compressive strength testing machine (WP 310 Materials Testing)

APPENDIX 9: PROCESS DEVELOPMENT MACHINE

Figure X Process Development System; Milling machine model: FU281

APPENDIX 10: FURNACESS USED IN HEAT TREATMENT OF DIES

Figure XI Furnace Used For Heat Treatment

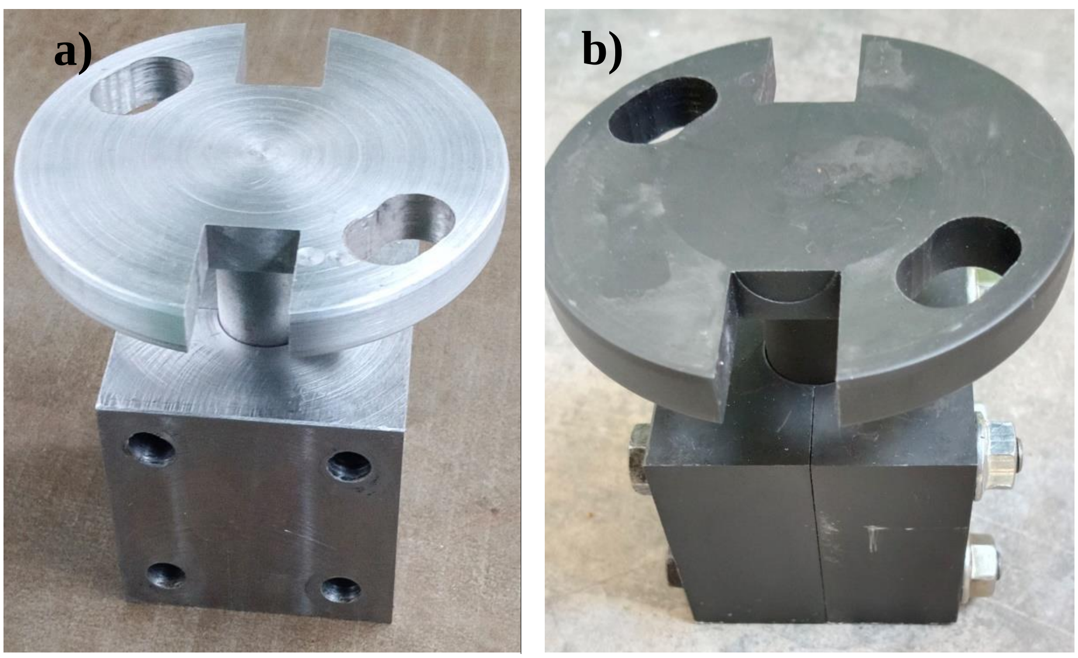

Figure XII fabricated dies a) beofre b) after heat treatment process

APPENDIX 11: 3D DESIGN OF DIES

The 3D models of dies were designed using Solidworks 2019 software. The sizes specified in the design were chosen in accordance with the spindle sizes of process development system

(Milling Machine's spindle size Model: FU281) which is used to assemble the dies. A) Chamber, B) Rotating Die and C) assembly of dies or exploded view of dies.

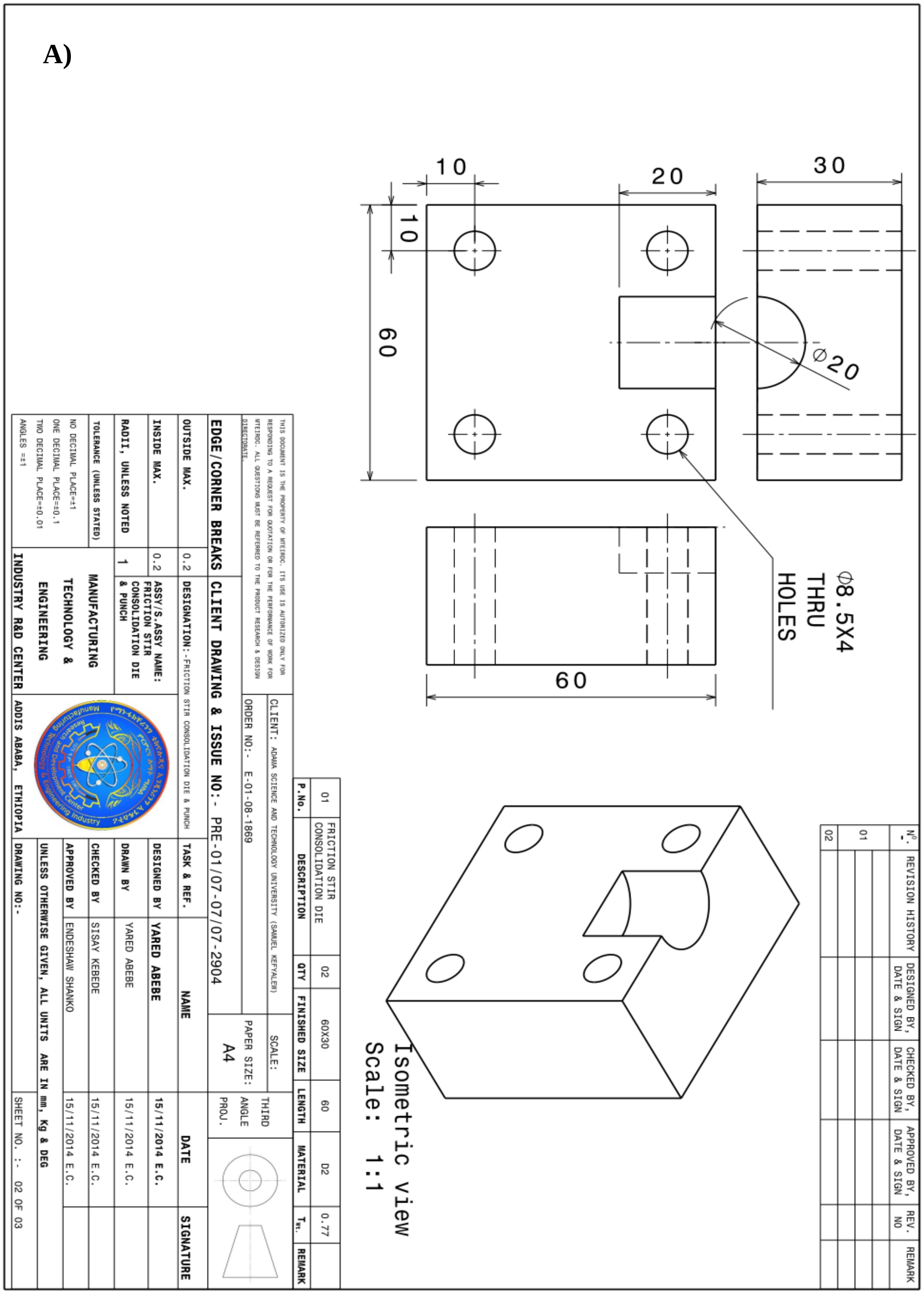

B)

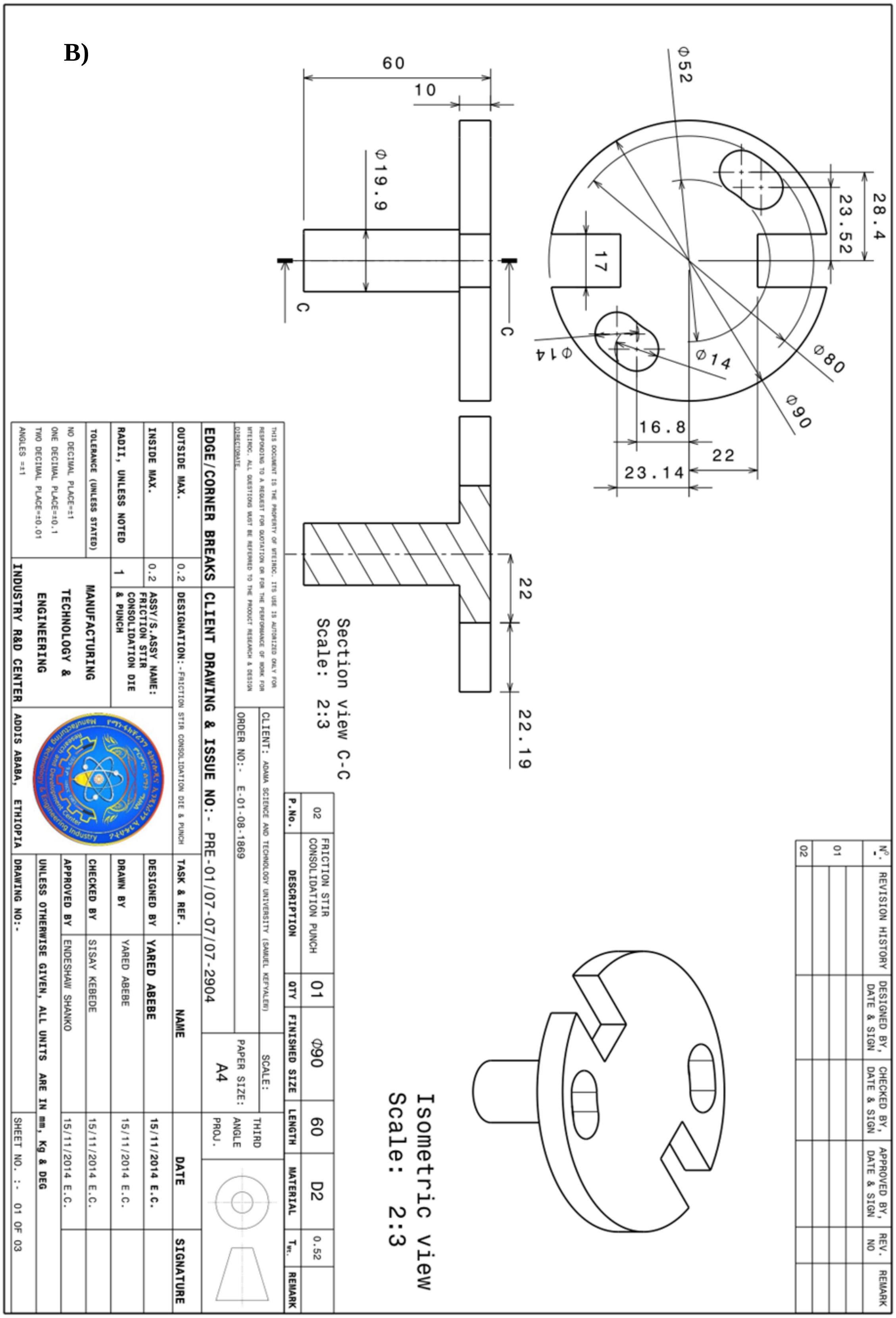
Ø52
60
10
28.4
23.52
Ø19.9
17
C
C
Ø14
Ø14
Ø80
Ø90
16.8
22
23.14
22
22.19
Section view C-C
Scale: 2:3
Isometric view
Scale: 2:3
Nº.
REVISION HISTORY
DESIGNED BY, DATE & SIGN
CHECKED BY, DATE & SIGN
APPROVED BY, DATE & SIGN
REV. NO
REMARK
01
02
02
FRICTION STIR CONSOLIDATION PUNCH
01
Ø90
60
D2
0.52
P.No.
DESCRIPTION
QTY
FINISHED SIZE
LENGTH
MATERIAL
REMARK
THIS DOCUMENT IS THE PROPERTY OF MTEIRDC. ITS USE IS AUTORIZED ONLY FOR RESPONDING TO A REQUEST FOR QUOTATION OR FOR THE PERFORMANCE OF WORK FOR MTEIRDC. ALL QUESTIONS MUST BE REFERRED TO THE PRODUCT RESEARCH & DESIGN DIRECTORATE.
CLIENT: ADAMA SCIENCE AND TECHNOLOGY UNIVERSITY (SAMUEL KEFYALEW)
ORDER NO:- E-01-08-1869
SCALE:
THIRD ANGLE PROJ.
PAPER SIZE: A4
EDGE/CORNER BREAKS
CLIENT DRAWING & ISSUE NO:- PRE-01/07-07/07-2904
OUTSIDE MAX. 0.2
INSIDE MAX. 0.2
RADII, UNLESS NOTED 1
DESIGNATION:-FRICTION STIR CONSOLIDATION DIE & PUNCH
ASSY/S.ASSY NAME: FRICTION STIR CONSOLIDATION DIE & PUNCH
TASK & REF.
NAME
DATE
SIGNATURE
DESIGNED BY YARED ABEBE 15/11/2014 E.C.
DRAWN BY YARED ABEBE 15/11/2014 E.C.
CHECKED BY SISAY KEBEDE 15/11/2014 E.C.
APPROVED BY ENDESHAW SHANKO 15/11/2014 E.C.
TOLERANCE (UNLESS STATED)
NO DECIMAL PLACE=±1
ONE DECIMAL PLACE=±0.1
TWO DECIMAL PLACE=±0.01
ANGLES =±1
MANUFACTURING TECHNOLOGY & ENGINEERING INDUSTRY R&D CENTER
UNLESS OTHERWISE GIVEN, ALL UNITS ARE IN mm, Kg & DEG
ADDIS ABABA, ETHIOPIA
DRAWING NO:-
SHEET NO. :- 01 OF 03

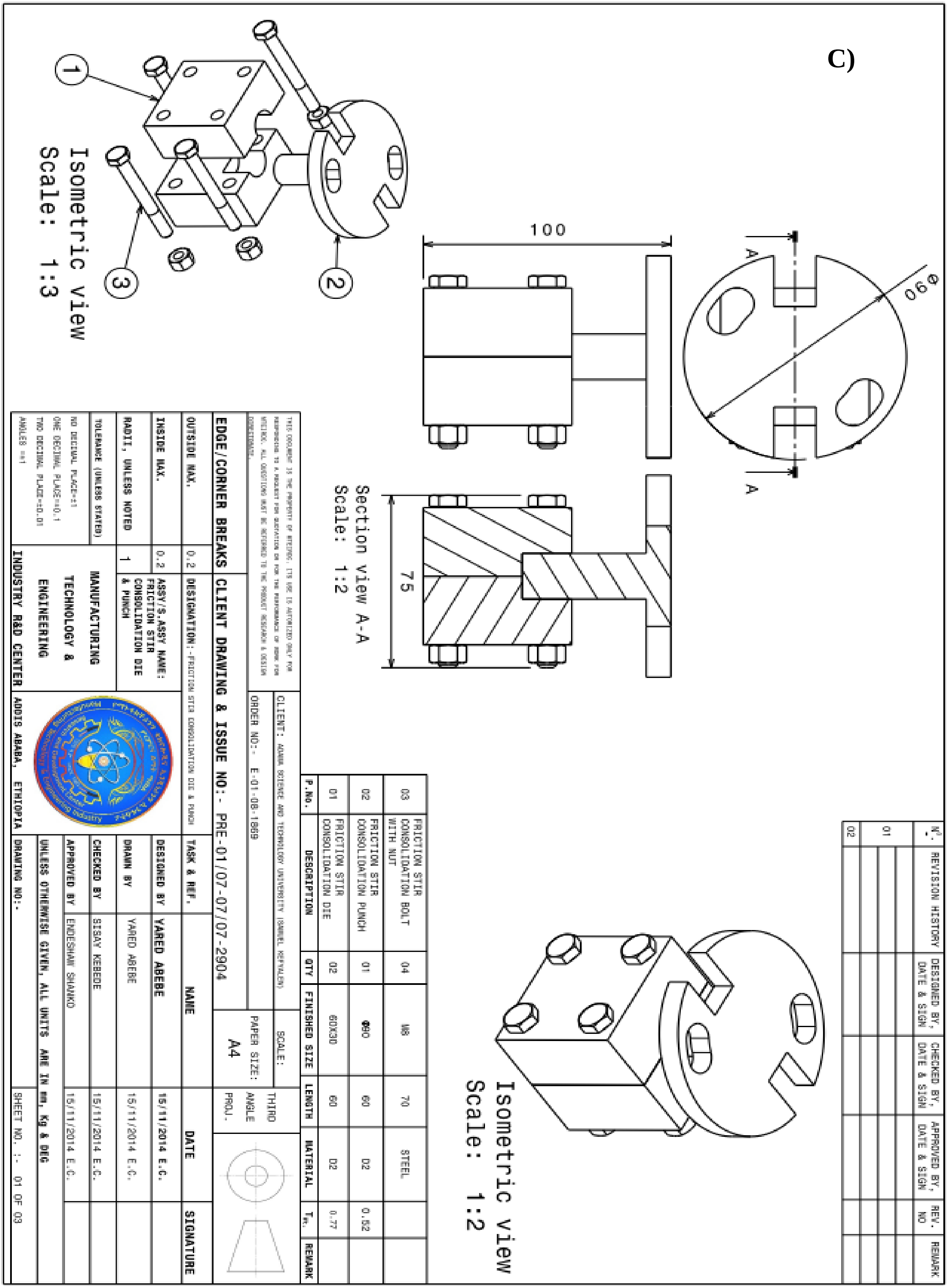

Figure XIII 3D Design of dies A) Chamber, B) Rotating Die and C) assembly of dies or exploded view of dies.